ETH
Eidgenössische Technische Hochschule Zürich
Swiss Federal Institute of Technology Zurich

IAC Institute for Atmospheric and Climate Science

Master's Thesis

Master's degree programme in Environmental Sciences

Swiss snow cover in a changing climate: Evaluation of a long-term high-resolution SWE analysis

---

Department of Environmental Systems Science, ETH Zurich
Institute for Atmospheric and Climate Science

Supervised by:
Dr. Sven Kotlarski, MeteoSwiss (main supervisor)
Dr. Regula Mülchi, MeteoSwiss
Dr. Stefanie Gubler, SCNAT
Dr. Christian Steger, ETH Zurich
Dr. Christoph Marty, SLF
Prof. Dr. Christoph Schär, ETH Zurich

Submitted by:
Sarina Danioth
18-924-597

Zurich / April 6, 2023

Abstract

Surface snow cover is an important and highly interactive component of global and regional climate systems and already has clearly responded to past warming trends in many regions of the world. Moreover, it is a key ingredient for tourism industry, water supply, irrigation, and hydro-power generation in many mountainous and high-latitude regions. Accurate information about the past, present and future evolution of snow cover is therefore of high importance. In Switzerland, to date, no state-of-the-art high-quality and spatially highly-resolved data set of surface snow cover at a climatological scale exists. For this reason, the Federal Office for Meteorology and Climatology (MeteoSwiss) and the WSL Institute for Snow and Avalanche Research (SLF), have generated a new daily snow water equivalent (SWE) data set (OSHD-CLQM) at a 1 km horizontal resolution, covering the hydrological years 1962 to 2022. Based on OSHD-CLQM, the spatio-temporal snow cover variability in Switzerland as a whole, as well as for different sub-regions and elevation classes employing a range of snow indicators is analyzed here. OSHD-CLQM is validated against existing data from station-based surface observations and from Advanced Very High Resolution Radiometer (AVHRR) and moderate resolution imaging spectroradiometer (MODIS) satellite data. A case study of the Swiss National Park (SNP) is conducted to assess the performance of OSHD-CLQM on a comparatively small area.

In accordance to previous studies, the analysis shows that the Swiss snow cover has changed strongly over the last decades. The comparison of two climatological long-term periods, 1962 - 1990 and 1991 - 2020, in terms of the mean SWE (September - May) and the number of snow days (SWE $>$ 10 mm) within the snow season, demonstrates a decrease in both indicators over the majority of the country. Low elevations ($<$ 1000 m a.s.l.) show relative decreases larger than 50 % of the mean SWE and larger than 30 % regarding the mean number of snow days (about - 22 days). The largest absolute difference of the mean SWE is found at medium elevations (between 1500 - 2000 m a.s.l.) with a decrease of about 45 mm (about $-$ 26 %). The validation of OSHD-CLQM indicates in general a high agreement between it and the in-situ observations. At the considered 59 measurement stations and their corresponding nearest grid cells in OSHD-CLQM, a median correlation of 0.82 is found for the time series of the mean SWE over the winter half year. Further, OSHD-CLQM lies within the range of AVHRR and MODIS. However, a clear statement regarding the comparison between OSHD-CLQM and the remote sensing data sets is difficult because of large differences between AVHRR and MODIS. Larger uncertainties and limitations of OSHD-CLQM are found, in particularly at the highest elevations (i.e. $>$ 3000 m a.s.l.). They originate from different sources, such as temporal inconsistencies in the input data grids of the underlying OSHD snow model or the lack of stations at high elevations that are needed for bias correction of the model. Nevertheless, overall OSHD-CLQM is able to provide adequate information on past snow cover for Switzerland as a whole, as well as for the selected sub-regions and the comparably small region of the SNP.

Contents

Chapter 1

Introduction and Background

Snow is of high importance for the climate system as well as for numerous socio-economic aspects in many mountainous and high-latitude regions. Therefore, information about the past, present and future spatio-temporal evolution of snow cover is extremely relevant. To date, no state-of-the-art high-quality and spatially high-resolved data set of snow cover at a long-term time scale over Switzerland exists. For this reason, the Federal Office for Meteorology and Climatology (MeteoSwiss) and the WSL Institute for Snow and Avalanche Research (SLF), have generated a new snow water equivalent (SWE) data set named OSHD-CLQM at a 1 km horizontal resolution and on a daily temporal resolution, covering the hydrological years 1962 to 2022. The first version of this newly developed data set was released in summer 2022 and is analyzed and validated in this Master's Thesis project.

The main objective of the thesis is the evaluation of the new gridded snow cover climatology over Switzerland, and thereby the validation of the data set against existing snow cover data from in-situ and remote sensing observations. In-depth analyses of temporal and spatial variabilities and trends of different snow indicators are performed. In a case study, the region of the Swiss National Park (SNP) in the Engadin is investigated in more detail. For these analyses, different snow variables and indicators are analyzed over Switzerland as a whole as well as for sub-regions and different elevation classes. The analyses are based on the variables SWE and fractional snow cover, and provide results on numerous snow indicators such as yearly mean SWE, the seasonal mean SWE, the monthly mean SWE and the number of snow days.

In the following a short background to snow in general, snow climatologies and the current state of research is given. Chapter 2 describes the data and methods used. Thereafter, chapter 3 presents the results and their discussion followed by the conclusions in chapter 4.

1.1 Snow

Surface snow cover is not only an essential component of the climate system (see subsection 1.1.1), but also has high economic and societal relevance in snow-rich regions such as the European Alps. For instance, snow cover is an important water storage in the hydrological cycle. As a consequence, snow melt and the total amount of water stored in snow is critical for water supply, irrigation and hydro-power generation (Armstrong et al., 2008; Anghileri et al., 2018). Further, snow is an essential contributor for the tourism industry in mid-latitudinal mountain regions. In many of Switzerland's Alpine regions, winter tourism is the major source of income (Elsasser et al., 2002). Thus, sufficient snow availability (snow-reliability) in the Alps is of high relevance (Elsasser et al., 2002). However, snow can also be associated with natural hazard, as it can cause reduced visibility from blowing snow, buildings to collapse due to heavy snow load, floods due to rapid snow melt, and avalanches (Armstrong et al., 2008).

1.1.1 Snow cover in the climate system

Snow is an essential component of the climate system. Snow cover, defined as the blanket of snow covering the surface, plays a crucial role in modifying energy and moisture fluxes between the surface and the atmosphere (Brown et al., 2005). Fresh snow has a high reflectance with an albedo between 0.8 and 0.9 (Armstrong et al., 2008). In addition, deeper snow packs have a strong insulating property due to its low thermal conductivity, which leads to a reduction of the energy exchange between the surface and the atmosphere (Armstrong et al., 2008). According to empirical studies, these two properties of snow lead to lower mean near-surface air temperatures in the vicinity of snow (Groisman et al., 2001). Scherrer et al. (2012) showed that in Switzerland, the daily mean near-surface temperature of a spring day without snow cover is on average 0.4 °C higher than one with snow cover at the same location. This is caused by the snow-albedo feedback, one of the most important positive feedbacks in the climate system, which impacts the surface energy balance (Hall, 2004). Moreover, the insulating nature of snow cover is also decisive for ecological systems. A snow thickness of 30 cm is sufficient to protect organisms living underneath from the diurnal cycle of temperature and therefrom from freezing (Brown et al., 2005). Up from a snow thickness of 60 cm, the insulating effect protects permafrost from the warmer temperatures outside and thus from thawing (Luetschg et al., 2008).

1.1.2 Distribution and variability of snow cover

On a global scale, the presence of snow coverage is clearly linked to air temperature and is most abundant at high latitudes and/or high elevations (Gutzler et al., 1992). The spatial extent typically peaks in the respective hemispheric winter, when incoming solar radiation is close to its annual minimum and temperatures are low. Despite this regular forcing, large interannual variability in both snow cover extent and amount can occur, which is typically linked to atmospheric circulation patterns affecting temperature and precipitation. For instance over Eurasia and North America, the North Atlantic Oscillation (NAO) and the Pacific-North America Oscillation are correlated to the snow cover extent (Gutzler et al., 1992). For the Swiss Alps, the examination of the linkage between the NAO and snow variability is difficult. Scherrer et al. (2006) identified the NAO index as the third major pattern which explains about 10 % of the total variance of interannual Swiss Alpine snow pack variability.

Another factor with strong influence on the spatio-temporal variability of snow in Switzerland is the elevation. Grünewald et al. (2014) showed that mean snow depths generally increase with elevation until a peak is reached, then a decrease follows at the highest elevations at the mountain peaks again. They have explained this shape with the positive elevation gradient of snowfall, which is modified by the interaction of snow cover and topography. These interactions include preferential deposition of precipitation and redistribution of snow by wind, sliding, and avalanche formation (Grünewald et al., 2014; WSL, 2012). Wirz et al. (2011) analyzed the effect of snow depth in rock face areas. They found that the snow depth is in general lower in steep terrain than in a flat area due to avalanching, radiation differences and wind-terrain-interactions. Additionally, the vegetation has an effect on snow depth. Stähli et al. (2006) showed that areas covered by forest have about half the SWE values of open areas since forests influence snow accumulation by interception as well as ablation by radiation shading and reduced turbulent exchange above the snow. With increasing snowfall this forest effect decreases (Stähli et al., 2006).

1.1.3 Snow cover in a changing climate

Global warming has a strong influence on the presence of snow cover (IPCC, 2021). The latest report of the Intergovernmental Panel on Climate Change (IPCC) states that human influence has very likely contributed to the decrease in northern hemisphere spring snow cover since 1950 (IPCC, 2021). Moreover, the IPCC is highly confident that the onset of spring snow-melt occurs earlier.
In a local perspective, Marty (2008) has shown that the amounts of snow in Switzerland have diminished over the last decades. Marty (2008) detected a step-like decrease (20 % to 60 %) in snow days at the end of the 1980's in Switzerland, whereby low elevation zones experienced the most dramatic reduction. Figure 1.1 depicts these descending trends including the step like shift at the end of the 1980s. This shift coincides with an increase in mean winter temperature, which is related to the increase in annual temperature (Marty, 2008).

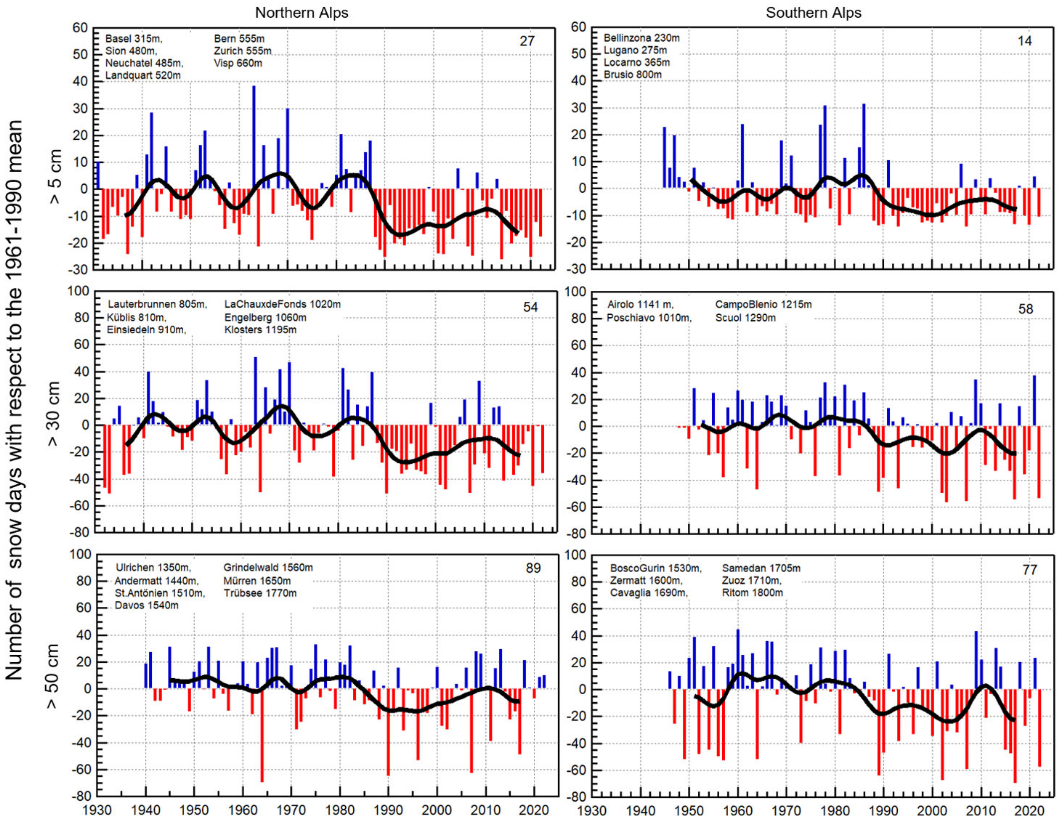

Figure 1.1: Annual snow days anomalies relative to the climate between 1961 and 1990 for three different elevation zones (low, middle and high) and the northern (left) and southern (right) slope of the Alps. Figure taken from Marty (2008); SLF (2023b).

Further, Marty et al. (2017b) analyzed SWE and found a reduction of snow mass in the European Alps. This reduction was explained by the increasing temperatures and the coincident weak reduction in precipitation (Marty et al., 2017b). Hüsler et al. (2014) found that regional snow cover duration in the European Alps significantly shortened at lower elevations in the south-east and south-west. These findings are supported by the study of Matiu et al. (2021). In an Alpine-wide analysis of the seasonal mean snow depth, they found an average trend of $-8.4\,\%$ per decade.

With additional warming further loss of seasonal snow cover is expected (IPCC, 2021). Beniston et al. (2018) stated that by the end of the 21st century, Europe's mountain cryosphere will have changed

dramatically. They showed that the landscape, the hydrological regimes, the water resources, the infrastructure of the mountain area and the downstream lowlands will be severely impacted by climate change until then, which will result in enormous socio-economical consequences. The increase in air temperatures and the related shift from solid to liquid precipitation, will lead to seasonal snow lines at higher elevations as well as to shorter snow seasons compared to today (Beniston et al., 2018). Furthermore, there will be a shift in the timing and discharge maxima (Beniston et al., 2018).
Projections of regional climate models show high inter-model agreement on reduction of winter mean SWE in the European Alps of about 40 - 80 % by the mid century relative to 1971 - 2000, with the strongest trend occurring at elevations below 1500 m a.s.l. (Steger et al., 2013). Similar trends were found in other studies, like Kotlarski et al. (2022) or Marty et al. (2017a). Kotlarski et al. (2022) have shown that alpine-wide snow cover will undergo a widespread decrease in the course of the 21st century as a result of higher temperatures, which will outweigh the effect of increased precipitation during winter. The study of Marty et al. (2017a) revealed, depending on the emission scenario and elevation zone, that the winter season could start half a month to a month later and could end one to three months earlier at the end of the twenty-first century compared to the reference period 1999 - 2012. Moreover, the number of snow days is projected to be halved at elevations around 1500 m a.s.l. by the end of the century relative to 1999 - 2012 under high-emission scenarios (Marty et al., 2017a).

1.2 Snow climatologies

The glossary of the American Meteorological Society (AMS, 2021) defines climatology as the description and scientific study of climate. Broad applications speak of climatology as the study of the atmosphere and weather over space and time. More precisely, descriptive climatology describes the observed geographic or temporal distribution of meteorological observations over a given period of time. To produce climatological standard normals and / or to filter random year-to-year fluctuations, climatological data is often averaged over 30 years. On the other hand, scientific climatology focuses on the nature and control of the Earth's climate and the causes of climate variability and change on all time scales (AMS, 2021).
Long-term climatologies are useful for two main reasons. First, they are used for the quantification of the past and current spatio-temporal variability of a climatological variable and its statistical distribution. Second, they serve as benchmarks against which recent or current observations can be assessed, and provide the basis for many anomaly-based climate data sets (WMO, 2007; WMO, 2017). The application of statistical methods allows detection and quantification of climate change, as well as the estimation of the probability of extreme events. Moreover, the assessment of uncertainties in the current understanding of the climate system and climate models is possible (Robeson, 2005).

In the specific case of snow cover, climatologies are valuable for various practical applications (SLF, 2023b). The snow reliability assessment of a specific region or the identification of ideal preventive measures such as avalanche barriers or snow load standards are two examples (SLF, 2023b). Information about the spatial and temporal distribution of SWE is critical for water resource management (i.e. agriculture, hydro power generation, flood forecasting) (Brown et al., 2005). In subsection 1.1.3 the change of snow pack with global warming was reviewed. Long-term data sets are important for the identification and quantification of such resulting trends and / or variability (SLF, 2023b).
However, the establishment of snow climatologies is challenging due to the lack of spatially dense measurement networks in many regions. Often, surface-based observation networks only exist in populated regions at low elevations (Brown et al., 2005). Additionally, measuring snow itself is a challenging task for numerous reasons. Snow is a dynamical material and its properties can change substantially on short time

scales (Doesken et al., 2009). Therefore, the time of measuring snow plays a role. Further, it is difficult to find representative measuring locations in areas with spatially highly variable snow coverage, which is the case in complex terrain, in which the snow coverage is influenced by inhomogeneities in wind and received surface radiation (Lehning et al., 2008). Measurement errors at site stations can occur when wind carries old or new snow towards or away from the measuring station. Also, avalanches or heavy snowfall can cause the measuring station to fail (SLF, 2023a). In summer, grass may be accidentally measured by the sensors (SLF, 2023a). Long-term snow series are often subject to inhomogeneities as a result of changes in the measurement locations, the measurement practices or observer changes (Buchmann et al., 2022).

1.3 State of research in Switzerland

To date, various snow cover data sets are available for the analysis of snow in Switzerland. The data sets originate from different sources, both in-situ and satellite measurements, atmospheric reanalysis, and / or snow models. The horizontal resolution ranges from coarse scales of about 30 km down to the point scale. As an example, Figure 1.2 shows the relative snow depth of the winter months (November - April) over Switzerland between 1971 and 2021 from spatially interpolated point measurements (Neukom, 2006; SLF, 2023b).

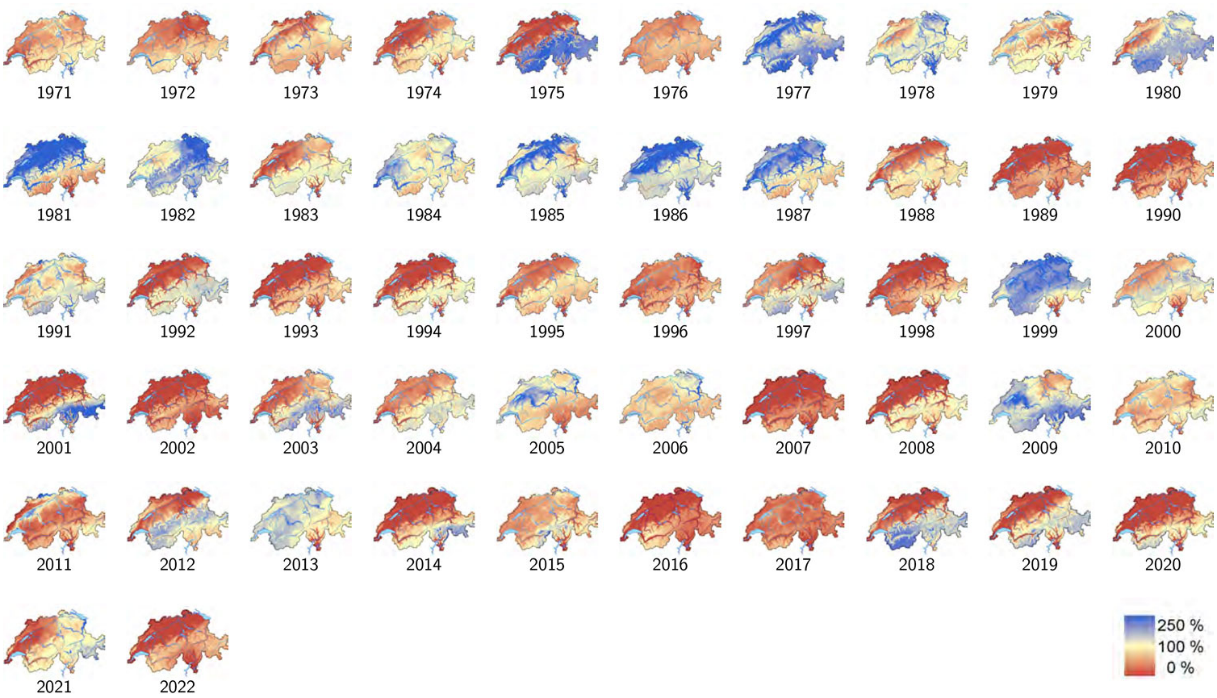

Figure 1.2: Relative snow depth of the winter months (November to April) over Switzerland between 1971 and 2021 compared to the reference period 1971-2000. Figure taken from SLF (2023b).

These data sets enable the analysis of the spatio-temporal distribution of snow over Switzerland. Different studies in the past have analyzed various snow indicators (see section 1.1). Göldi (2021), for instance, analyzed different snow indicators in several different data sets between 1982 and 2019 in order to evaluate their performance. The study revealed that all available data sets are subject to major or minor deficits like low horizontal resolution, weak correlations with validation data, irregular performance in different elevation zones and regions or short time periods of availability (Göldi, 2021). Possible factors for that include temporal and spatial gaps in station measurement networks, as well as difficulties in

measuring snow on site and remotely, which make the development of a spatial climatological snow data set challenging (Göldi, 2021). Remote sensing data are maximally available back to the early 1980's. The lack of temporal homogeneity of data series and complex processes in the snow pack, which are difficult to model, are further causes. Although Switzerland has one of the densest networks of snow measurements, the large spatial variability, primarily caused by the complex topography, makes interpolation a challenging endeavour.
To conclude, various snow data sets with different strengths and weaknesses over Switzerland for various time periods exist. Nevertheless, there is currently no state-of-the-art spatially high-resolved (1 km) and high-quality snow cover data set at a climatological scale available. Within this context, a new reliable snow climatology with high spatial and temporal resolution over a longer time period allows new relevant insights and applications in a number of fields such as hydrology, tourism and ecology.

1.4 Objectives

To fill this research and data gap, MeteoSwiss and the SLF have produced a new climatological snow cover data set for Switzerland at high temporal (1 day) and high spatial (1 km) resolution, covering the hydrological years between 1962 and 2022. This data set is named OSHD-CLQM and is described in detail below (subsection 2.2.1). A first version of this new Swiss snow climatology has been released in summer 2022. The main purpose of the present thesis is the analysis and evaluation of this spatially and temporally high-resolved snow data set of Switzerland on a climatological scale. The specific objectives are listed in the following.

- Based on OSHD-CLQM the spatio-temporal snow cover variability is analyzed in Switzerland as a whole as well as for different sub-regions and elevation classes employing a range of snow indicators.
- Uncertainties and limitations of OSHD-CLQM are identified.
- OSHD-CLQM is validated against existing dependent and independent snow cover data from ground and remote sensing observations.
- A case study in the region of the SNP is conducted to assess the performance of OSHD-CLQM on a comparatively smaller area.

Chapter 2

Data and Methods

2.1 Study region

The study is conducted over Switzerland. The 41 285 km^2 of Switzerland can be divided into three geographical regions: the Alps (make up about 58 % of the country), the Swiss Plateau (31 %) and the Jura (11 %) (EDA, 2021). The topography of Switzerland is shaped by the Alps, the lowest point is located at Lake Maggiore at 193 m a.s.l. and the highest at the Dufourspitze at 4634 m a.s.l. About 50 % of the country is located above 1000 m a.s.l. and roughly 23 % lies above 2000 m a.s.l. (EDA, 2021). The Swiss climate is characterized to a large extent by the complex topography of the Alps and the Jura. The geographical location, low temperatures as well as topographical factors such as orographic lifting yield to snow as a significant precipitation quantity, especially at high elevations. At elevations around 1500 m a.s.l., one third of the annual precipitation consists of snow, and above 2000 m a.s.l. the proportion is greater than 50 % (WSL, 2012).

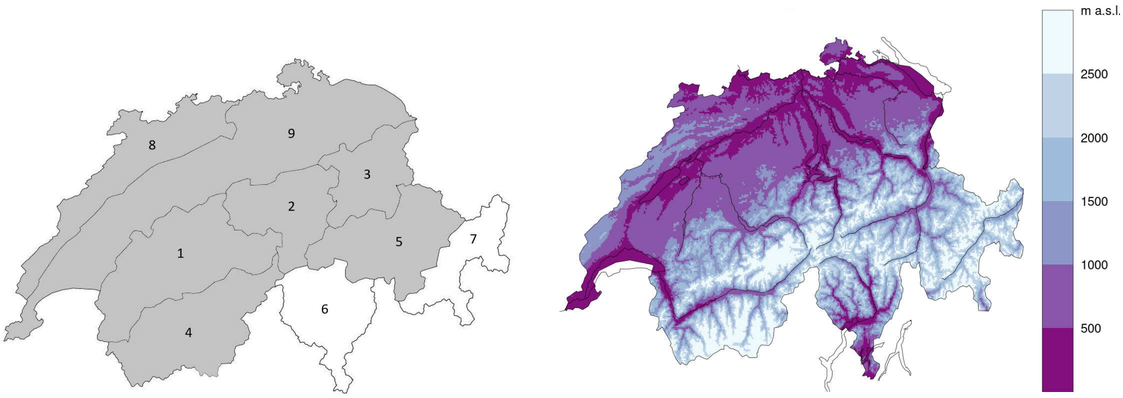

(a) The selected sub-regions. (b) The selected elevation classes.

Figure 2.1: Overview of the study region. **(a)** 1: North-Western Alpine Slope, 2: North-Central Alpine Slope, 3: North-Eastern Alpine Slope, 4: Valais, 5: Northern and Central Grisons, 6: Ticino, 7: Engadin, 8: Jura, 9: Swiss Plateau. The sub-regions indicated by the grey shading built together Northern Switzerland, the white area represents Southern Switzerland. Figure taken from Göldi (2021). **(b)** $<$ 500 m a.s.l., 500 - 1000 m a.s.l., 1000 - 1500 m a.s.l., 1500 - 2000 m a.s.l., 2000 - 2500 m a.s.l. and $>$ 2500 m a.s.l.

In the study, Switzerland as a whole is analyzed first. Owing to the high spatial resolution of the data, it is possible to look at different sub-regions. Figure 2.1 shows the sub-regions, which were defined according to the warning regions of the SLF (SLF, 2022a): North-Western Alpine Slope (NWA), North-Central Alpine Slope (NCA), North-Eastern Alpine Slope (NWA), Valais (VAL), Northern and Central Grisons (GRI), Ticino (TIC), Engadin (ENG), Jura (JUR) and Swiss Plateau (PLA). This division is based on climatological and / or political criteria and has the advantage that a previous study has used the same sub-regions and thus a comparison of the results is possible (i.e. Göldi (2021)). In addition, Switzerland (CH) was divided into south (S, consisting of the sub-regions Ticino and Engadin) and north (N, all other sub-regions). Moreover, different elevation classes are evaluated, in order to detect potential elevation-dependent trends and patterns. In accordance with previous studies, (e.g. Göldi (2021); Marty et al. (2017a); Steger et al. (2013)) the following elevation classes were selected: < 500 m a.s.l., 500 - 1000 m a.s.l., 1000 - 1500 m a.s.l., 1500 - 2000 m a.s.l., 2000 - 2500 m a.s.l. and > 2500 m a.s.l. (Figure 2.1b). Finally, a case study of a comparatively smaller sub-region, namely of the SNP, is conducted. The SNP is described in more detail in section 3.4.

In Figure 2.2 the relative distribution of the grid cells of the main data set (OSHD-CLQM) among the elevation classes in the sub-regions is presented in a hypsograph. The data grid used represents Switzerland with a total of 41'547 grid cells. The absolute numbers of grid cells for each sub-region and elevation class are shown in Appendix A. It makes clear that the Jura and the Swiss Plateau are dominated by grid cells with relatively low elevations, whereas the Engadin and the Northern and Central Grisons, for example, have most grid cells in higher elevations.

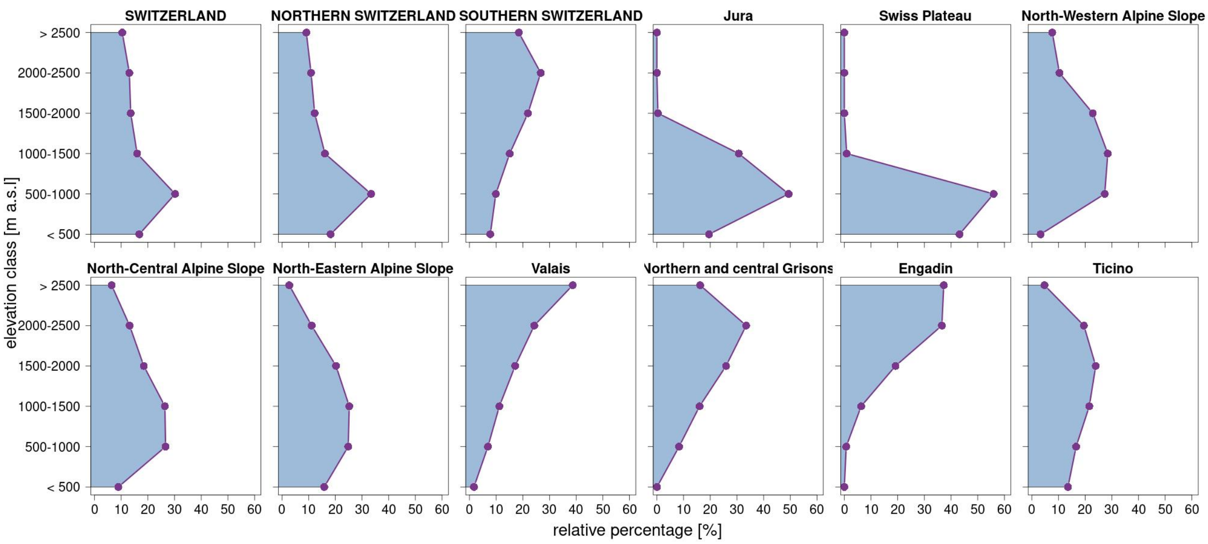

Figure 2.2: Hypsograph showing the relative distribution of the number of grid cells among the elevation classes in every selected sub-region.

2.2 Data

The gridded data set analyzed in the present work is based on modeled and bias-corrected SWE. Information about the variable SWE can be found in subsection 2.3.1. Additionally, observational data sets were used for validation and comparison. These data sets are based on both ground measurements as well as on remote sensing observations. In the following, all data sets are shortly presented.

2.2.1 Modeled snow water equivalent from OSHD-CLQM

As reviewed in section 1.3, to date no state-of-the-art high-quality and spatially high-resolved snow cover data set covering climatological time scales is available over Switzerland. For this reason, the SLF and MeteoSwiss initiated the joint research project "A spatial Snow Climatology for Switzerland (SPASS)" in order to develop such a data set (MeteoSwiss, 2021f). The first version of the data set has been released in summer 2022. The data set is called OSHD-CLQM and currently provides modeled and bias-corrected SWE data (in m w.e.) from September 1961 until September 2022 (hydrological years 1962 to 2022) for entire Switzerland. The spatial resolution of OSHD-CLQM is 1 km, and the data has a daily temporal resolution. In the following, the methodological approach behind OSHD-CLQM is described in more detail. Further information can be found in Michel et al. (2023).

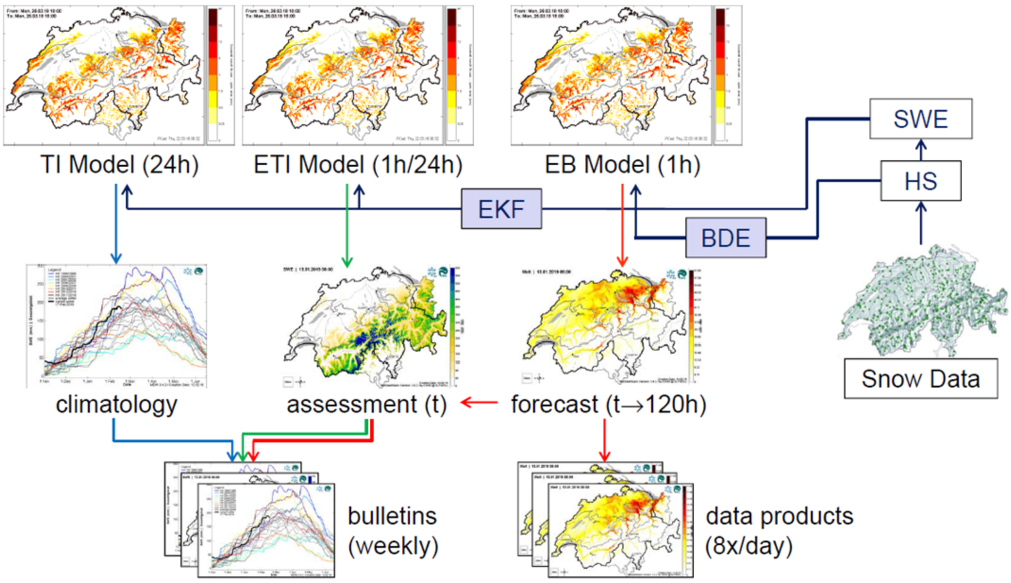

Figure 2.3: Overview of the OSHD framework. Figure provided by T. Jonas (pers. comm., 2023).

The operational snow-hydrological service (OSHD) of the SLF operates various snow models (OSHD, 2023). An overview is provided in Figure 2.3. OSHD-CLQM has been produced based on a simple baseline simulation and a training data set that additionally assimilates observations from stations (Michel et al., 2023). For the baseline simulation of the daily SWE grids a standard temperature index model is employed (Magnusson et al., 2014) (upper left in Figure 2.3). The resulting data set is called OSHD-CL. The atmospheric forcing of OSHD-CL consists of daily 1 km gridded temperature (TabsD, (MeteoSwiss, 2021a)) and precipitation (RhiresD, (MeteoSwiss, 2021b)) data sets developed by MeteoSwiss. OSHD-CL is available from September 1961 to the present.

The training data set, called OSHD-EKF, is based on the same temperature index model. Additionally, measured snow depth data from 320 different monitoring stations are assimilated into OSHD-EKF using the Ensemble Kalman Filter (Magnusson et al., 2014). OSHD-EKF is available since September 1998. As OSHD-EKF was produced with the goal to have a homogeneous data set over time, homogeneous and consistent observational data had to be assimilated. Numerous stations only begun to measure in the late nineties or the station location changed over time, thus, the temporal availability of OSHD-EKF is limited.

To adjust the OSHD-CL baseline model towards the more accurate OSHD-EKF data set, Michel et al. (2023) created a R Package named SnowQM based on a quantile mapping approach. Quantile mapping can be used for correcting systematic biases of long-term data series against shorter higher-quality data series (Rabiei et al., 2015). For the development of OSHD-CLQM, the quantile mapping of SnowQM was calibrated and validated from 1998 to 2021 using the OSHD-EKF data set (higher-quality data series) and was then applied to the OSHD-CL data set over the period from September 1961 to today (Michel et al., 2023). An overview is provided in Figure 2.4. For the SWE adjustment through quantile mapping, quantile distributions were calculated over the training period depending on the following free parameters: size of the time window, minimum number of pixel to be included in the spatial clustering, step in the spatial direction, step in the elevation direction, step in the slope angle direction, step in the aspect angle direction and step in the curvature direction (Michel et al., 2023). The correction of the SWE data is based on the cumulative distribution function of the modeled SWE data and the inverse of the cumulative distribution function of the ground truth data. More specifically, these functions were approximated by the empirical quantile distribution and then sorted in ascending order and separated, in this case, into 101 quantiles (Michel et al., 2023). Then the SWE value to be corrected was compared to the quantile distribution of the modeled SWE data set to determine in which quantile it falls into. The difference between this specific modeled SWE value quantile and the related training SWE value quantile has then be used as an adjustment. For each pixel and every day of the year the quantile mapping approach was applied separately (Michel et al., 2023).

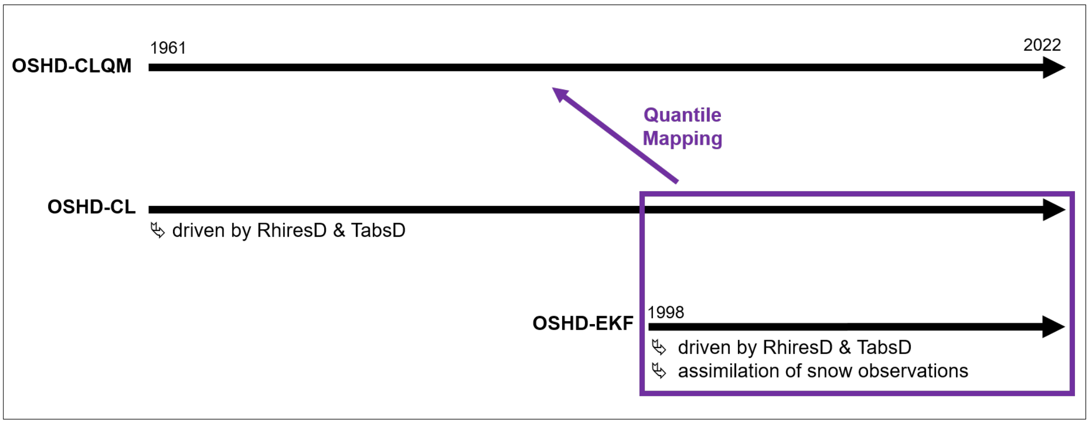

Figure 2.4: Overview of the modeled SWE data sets.

Michel et al. (2023) state that there might exist larger spatial uncertainties in OSHD-CLQM at elevations above 3000 m a.s.l. as there are no monitoring stations and therefore no possibility to assimilate data into the OSHD-EKF training data set. Moreover, the Alpine topography is steep at high elevations and therefore not well captured by the 1 km grid spacing of OSHD (Michel et al., 2023). These factors especially also impact summer, when snow is usually mainly present at high elevations. In addition, there are generally fewer snow observations available over summer (A. Michel, pers. comm., 2023).
In the context of other temporal uncertainties, there might occur inconsistencies as the model can produce snow towers at certain high elevation pixels (Michel et al., 2023). This means that snow does not melt over summer at some pixels and thus accumulates from year to year. Multi-year snow accumulation can be a realistic phenomenon at high Alpine elevations. Nevertheless, modeling such features is challenging. Therefore, the SWE values produced by the model were set to zero every year on September 01, to make sure that the model delivers snow accumulation for each hydrological year individually (Michel et al., 2023).

2.2.2 In-situ observations

For the validation of OSHD-CLQM, snow depth data from two different station-based measurement networks were used. On one hand, manual measurements from 54 monitoring stations of the SLF and MeteoSwiss were included (Haberkorn, A., 2019). Some of these measurement data was evaluated by Buchmann et al. (2021). On the other hand, 5 automatic snow measurement stations from the IMIS-network (Interkantonales Mess- und Informationssystem) supervised by the SLF available at remote regions in the Swiss Alps were included. They reach back to 1996 and were used for example by Egli (2008). Figure 2.5 provides an overview of the stations used from the two networks, their spatial distribution as well as their division among the six elevation classes. The selection of the stations was made based on their respective data availability between 1999 and 2021 to enable the comparison against OSHD-CLQM and its preceding data sets. Moreover, their quality, continuity and spatial distribution were considered. Numerous stations are available over the whole time period of OSHD-CLQM reaching back to the 1960s. Within the hydrological year, the availability of the data is limited to the winter months (November to April).

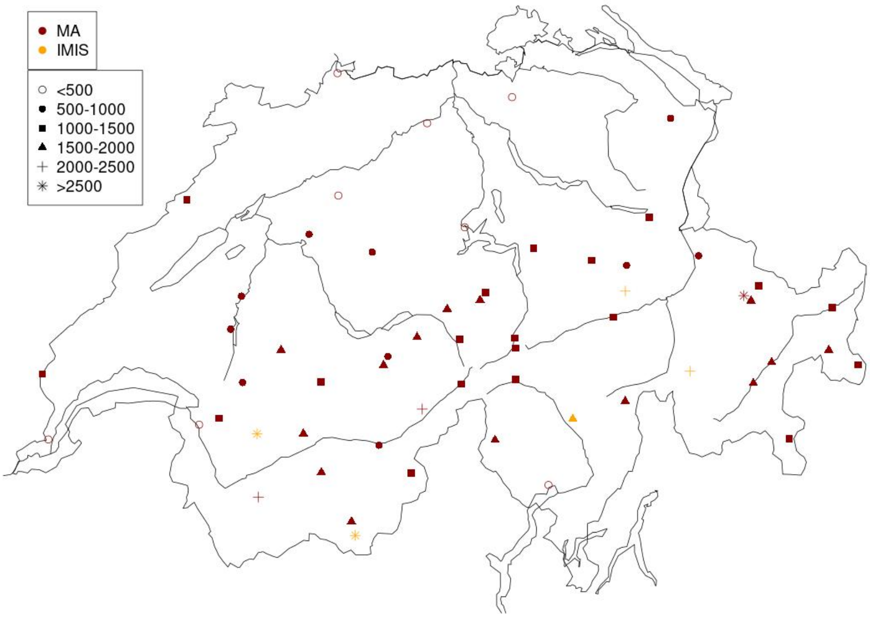

Figure 2.5: Overview of the measurement stations. Brown: manual measurement stations. Yellow: stations from the IMIS network. The symbols indicate to which elevation class the stations belong to.

It has to be mentioned here that the in-situ data do not allow for a completely independent assessment of OSHD-CLQM's performance because some of the data were used in the data assimilation step of OSHD-EKF. Moreover, the time series at the stations may be prone to inhomogeneities. As mentioned in section 1.2 measuring snow itself is a challenging task. Inhomogeneities in the time series can occur if there were changes in the station's location, observer personnel or measurement practices (Buchmann et al., 2022). Moreover, finding representative measuring sites, especially in areas with spatially highly variable snow cover in complex terrain, is challenging due to inhomogeneities in wind and received surface radiation (Lehning et al., 2008). To avoid resulting discrepancies, the validation primarily looked at anomalies and trends, rather than at absolute values. Nevertheless, these observational data are very important for the validation as they have a high temporal (1 day) and spatial (point) resolution and some

stations are available over the whole temporal range of OSHD-CLQM (back to 1961).
As the stations provide data on snow depth and OSHD-CLQM on SWE, a conversion of the snow depth data was needed. This conversion of the data was done using the semi-empirical multi-layer model developed by Winkler et al. (2021), with the difference that slightly different calibration coefficients were used for elevations below 800 m a.s.l. (C. Marty, pers. comm., 2023).

2.2.3 Remote sensing data

The station-based validation does not allow for a completely independent assessment of OSHD-CLQM and enables rather local analyses. Remote sensing data allow independent and spatial insights. However, the length of the measurement series is limited to the presence of satellites. OSHD-CLQM was validated against two different remote sensing data sets from Advanced Very High Resolution Radiometer (AVHRR) and moderate resolution imaging spectroradiometer (MODIS) satellite data.

In order to coordinate systematic climate observations worldwide, the Global Climate Observing System (GCOS) was established in 1992 (MeteoSwiss, 2018). Within the framework of GCOS Switzerland, a novel fractional snow cover time series based on AVHRR satellite data was recently generated by the University of Bern (Weber et al. (2022); MeteoSwiss (2022b)), which is the follow-up of the data set by Hüsler et al. (2014). For the comparison with OSHD-CLQM a Beta-version of this AVHRR product is used, as the final version is not available yet. The data set covers the time period from 1981 until 2021 and provides temporal and spatial homogeneous information of Switzerland's snow cover. As about 30 % of the country is forested and snow on the ground in forests is (partially) obstructed by the canopy, Weber et al. (2022) corrected fractional snow cover for this effect. The spatial resolution of AVHRR is 1 km and the data product delivers the 10-day running mean fractional snow cover. The validation of this product by Weber et al. (2022) pointed out that the performance of AVHRR increases for larger fractional snow cover values ($> 40\,\%$). They also found a superior performance when limiting the viewing zenith angle for the satellites acquisitions to less than $40°$. Thus, the AVHRR product used for the validation against OSHD-CLQM follows these definitions.
There are frequently missing days and years in this Beta-version of AVHRR. In the beginning of 1981, there is a missing period because of the lack of satellite data. Afterwards, the years between 1986 and 1989 are missing due to processing errors. Parts of 1991 and the years 1997 - 2003 are missing due to low data quality. Thus, these years could be used for the validation. Remaining years still contain spatially confined temporal gaps with lengths of several days.

The second remote sensing data set used for validation of OSHD-CLQM is based on MODIS satellite data and was developed by Matiu et al. (2019). It delivers daily fractional snow cover data at a spatial resolution of 250 m. The availability is limited to the years 2002 to 2019. Due to data quality issues the year 2019 is not considered here (Matiu et al., 2019). Matiu et al. (2019) applied temporal and spatial filters in order to reduce data gaps stemming from cloud coverage. In contrast to AVHRR, there are almost no missing values in MODIS, which enables a virtually gap-free validation, however, on a shorter time scale.

For the comparison of OSHD-CLQM with the remote sensing data, the data sets needed to be on a comparable grid. For this reason, the remote sensing data sets were re-mapped to the OSHD 1 km grid. For the re-gridding of AVHRR (horizontal resolution of 1 km), a nearest-neighbour method was used (according to Matiu et al. (2022)) to conserve the distribution and avoid the smoothing of extrema. On the other hand, a conservative approach was used for MODIS to preserve all available information from the fine MODIS grid (horizontal resolution of 250 m).

2.3 Methods

2.3.1 Snow variables and indicators

The main snow variable investigated is snow water equivalent (SWE) since this is the basic variable provided by OSHD-CLQM. SWE corresponds to the depth of water if all available snow is melted. The relation between SWE and snow depth is given as follows,

$$SWE\,(m) \;=\; \frac{\rho_s}{\rho_w} \,*\, h_s\;,$$

where h_s stands for the depth of snow in m and ρ_s and ρ_w are the densities of snow and water in kg m^{-3}, respectively (DeWalle et al., 2008). Snowfall density is affected by differences in crystal type, size and liquid water content and varies as a function of regional variations based on temperature and precipitation climates. Typical values are in the range of 50 to 120 kg m^{-3} (DeWalle et al., 2008). Once the snow flakes are deposited on the ground, snow crystals change their size, shape and bonding over time by water vapor gradients, crystal settlement and wind packing, leading to large density modifications (called metamorphism). Typical density values for melting snow lie between 350 and 500 kg m^{-3} (Brown et al., 2005). Jonas et al. (2009) showed that the bulk snow density in Switzerland is strongly dependent on the season, snow depth, site elevation and site location. Densities for snow that has been on the ground for a longer time and underwent significant metamorphism and settling processes are larger than of fresh and smaller than of melting snow.

Snow indicators were obtained from the SWE provided by OSHD-CLQM as well as from the converted SWE provided by the in-situ snow depth observations and from the fractional snow cover data provided by remote sensing observations. The following main indicators were considered in this study to analyze snow cover and to intercompare the data sets:

- **Mean SWE**: The daily SWE provided by OSHD-CLQM as well as the daily SWE from the station-based snow depth data, were averaged over different time periods (see subsection 2.3.2).
- **Number of snow days**: The threshold value of 10 mm was used to define a snow day based on the SWE values provided by OSHD-CLQM and the station-based data (according to e.g. Da Ronco et al. (2016)). The threshold for defining a snow day in the remote sensing data sets, which provide fractional snow cover data, was set to 0.5. More details on the computation is provided in subsection 2.3.3.

2.3.2 Time periods and statistical metrics

Analyses in the field of hydrology are generally conducted over the hydrological year, which is defined as the year from September 01 of the previous year to August 31 of the year under consideration. As stated in subsection 2.2.1 the summer months of OSHD-CLQM may contain larger uncertainties and thus, analyses including summer might be prone to errors. Therefore, we decided to exclude June, July and August for the analysis part of this work. For the comparison of OSHD-CLQM against the in-situ observations, only the winter months were considered, as the availability of the measurements is limited. The different time periods considered, are defined in the following:

- **Hydrological year**: from September 01 of the previous year to August 31 of the year under consideration. E.g. the hydrological year 1962 begins on September 01, 1961, and ends on August 31, 1962.
- **Snow season**: from September 01 of the previous year to May 31 of the year under consideration.
- **Winter half year**: from November 01 of the previous year to April 30 of the year under consideration.
- **Meteorological seasons**: SON (September, October, November), DJF (December, January, February), MAM (March, April, May) and JJA (June, July, August).

Whenever the time period is not explicitly specified below, the snow season was considered.

In climatological applications it is common to use long-term averages of meteorological observations (see section 1.2). The averaging periods (30 years) to produce climatological standard normals are globally standardized. Those periods are shifted frequently as the climate is evolving. Currently, MeteoSwiss uses the period 1991 - 2020 as the normal period (MeteoSwiss, 2022a). For quantifying and illustrating long-term climate change, the period between 1961 and 1990 is often used as reference. As OSHD-CLQM is available from September 1961 until September 2022, the following two norm periods were used: hydrological years resp. snow seasons 1962 - 1990 and hydrological years resp. snow seasons 1991 - 2020. Those two periods were compared to each other in order to identify changes in the climatological normals.

For the calculation of the climatology, the snow indicators were averaged over a chosen time (hydrological year, season or month) and over the norm periods for every grid cell. In order to get sub-regional results, the grid cells over the specific sub-regions of interest were averaged again. To obtain deviations from the climate normal, relative and absolute anomalies were computed. The SWE was averaged on a monthly base to investigate the annual cycle. The time series of the mean SWE and the number of snow days over the snow season was analyzed to get an insight about variability and changes over time. Here, also the pearson correlation between those two indicators was calculated.

Trends of the snow indicators were investigated using a smoothing function. More exactly, a trend line is fitted by local linear regression to the obtained time series of the indicators. This procedure is called LOESS smoothing and was developed by De Valk (2020). Here, an adaption of this function by Scherrer et al. (2023) was used. A bicubic weight function over different window sizes, which controls the span parameter of the function, could be chosen. For the SWE and snow days time series in this study, the window sizes were set to 14 (corresponding to a 10-year average) and 42 (corresponding to a 30-year average). The confidence level for the error bound was set to 0.95.

2.3.3 Intercomparison of data sets

For a local comparison of OSHD-CLQM with the station-based data, the mean SWE values and the number of snow days at the stations were compared to a specific grid cell of OSHD-CLQM through an adapted nearest grid cell approach (as done by e.g. Göldi (2021)). The grid cell that contains the station of interest as well as the eight surrounding grid cells were selected in a first step. Then, the elevation of these totally nine grid cells were compared to the elevation of the station. The grid cell with the smallest elevation difference to the station was chosen for the comparison. Figure 2.6 shows an overview of the elevations of the stations (turqoise) and their corresponding grid cells in OSHD-CLQM (pink) identified

by this procedure. The largest elevation difference occurs between the station of Airolo (*AIR) and its selected nearest grid cell (77.25 m) and the smallest difference is located at the station of Guttannen (*GTT) (0.13 m).
Due to missing values and gaps in the station data set, some criteria for the comparison with OSHD-CLQM were set. For monthly averages, a maximum of 10 daily values were allowed to miss. For the average over all available months (November to April), this maximum was set to 30 missing daily values. When considering climatological periods, less than 5 years were allowed to miss.

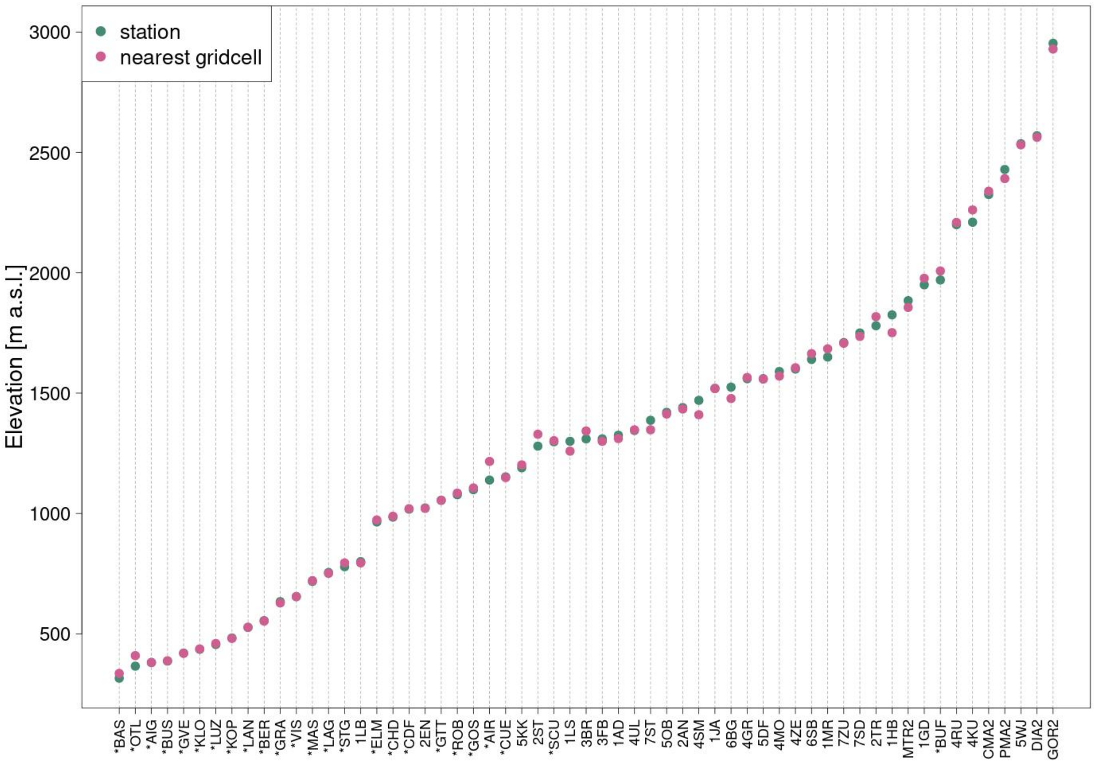

Figure 2.6: Comparison of the elevations at the stations (turquoise) and their corresponding nearest grid cell (pink). The station names according to the abbreviations are given in Appendix B.

The intercomparison of OSHD-CLQM and the remote sensing data sets is based on the number of snow days. AVHRR and MODIS provide fractional snow cover, which is given as the percentage of the grid cell or a certain reference area covered with snow. Snow coverage was obtained from the SWE values of OSHD-CLQM using a simple parameterization. The SWE value of 20 mm was defined as 100 % snow coverage and was then calculated linearly until 0 mm which corresponds to 0 % snow coverage (10 mm corresponds to 50 %). Since AVHRR provides fractional snow cover as 10-day composites, a moving average based on the preceded 10 days was applied on each hydrological year provided by MODIS and OSHD-CLQM, when a comparison with AVHRR was made. The first 9 days of each September were excluded then. Moreover, as AVHRR contains numerous spatially confined temporal gaps, a common mask was applied for all three products. A spatially and temporally more comprehensive comparison, based on daily values rather than 10-day composites and without applying the mask, was done between OSHD-CLQM and MODIS. According to subsection 2.3.1, the threshold value of 0.5 was used to define snow days based on the fractional snow cover given by AVHRR and MODIS and the parameterized snow coverage obtained from the SWE values.

Chapter 3

Results and Discussion

In the following chapter, the results are presented and discussed. First, an overview about the past and present snow variability according to OSHD-CLQM is given. Then, limitations and uncertainties of this data set are reviewed. After that, the validation of the data set against surface observations as well as remote sensing data is shown. Finally, the case study of the SNP is presented.

3.1 Spatio-temporal snow cover variability

3.1.1 Climatological overview

Figure 3.1a and 3.1b show the mean SWE (Sep - May) over the periods 1962 - 1990 and 1991 - 2020, respectively. Light colors represent smaller mean SWE and darker colors represent larger mean SWE values. The small gray pixels indicate missing grid cells due to the occurrence of water (lakes).

Owing to the high spatial resolution of OSHD-CLQM an adequate representation of the Swiss topography and geographic features is possible. While the mean SWE on the Swiss Plateau shows values mostly below 20 mm w.e., the values in the Alps are much larger (> 100 mm) over both periods. This demonstrates directly the high spatial variability of snow in Switzerland. Further, it is clearly recognizable that the mean SWE amounts in the two periods differ substantially from each other. A quantification of the spatial pattern of change can be made investigating the absolute (Figure 3.1c) and relative difference (Figure 3.1d) between the periods taking the previous period, 1962 - 1990, as reference. The largest relative reduction is visible in the lowlands with values around - 50 %. The absolute reduction in these regions is quite small with values mostly between - 1 and - 10 mm w.e. In contrast, in most areas at higher elevations, i.e. in the Jura and especially the Alps, where the absolute amount of SWE is large, the absolute change of SWE is larger too (around - 50 mm w.e.), whereas the relative change is rather small (around - 10 %). There are a few smaller areas that show a distinctive increase of the mean SWE. These areas are primarily located at high elevations in the Valais and Bernese mountains in areas with glacier occurrence. However, these regions might be impacted by larger uncertainties or even artifacts occurring during the creation of OSHD-CLQM. Therefore, those areas should not be over interpreted here nor in the further analysis. These limitations and uncertainties are discussed in more detail in section 3.2. Also the outstanding anomaly in the south-western region of Yverdon should be considered carefully as an artifact in the input data of the underlying snow model of OSHD-CLQM was found there (see subsection 3.2.1 for more details).

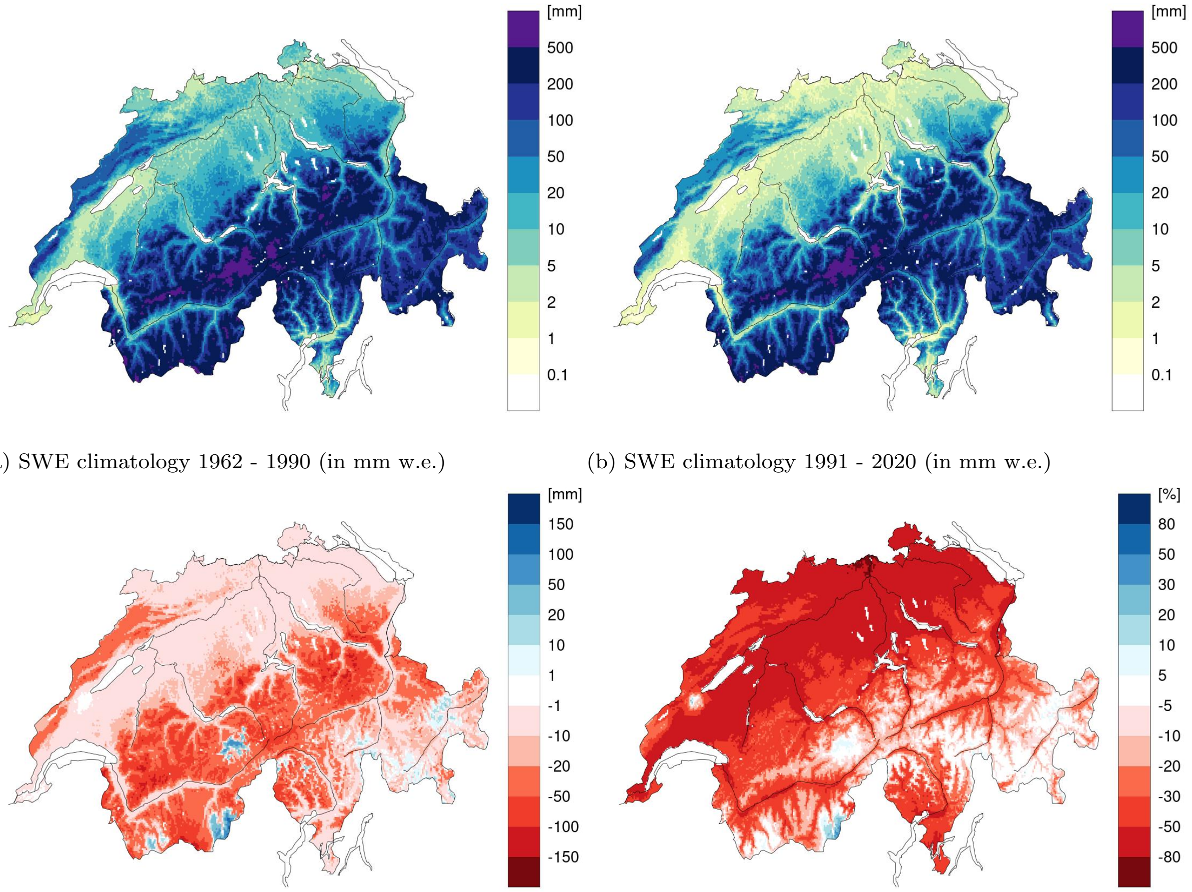

(a) SWE climatology 1962 - 1990 (in mm w.e.)

(b) SWE climatology 1991 - 2020 (in mm w.e.)

(c) Absolute difference (in mm w.e.)

(d) Relative difference (in %)

Figure 3.1: Comparison of the mean SWE (Sep - May) between the periods 1962 - 1990 and 1991 - 2020. The reference period for the differences is 1962 - 1990.

The large relative difference in the lowlands can be explained by the generally small absolute mean SWE values there and the fact that already small absolute changes can result in strong relative anomalies. This is exactly the opposite in areas at higher elevations with large absolute mean SWE values. Moreover, a temperature rise has a stronger effect at lower and medium elevations in comparison to higher elevations (Beniston, 2012). In high elevated areas ($>$ 2000 m a.s.l.), temperatures are usually markedly below the freezing point. Despite the warming trend over the last decades, the temperatures remained below the freezing point during most of the snow season (Beniston, 2012; Serquet et al., 2011). Beniston (2012) stated that the snow evolution at higher elevations is the result of changes in precipitation instead of temperature. An increase in precipitation may lead to an extent of the amount of snow there (Beniston, 2012). At lower elevations minimal warming can have a strong influence as temperatures may exceed the freezing point and thus, the form of precipitation changes from snow to rain (Beniston, 2012; Serquet et al., 2011). The critical elevation at which temperature has the greatest influence on snow accumulation may increase with ongoing future warming (Morán-Tejeda et al., 2013).

A similar analysis for the number of snow days (SWE $>$ 10 mm, see subsection 2.3.1) within the snow season is shown in Figure 3.2. The mean number of snow days over 1962 - 1990 and 1991 - 2020 reveal similar spatial patterns compared to the mean SWE over the same periods (Figure 3.1). Larger numbers of snow days are found at higher elevations, whereas fewer snow days occur in the lowlands. In some

high-elevated areas the number of snow days approaches the maximum of 273 / 274 possible snow days (number of days over the snow season). However, the fact that the SWE values in OSHD-CLQM are set to zero on September 01 every year (see subsection 2.2.1), has an effect on the number of snow days. Especially at high elevations, where a certain snow coverage could remain throughout the summer season, less snow days are counted as it has first to snow in September to be counted as a snow day again. Thus, reaching the maximum of 274 snow days is difficult if not impossible.
Figure 3.2c shows the absolute and Figure 3.2d the relative spatial pattern of change of the mean number of snow days between 1962 - 1990 and 1991 - 2020, using the period 1962 - 1990 as reference. In most parts of the country, a reduction of the mean number of snow days is found. In contrast to the SWE-analysis, the largest absolute reduction does not occur at medium or high elevations but rather at lower elevations. The largest absolute as well as relative decrease of the number of snow days is visible in the lowlands of the Swiss Plateau and Ticino (around - 30 days). This corresponds to a reduction of more than 50 % in some places. Also, the valleys of the Alps are affected by a rather large decline. Areas at higher elevations experienced a less pronounced change. In some high places no change at all or even a small increase is recognizable again.

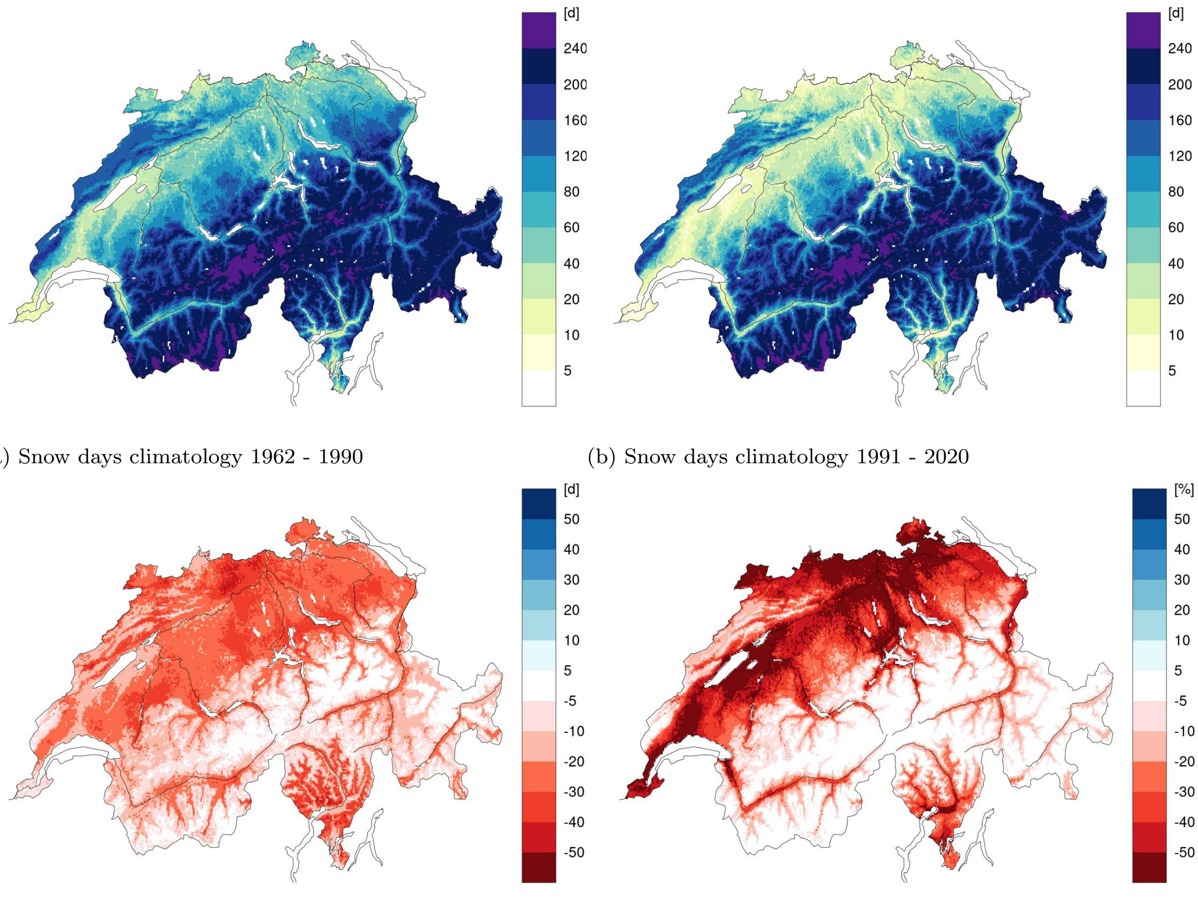

(a) Snow days climatology 1962 - 1990

(b) Snow days climatology 1991 - 2020

(c) Absolute difference (in days)

(d) Relative difference (in %)

Figure 3.2: Comparison of the number of snow days (SWE $>$ 10 mm) within the snow season between the periods 1962 - 1990 and 1991 - 2020. The reference period for the differences is 1962 - 1990.

Similar to the SWE analysis, the sensitivity of the number of snow days to changes in temperature or precipitation is larger at lower regions because the absolute snow amount is smaller there. The SWE

threshold for a day being counted as a snow day was set to 10 mm (see subsection 2.3.1). Even with a reduction of the absolute snow amount, areas with larger absolute snow amounts still have SWE values above the threshold on most days. They are most sensitive to reductions in the beginning and end of the snow period, when the SWE values are around the threshold. At lower elevations (i.e. in the Swiss Plateau or the lowlands of the Ticino), the SWE values are more often around the threshold and often there is no continuous snow season. Therefore, reductions in the number of snow days are realistic throughout the whole snow season.
These results basically agree with previous works, such as e.g. Klein et al. (2016). In an analysis of the Swiss Alps between 1970 and 2015, Klein et al. (2016) found a decrease in the number of days with snow on the ground at all elevations (between 1139 - 2540 m a.s.l.) and sub-regions considered (on average -8.9 days / decade).

More detailed temporal analyses of the mean SWE values during the snow season are presented in Figure 3.3, where seasonal climatologies and their differences are investigated. The same analysis on a monthly resolution is depicted in Appendix C. Investigations of the upper two rows, where the 1962 - 1990 and 1991 - 2020 climatologies are shown respectively, reveal that lower elevated regions in and around the Swiss Plateau reach their maximum in SWE during the winter season (DJF). Higher regions, especially in the Alps, reach their maximum later, namely during spring (MAM). Furthermore, it is shown that differences between the periods 1962 - 1990 and 1991 - 2020 occurred in all three seasons investigated. For the interpretation, especially of autumn (SON, left column), it is important to be aware of the fact that the SWE values were set to zero on September 01 (see subsection 2.2.1). Therefore, especially higher elevations show smaller SWE values than they actually have, because there is no snow from previous months present. Overall, there is a loss of mean SWE visible over most parts of the country during all three seasons. Again, it can be seen that the SWE values at lower elevations decrease relatively stronger than at higher elevations. The opposite is the case for absolute values, which decrease stronger at medium and high elevations where generally larger absolute mean SWE values are present. At the highest elevations, even a small increase of the mean SWE is visible once more (around + 20 mm). This increase is strongest and spatially most widespread during winter (DJF). The absolute change in the Swiss Plateau is smallest in autumn since there is almost no occurrence of snow and largest in winter when there is most absolute SWE present. In spring, the absolute change at low elevations is smaller again, since less absolute SWE is available. In the Alps and the Jura the absolute decrease of SWE is largest in spring, when most SWE is present and smallest in autumn, when least snow is available.

The finding of the largest absolute negative change from the period 1962 - 1990 to 1991 - 2020 during the spring months is supported by previous studies (e.g. Klein et al. (2016)). The most likely explanation for this is the stronger rise in temperature during spring (Rebetez et al., 2008). As shown by Rebetez et al. (2008) the temperature trends in the Swiss Alps are strongest in spring. Moreover, Klein et al. (2016) suggested that the trend of increasing sunshine duration (e.g. showed by Sanchez-Lorenzo et al. (2012); Philipona et al. (2023)) has a large impact in spring as the sun has a higher (daily averaged) elevation angle in these months compared to the preceding winter months. The changing albedo due to melting snow and the increase in energy availability resulted may additionally even amplify the temperature effect (Rebetez et al., 2008; Klein et al., 2016).

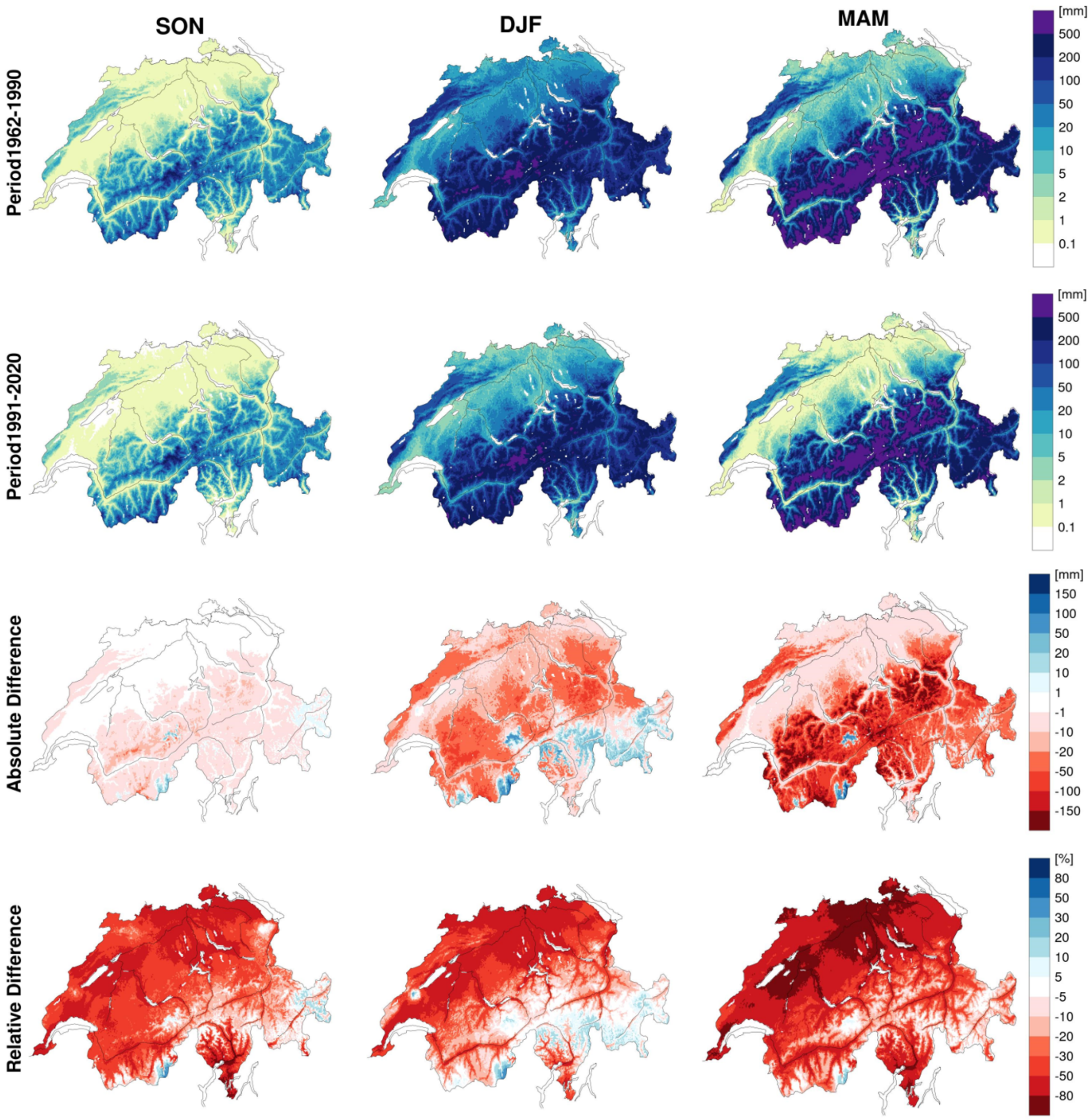

Figure 3.3: Analysis of the mean seasonal SWE. Left column: autumn (September, October and November), middle column: winter (December, January and February) and right column: spring (March, April and May). First resp. second row: SWE climatology over the period 1962 - 1990 resp. over 1991 - 2020 (mm w.e.), third resp. fourth row: absolute (mm w.e.) resp. relative (%) difference (Reference period: 1962 - 1990).

3.1.2 Inter-annual variability

After the spatial investigation of climatological periods, individual snow seasons are presented in the following. The spatial patterns of the absolute mean SWE of the snow seasons 1962 - 2022 are shown in Appendix D. Figure 3.4 shows the spatial absolute anomaly patterns for these snow seasons compared

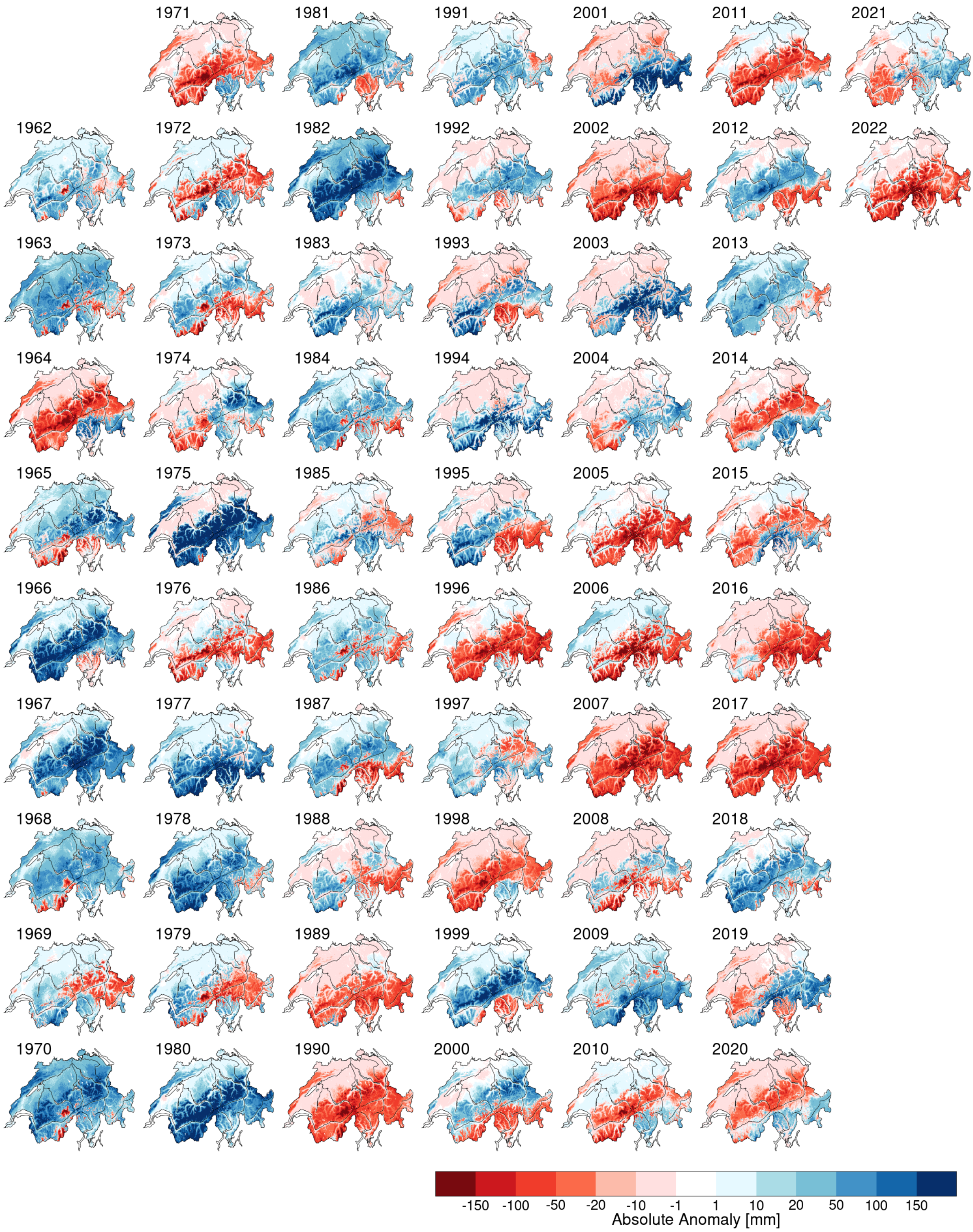

Figure 3.4: Absolute SWE anomaly for the snow seasons 1962 to 2022 (in mm w.e.). Reference period: 1991 - 2020.

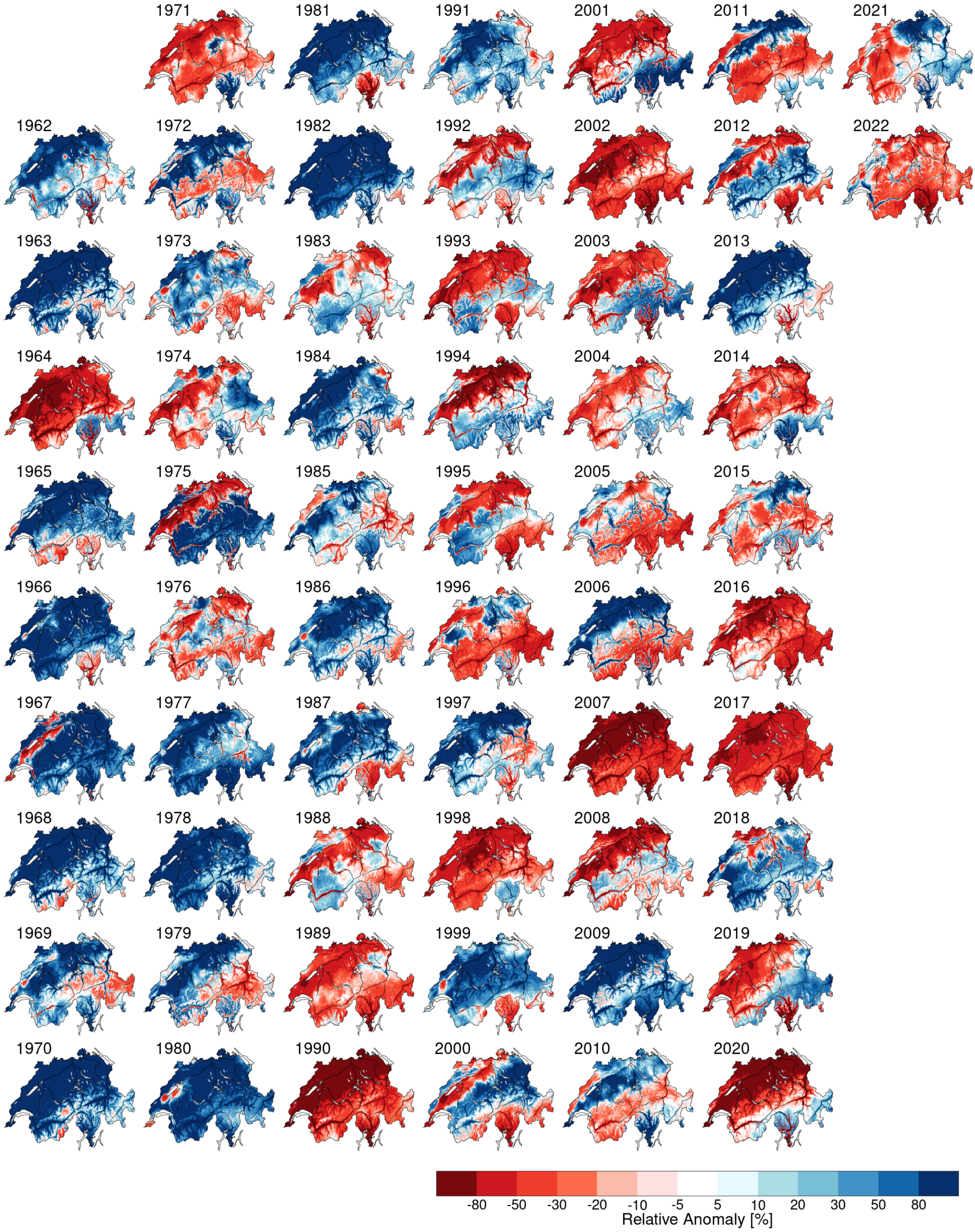

Figure 3.5: Relative SWE anomaly for the snow seasons 1962 to 2022 (in %). Reference period: 1991 - 2020.

to the reference 1991 - 2020. The same analysis but in relative terms is depicted in Figure 3.5.
At first glance, it may be noted that the year-to-year fluctuations as well as the spatial variations within the country and a snow season are large. Especially at lower elevations relative anomalies show strong positive or negative patterns. These patterns may be largely influenced by individual snow events. For

this reason the spatial anomaly patterns in the Swiss Plateau look quite patchy in some snow seasons (e.g. 1974, 1989 or 2021). For instance, the large relative positive anomaly in northern Switzerland in 2021's snow season was probably made up to a large extent by the extreme event occurred in January 2021 as documented in MeteoSwiss (2021d).

Some snow seasons show quite similar anomaly patterns. For example, the snow seasons 1964, 1971, 1998, 2001, 2003, 2004, 2013, 2014 and 2020 all have relatively little mean SWE values in northern Switzerland and above average amounts in the south compared to 1991 - 2020. The opposite is the case for the snow seasons 1965, 1966, 1981, 1987, 1999 and 2000. A rather east-west contrast is found for the snow seasons of 1974, 2019 and 2021, where eastern Switzerland has relatively higher and western Switzerland shows relatively lower mean SWE amounts compared to the reference. Moreover, there are snow seasons with positive anomalies spatially located over the Alps (i.e. 1992, 1993, 1994, 1995, 2000, 2003, 2008 and 2012) and negative anomalies over the rest of the country. The opposite is the case for 1969, 1972, 1979, 1996, 2010, and 2011. However, there are snow seasons in which almost the whole country shows the same sign in the anomaly pattern. For instance, over the snow seasons 1968, 1970, 1977, 1978, 1980, 1982, and 2009 the mean SWE values are higher than the 1991 - 2020 average over entire Switzerland. The opposite can be observed for the snow seasons 1990, 2002, 2007 and 2017, in which almost the whole country shows negative anomalies. Nevertheless, also anomaly patterns which cannot be grouped with others exist (e.g. 1967, 1996, 2018).

3.1.3 Annual Cycle

Figure 3.6 presents the annual cycle of SWE for Switzerland as a whole, as well as for the selected sub-regions. The annual cycle was obtained calculating monthly averages over the respective sub-region and climatological period. The green line corresponds to the period 1962 - 1990, whereas the purple line represents 1991 - 2020. The calculation was done for the entire hydrological year. However, the summer months (June, July and August), which are indicated by the gray shading, contain larger uncertainties and should be interpreted with caution (see subsection 2.2.1).

In September, the annual cycle of the hydrological year starts. Since the SWE values in OSHD-CLQM are set to zero on September 01, the monthly average is close to zero in all the specified sub-regions. Thereafter, the monthly SWE averages start to increase in all sub-regions up to a maximum in winter or spring, after which they decrease again. The annual cycle of the two climatological periods differs in all sub-regions, depending on the elevation distribution in the respective sub-region (see Figure 2.2 for elevation distribution). The annual cycle of Switzerland as a whole has its maximum in April (at 219 mm) during the period 1962 - 1990. Towards the period 1991 - 2020, a decrease of the maximum (- 40 mm) and a shift to March occur. Moreover, the monthly SWE average of each month decreased, with the strongest reduction during the spring months (monthly average of - 45 mm over MAM).
The annual cycle of Northern Switzerland is comparable to the one of Switzerland as a whole, as it contains the same grid cells to a large extent. In contrast, the annual cycle of Southern Switzerland differs more, which can be explained by the distribution of the grid cells over the elevation classes. Southern Switzerland contains more higher elevated grid cells. This effect is even more visible in the sub-regions. On one hand, lower sub-regions such as the Jura or the Swiss Plateau have a shorter snow period and their monthly SWE maximum occurs in February. Here, the monthly reduction of the mean SWE from the period 1962 - 1990 to the period 1991 - 2020 is clearly visible from November / December onward until April / May. This reduction seems to be more symmetric, which means that the reduction in autumn, winter and spring is similar. Thus, the snow period there underwent a shortening from both sides as the remaining months have very little SWE values and therefore do not represent a change. On the other hand, high-elevated sub-regions such as the Valais, Northern and central Grisons and the Engadin have a longer snow period with the maximum occurring in April. In contrast to the comparatively symmetric reduction of the monthly averaged SWE values from the period 1962 - 1990 to the period 1991 - 2020 in the lower sub-regions, the higher sub-regions show the strongest reduction clearly in spring (MAM). From September to January / February there is no reduction recognizable. Rather the opposite is the case for January and February in the Engadin. However, also here it has to be mentioned that very high grid cells (> 3000 m a.s.l.) might be prone to larger uncertainties and errors and thus, these sub-regions have to be interpreted with caution (see section 3.2). The remaining sub-regions at medium elevations (i.e. North-Western Alpine Slope, North-Central Alpine Slope, North-Eastern Alpine Slope and Ticino) show their monthly maximum in April (except the sub-region North-Eastern Alpine Slope in March) during the period 1962 - 1990. Towards the period 1991 - 2020 the maximum is reduced and shifted to March for all these sub-regions.

In a study of Klein et al. (2016), in which the snow depth at stations at elevations from 1139 to 2540 m a.s.l between 1970 and 2015 was analyzed, it was found that the snow cover duration has significantly shortened at all study locations. Likewise the findings of Figure 3.6, the shortening occurred more strongly in spring, while the later snow onset was not significant in every sub-region. They found an average shift to later snow onset of 12 days and an earlier end of the snow cover duration of 26 days compared to 1970

(Klein et al., 2016). Even though daily values were not analyzed in this study, the signal is comparable. The annual cycle showed a shift to earlier snow melt in spring in all considered sub-regions and a shift to later snow onset in some, especially the low-elevated sub-regions.

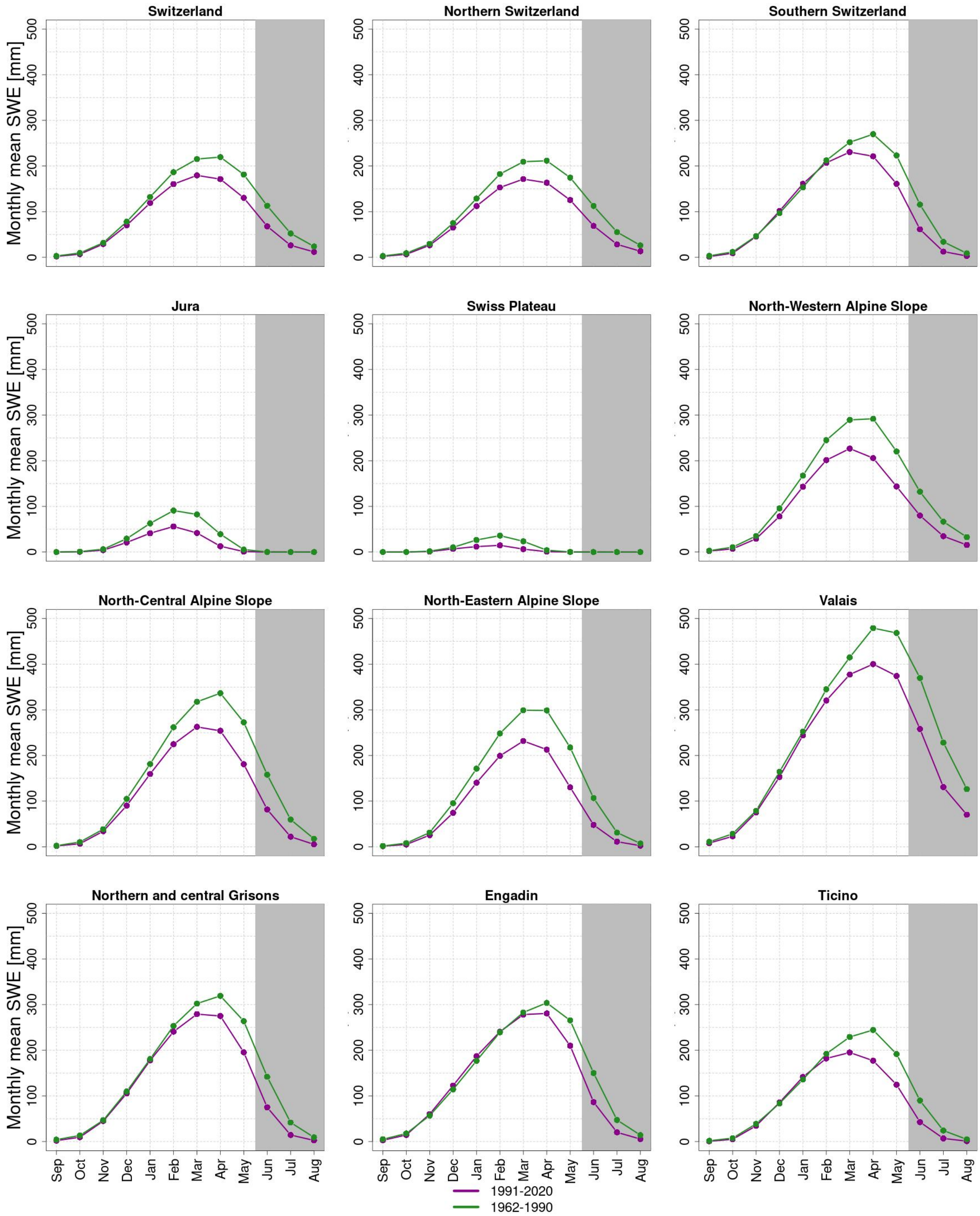

Figure 3.6: Comparison of the annual cycle (based on monthly SWE averages) over the period 1962 - 1990 (green) and the period 1991 - 2020 (purple) in the different sub-regions. The gray shading indicates the summer months, which should be considered with caution as they contain larger uncertainties (subsection 2.2.1).

3.1.4 Time series

The time series of the snow indicators are investigated in the following. Figure 3.7 shows the time series for the mean SWE (Sep - May) between 1962 and 2022. The dashed horizontal lines represent the averages over the climatological periods 1962 - 1990 (green) and 1991 - 2020 (purple). Please note that the scale of the y-axis is different for each sub-region.
The two climatological averages show a reduction from the period 1962 - 1990 to 1991 - 2020 in every selected sub-region. This reduction is relatively higher in lower sub-regions such as the Jura and the Swiss Plateau. In these two sub-regions the highest mean SWE amounts are found for the snow season

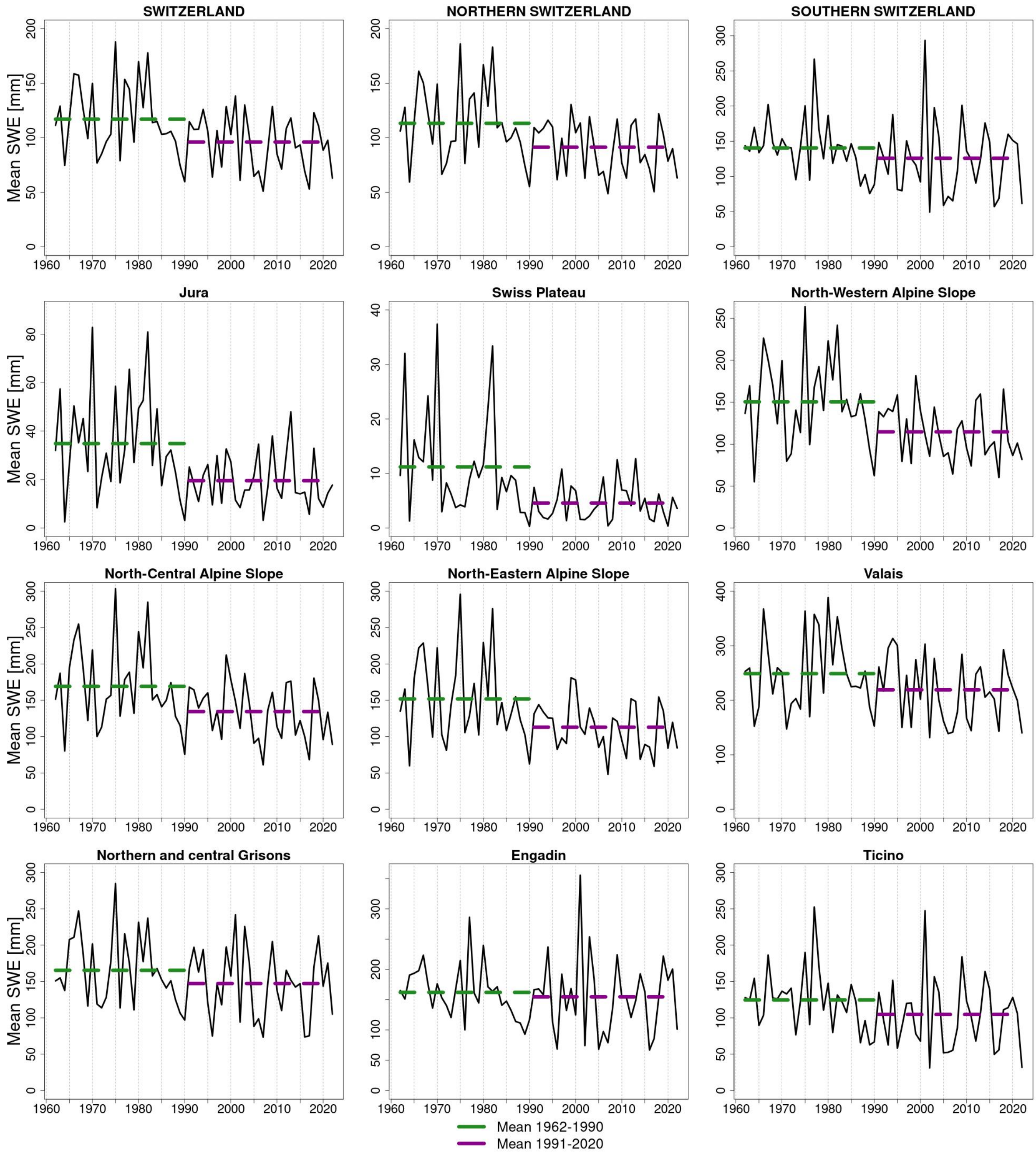

Figure 3.7: Time series of the mean SWE (Sep - May) for every sub-region. Green: climatological mean over the period 1962-1990. Purple: climatological mean over the period 1991 - 2020.

1970 (at 83 mm in the Jura and 37 mm in the Swiss Plateau). Generally, it stands out that most of the rather high mean SWE values are present in the 1960s to 1980s. Later on, the snow seasons never reach such high mean SWE values again. The maximum in the latter period corresponds to 48 mm in the Jura and to 13 mm in the Swiss Plateau for the snow season 2013, respectively. The same statement can be made for most of the other sub-regions. However, the change there is not that extreme. And in Southern Switzerland, particularly in the Engadin, the all-time maximum occurs in the snow season 2001 (at 355 mm) and thus, in the latter period.

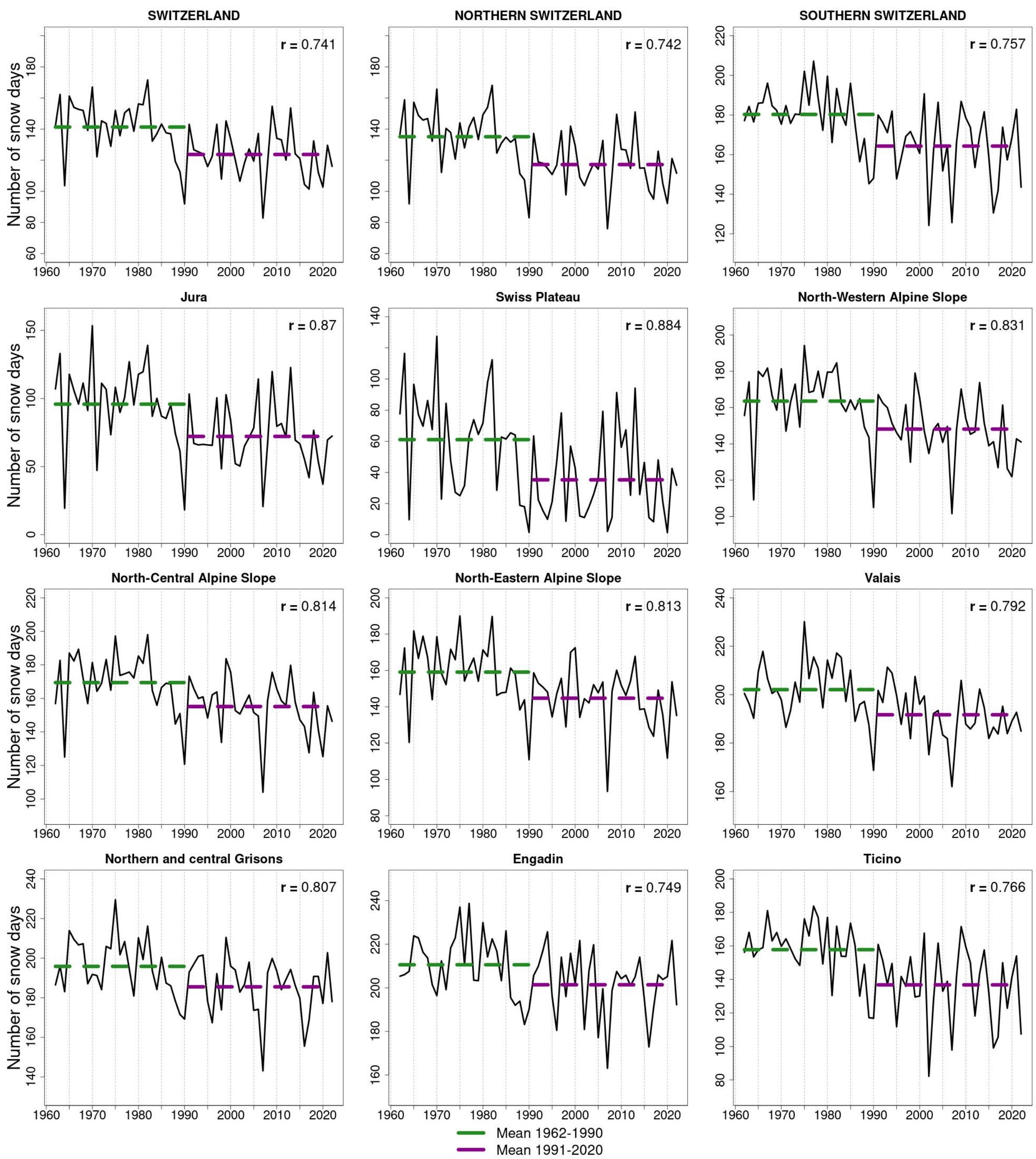

Figure 3.8: Time series of the number of snow days within a snow season for every sub-region. Green: climatological mean over the period 1962 - 1990. Purple: climatological mean over the period 1991 - 2020. r: Pearson correlation between the illustrated snow days time series and the mean SWE time series shown in Figure 3.7).

The same analysis for the number of snow days within the snow season is presented in Figure 3.8. The time series contain additionally the correlation coefficient (r) between them and the mean SWE time series (Figure 3.7) in the upper right corners. All in all, it can be stated that the main results of this snow indicator are comparable to the mean SWE time series. The climatological averages over the period 1962 - 1990 are higher over Switzerland including every sub-region than the averages over the 30-year period 1991 - 2020. Again, sub-regions dominated by grid cells lying in the lower elevation classes show a stronger relative reduction than sub-regions at higher elevations (see further discussion in subsection 3.1.5). The maximum of the 62-year long period occurs in the earlier period whereas most of the seasons with fewer than average snow days lie in the second period in every sub-region.
The correlation coefficient between the mean SWE and the snow days time series is largest in the Swiss Plateau (r = 0.884), followed by the Jura (r = 0.87). The smallest correlation coefficient is found over Switzerland as a whole (r = 0.741) and in the Engadin for the sub-regions (r = 0.749). Thus, all in all the two time series correlate strongly, whereas sub-regions dominated by grid cells at lower elevations generally have higher correlation coefficients. As specified in subsection 2.3.1, a snow day is defined as a day with at least 10 mm SWE. Lower elevations are more sensitive to this threshold value since the absolute SWE amount is rather small. Higher elevations have higher SWE amounts on most days with snow being present and are less sensitive to this threshold, since seasons with lower SWE values still exceed the threshold on most days.

3.1.5 Sub-regional and elevation dependent analyses

For a more detailed elevation-dependent overview on Switzerland's snow cover, Figure 3.9 presents the mean SWE (Sep - May) in 100 m elevation bins. The same analysis for the mean number of snow days within the snow season is shown in Figure 3.10. Again, the averages over the two climatological periods 1962 - 1990 (green) and 1991 - 2020 (purple) are compared. The gray shading above 3000 m a.s.l. indicates the elevations at which larger uncertainties must be expected (see section 3.2).
In general, the mean SWE values increase with ascending elevation to a maximum (of 540 mm over 1991 - 2020) at about 3500 m a.s.l. Then the values decrease again. Up to around 3000 m a.s.l., the mean SWE values over the period 1991 - 2020 are lower than over the period 1962 - 1990. For the elevations above, no clear statement can be made regarding a change between the periods. The largest absolute change between the two climatological periods is located in intermediate elevation classes. More exactly, the

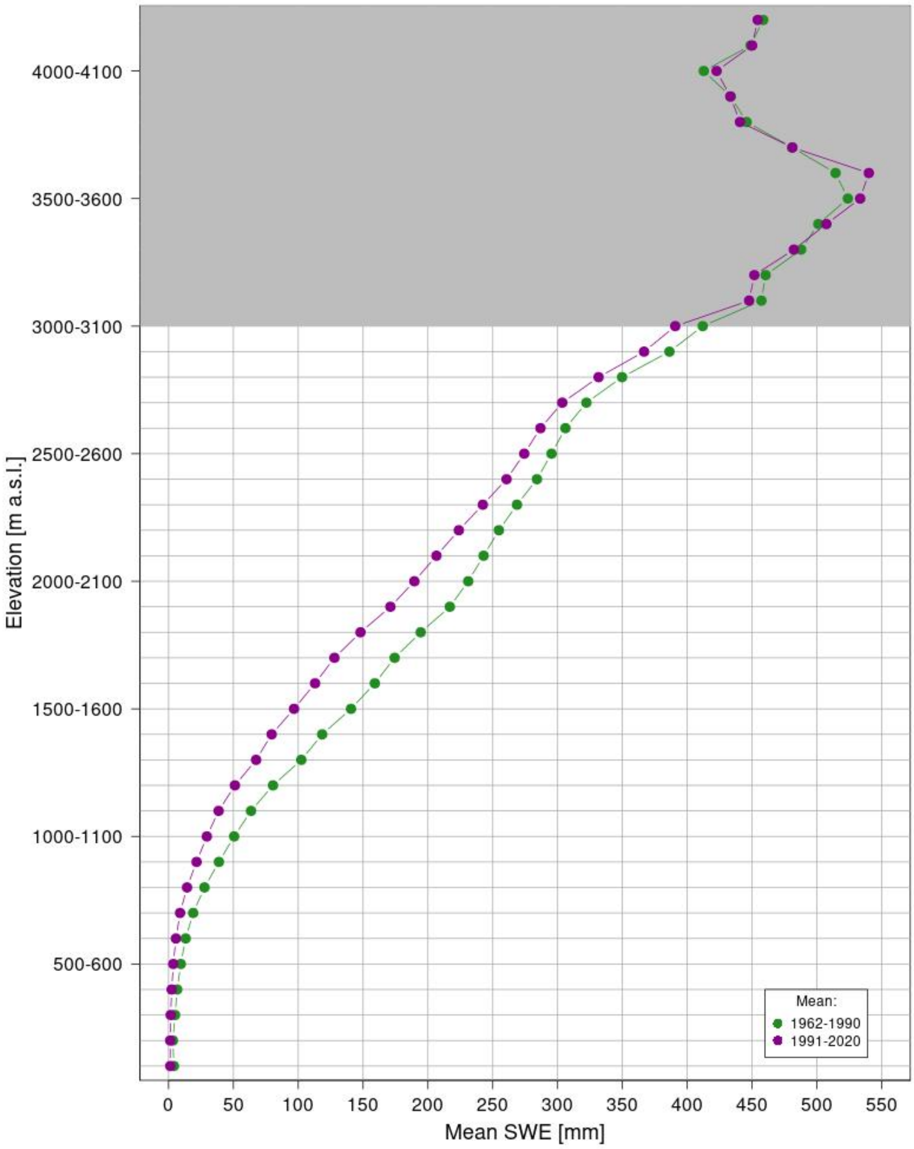

Figure 3.9: Elevation dependent analysis (100 m elevation bins) of the mean SWE (Sep - May) over Switzerland. Green: climatological mean over the period 1962 - 1990. Purple: climatological mean for the period 1991 - 2020.

elevation between 1700 and 1800 m a.s.l. experienced the largest decline with - 46 mm w.e. Nevertheless, also the lower three and the upper two elevation classes underwent a change exceeding - 40 mm w.e.

The mean number of snow days within a snow season over Switzerland increases steadily with elevation (Figure 3.10). At the highest elevations, the number of snow days is close to the possible maximum number at 273 / 274 days (number of days between September and May). Since the SWE values in OSHD-CLQM are set to zero on September 01 (see subsection 2.2.1), there might be missing snow days in these higher parts as snow from the previous summer would usually still be present. In contrast to the change of the mean SWE from the period 1962 - 1990 to the period 1991 - 2020, the absolute change here is largest at low elevations. The largest absolute change with - 29 days occurs between 700 and 800 m a.s.l. Also medium elevations show a distinct reduction. For example, the elevation between 1400 and 1500 m a.s.l. reveals a reduction of 17 days.

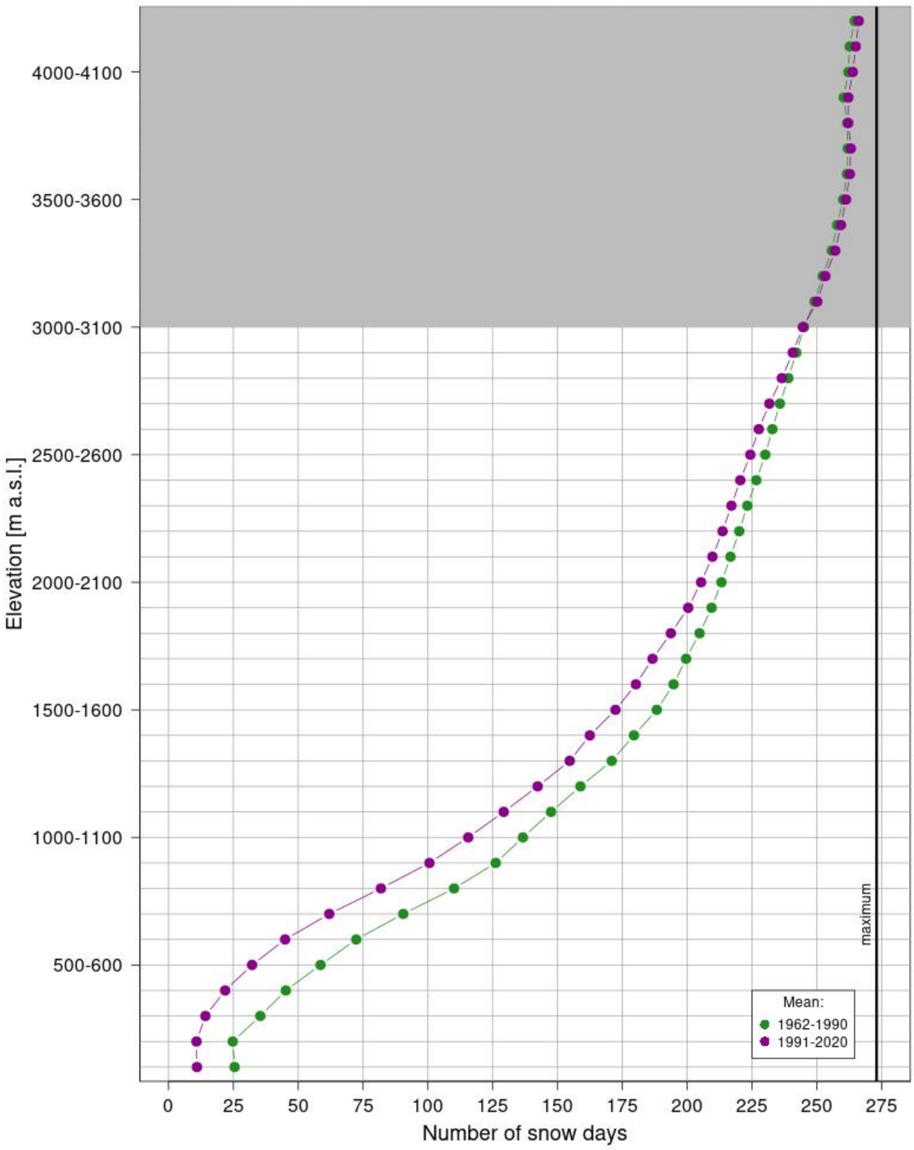

Figure 3.10: Elevation dependent analysis (100 m elevation bins) of the mean number of snow days within the snow season over Switzerland. Green: climatological mean for the period 1962-1990. Purple: climatological mean for the period 1991-2020.

The elevation dependence of the mean SWE can be compared to Grünewald et al. (2014). They analyzed remote sensing data in elevation steps of 100 m as well, but on a larger spatial resolution and looking at snow depth. The analysis showed overall similar results. Grünewald et al. (2014) showed that the snow depth increases with elevation up to a specific elevation and then decreases again at very high elevations. They explain this feature through interactions between the snow cover and the topography including preferential deposition of precipitation and redistribution through e.g. wind or avalanches. Even though, an exact comparison of the results is not possible due to the different resolutions and sub-regions looked at, the overall characteristics in Figure 3.9 are comparable. However, the described decrease at the highest elevations is not as clearly visible in Figure 3.9 as in the results of Grünewald et al. (2014). This might be caused due to the larger uncertainties of OSHD-CLQM at these elevations (see subsection 3.2.2).

A different perspective on the elevation-dependent and sub-regional distribution of snow is provided by Figure 3.11 and Figure 3.12. Those figures present boxplots for every selected elevation class in all sub-regions. The green boxes represent the period 1962 - 1990 whereas the purple boxes depict the period 1991 - 2020. A single boxplot in Figure 3.11 contains the 29 (green; 1962 - 1990) or 30 (purple; 1991 - 2020) average values of SWE over the snow seasons within the respective period. n denotes the number of grid cells in the specific elevation class of the selected sub-region (according to Appendix A). In the elevation class < 500 m a.s.l. the Engadin does not have any grid cells. The Swiss Plateau has no grid cells in the elevation class 1500 - 2000 m a.s.l. and the higher ones; the Jura has no grid cells in the uppermost two elevation classes. Thus, those fields are empty.
Comparable to Figure 3.9 the lowest mean SWE values are located in the lowest elevation class. With ascending elevation the mean SWE values generally increase. The medians over the period 1962 - 1990 have a higher values than the medians over the period 1991 - 2020 including all sub-regions for all elevation classes up to 2000 - 2500 m a.s.l. This statement does not hold for the elevation class > 2500 m a.s.l., where the medians are larger in the second period for most of the sub-regions (i.e. Switzerland, Northern Switzerland, North-Central Alpine Slope, Valais and Northern and central Grisons). However, the results at this upper elevations have to be interpreted with caution due to their larger uncertainties (see section 3.2).
In the lower four elevation classes the upper outliers occur almost solely in the first period. Further, the upper whiskers of the period 1962 - 1990 are larger than those of the period 1991 - 2020 in every sub-region in these lower elevation classes. In the fifth elevation class (2000 - 2500 m a.s.l.), the upper whisker is only higher in Ticino in the latter period, whereas in the sixth elevation class (> 2500 m a.s.l.) the upper whiskers are higher in the latter period over Switzerland as a whole, Southern Switzerland, Northern and central Grisons, Valais and Ticino. In contrast, the lower whiskers in the uppermost two elevation classes are smaller in the second period compared to the first period in every sub-region. The description of the whiskers in the lower elevation classes is more difficult, as the lower whiskers are generally smaller and so are the differences.
The analysis of the quartiles reveals that the upper ones are larger during the first period in all the sub-regions up to the fourth elevation class (1500 - 2000 m a.s.l.). In the fifth elevation class (2000 - 2500 m a.s.l.) and the sixth elevation class (> 2500 m a.s.l.) the upper quartile is larger in the latter period over Southern Switzerland including its sub-regions (Engadin and Ticino). This is also the case for the Valais in the sixth elevation class (> 2500 m a.s.l.). The lower quartiles are smaller in all sub-regions and elevation classes during the second period compared to the first with the exception of the fourth elevation class in the Jura. However, as the Jura in the fourth elevation class consists of only 17 grid cells, this result is probably not very robust.

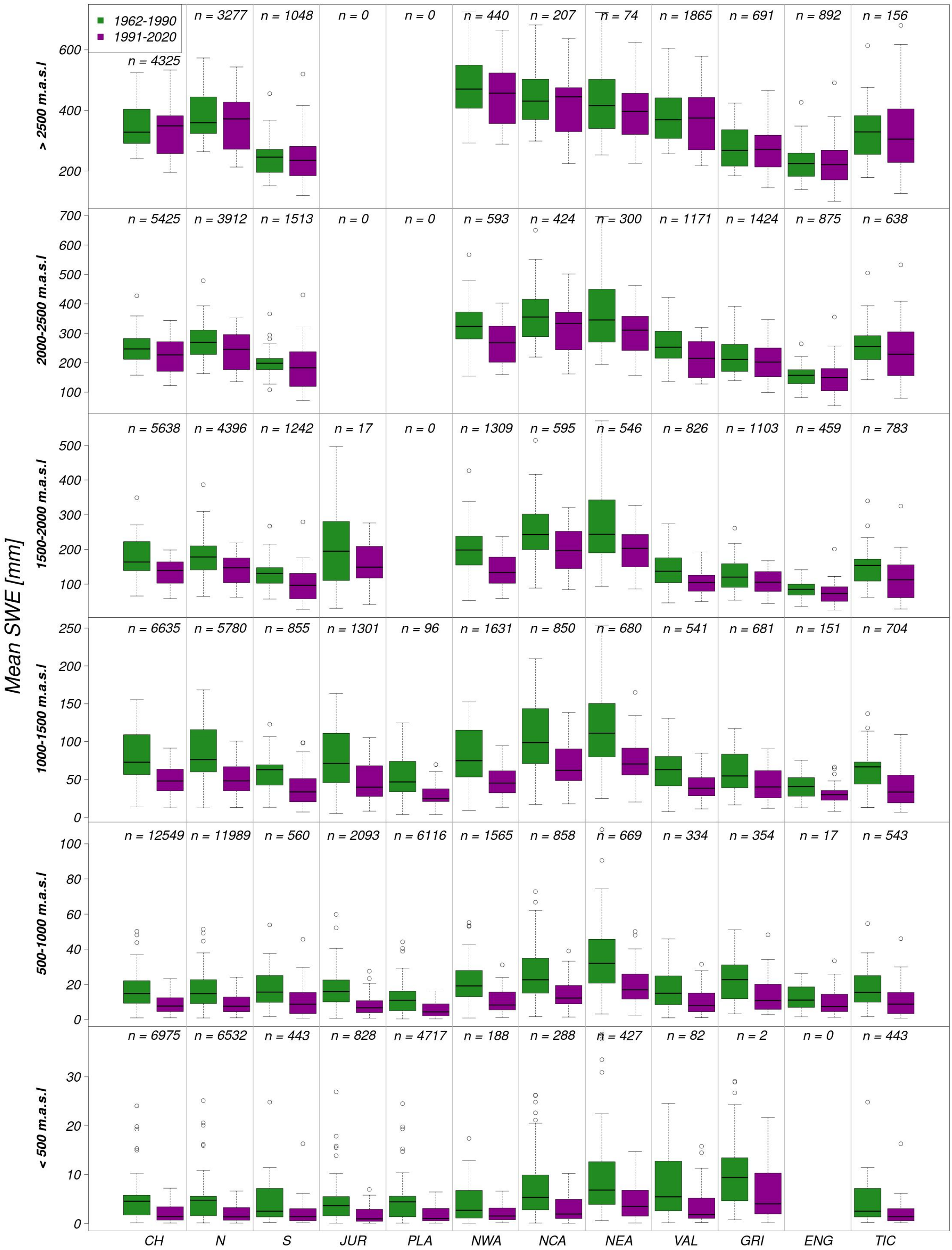

Figure 3.11: Overview of the distribution of the mean SWE (Sep - May) in the different elevation classes of each selected sub-region. Green: period 1962 - 1990. Purple: period 1991 - 2020. Each boxplot consist of the 29 resp. 30 mean SWE values within the respective period. n: number of grid cells in the specific elevation class of the sub-region. The boxplots show the median, the 25th / 75th percentiles (interquartile range, IQR) and the 1.5×IQR (whiskers).

The variance decreases in the lower elevation classes from the previous to the latter period. This can be seen in the reduction of the range from the upper to the lower whiskers and the reduction of the interquartile range in many of the sub-regions. However, this is not the case for the upper elevation classes.
Overall, Figure 3.11 suggests a decrease of snow seasons with very high mean SWE values from the first to the second period. Low snow seasons on the other hand occur more frequently in the latter period. The entire distribution from the mean SWE values seem to move to lower values. However, this is not the case for all sub-regions in all elevation classes. Especially in the uppermost elevation the signal is small or even reversed in some cases (note the larger uncertainties there - section 3.2).

In Figure 3.12 a single boxplot contains the 29 (green; 1962 - 1990) respectively 30 (purple; 1991 - 2020) averages of the number of snow days within the snow season over the respective period. All in all, the results of Figure 3.12 are very comparable to the results of the mean SWE distribution shown in Figure 3.11. The analysis of the medians in each sub-region and elevation class reveals a reduction of them from the previous to the latter period in almost every case. The reductions are larger in the lowermost elevation classes and smaller in the upper elevation classes. Looking at the quartiles shows that the upper ones lie at higher numbers in the period of 1962 - 1990 compared to the period 1991 - 2020 at all sub-regions and elevation classes. Further, the lower quartiles are reduced from the previous to the latter period in the lower four elevation classes. In the two uppermost elevation classes there are some exceptions in which the lower quartile shows an increase in numerous sub-regions (North-Western Alpine Slope, North-Central Alpine Slope and North-Eastern Alpine Slope). The upper and lower whiskers show a reduction of number of snow days in most sub-regions and elevation classes.
To conclude, this shows that the distribution of the mean number of snow days within a snow season, is shifted to lower numbers from the first to the second period. However, the signal is not equally clear in all elevation classes and sub-regions. Especially in the uppermost elevation classes the shift is not very pronounced or visible at all (again, note the uncertainties - section 3.2).

To summarize the comparison between the two climatological periods 1962 - 1990 and 1991 - 2020, Figure 3.13, 3.14, 3.15 and 3.16 present a summary of the main findings. Figure 3.13 depicts the absolute (blue) and relative (orange) change of the mean SWE from the previous to the latter period for the different sub-regions. It is shown that the highest relative decrease occurred in the Swiss Plateau with a change of - 59 % followed by the Jura (- 44 %). The smallest relative change is found in the Engadin (- 5 %). For the absolute change, the result is different. The highest absolute decrease occurs in the North-Eastern Alpine Slope (- 39 mm w.e.), followed by the North-Western Alpine Slope (- 36 mm w.e.) and the North-Central Alpine Slope (- 35 mm w.e.). The smallest absolute change is found in the Swiss Plateau (- 7 mm w.e.). A comparison of these results and the elevation distribution of the grid cells within the sub-regions (Figure 2.2) reveals that the sub-regions where a large relative change is found are dominated by grid cells in the lowermost elevation classes. The sub-regions where the absolute decrease decline is largest, grid cells dominate at medium elevations. These findings match with the results presented in Figure 3.14, which shows the same analysis for the mean SWE in the two periods for the elevation classes. As expected from the sub-regional analysis, the largest relative reduction occurs in the lowest elevation class ($<$ 500 m a.s.l.) corresponding to - 64 %. The extent of the decline decreases with ascending elevation, but can still be seen in the highest elevation class (- 5 %). The evaluation for the absolute decrease of the mean seasonal SWE from the previous to the latter period shows the largest value in the fourth elevation class (1500 - 2000 m a.s.l.) with - 46 mm w.e.

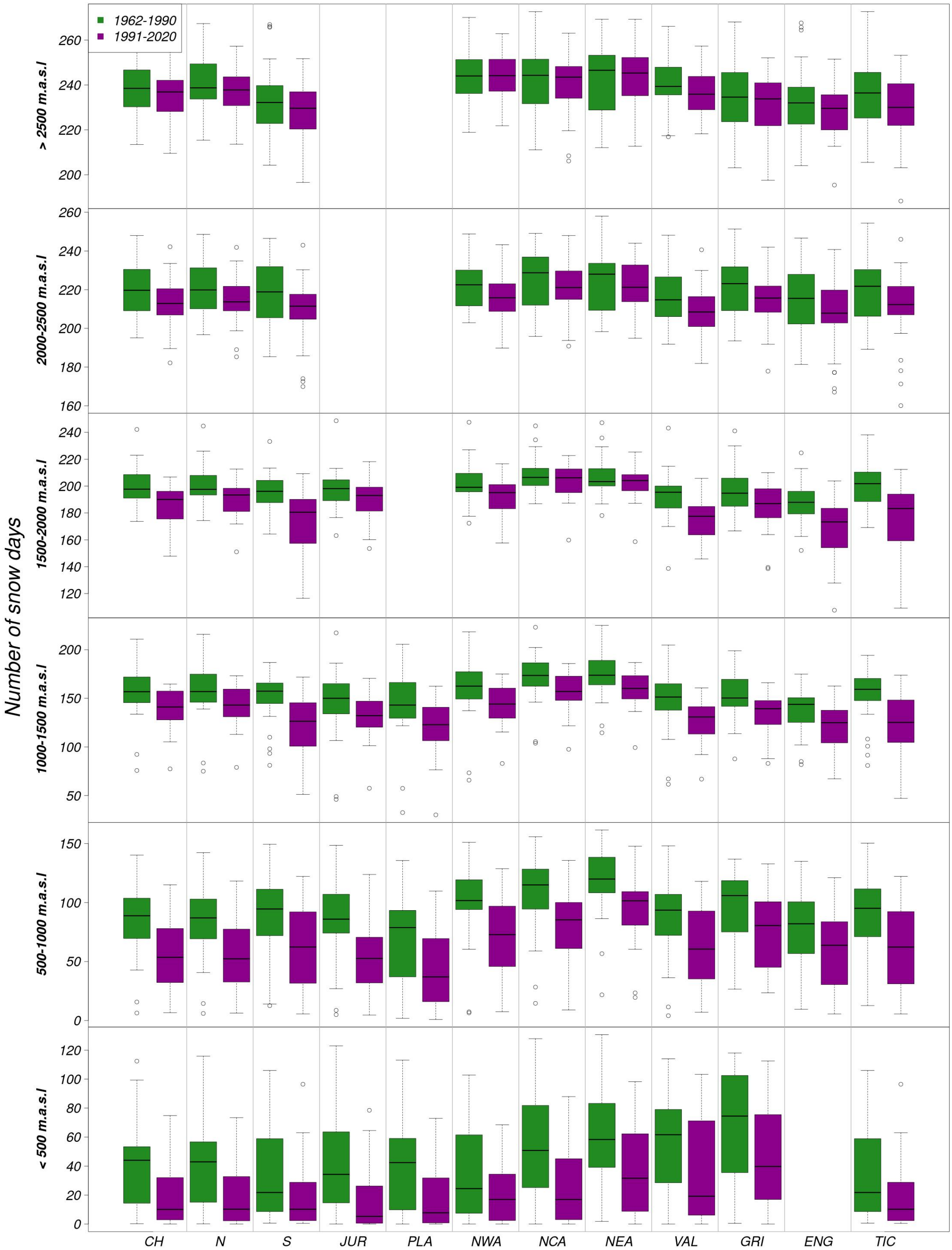

Figure 3.12: Overview of the distribution of the number of snow days within a snow season in the different elevation classes of each selected sub-region. Green: period 1962 - 1990. Purple: 1991 - 2020. Each boxplot consist of the 29 respectively 30 numbers of snow days within the snow seasons within the respective period. n represents the number of grid cells in the specific elevation class of the sub-region. The boxplots show the median, the 25th / 75th percentiles (interquartile range, IQR) and the 1.5×IQR (whiskers).

The analysis for the reduction of the mean number of snow days within a snow season from the period 1962 - 1990 to the period 1991 - 2020 delivers very similar regional results (Figure 3.15). As in the analysis of the mean SWE (Figure 3.13), the Swiss Plateau recorded the largest relative decline in the number of snow days (- 42 %) and the Engadin the smallest relative reduction (- 4 %). In contrast to the analysis of the mean SWE, where the absolute reduction was largest in sub-regions dominated by medium elevations, the absolute change of the number of snow days is largest in the Swiss Plateau and the Jura and therefore in lower sub-regions. This corresponds to the findings in Figure 3.16 where the elevation dependent reduction of the mean number of snow days is shown. The lowermost two elevation classes are not only the elevations where the largest relative change occurs but also the elevations where the largest absolute change is visible. In elevation class one (< 500 m a.s.l.) the relative reduction is - 53 % and the absolute reduction corresponds to - 23 days. One elevation class higher (500 - 1000 m a.s.l.), the relative change is - 32 %, whereas the absolute change reaches its maximum and corresponds to - 32 days. After that, the relative as well as the absolute reduction decline with elevation. In the highest elevation class, a small relative (- 1.4 %) and absolute (- 3 days) reduction are still visible.

Overall, the previous results can be summarized as follows. All sub-regions and elevation classes investigated show a decline in the mean SWE and the mean number of snow days within a snow season from the period 1962 - 1990 to the period 1991 - 2020. The relative reduction of both snow indicators as well as the absolute reduction of the number of snow days is most pronounced in lowlands. In contrast, the absolute decrease of the mean SWE is strongest in the fourth elevation class (1500 - 2000 m a.s.l.). Previous studies have found comparable elevation-dependent results (e.g. Marty (2008); Serquet et al. (2011); Beniston (2012)). Marty (2008) explained that winter mean temperature usually is close to the melting point at elevations below 1800 m a.s.l and thus, the sensitivity of snow to temperature increases is more pronounced there. Minimal warming can change the form of precipitation from snow to rain and therefore have a strong influence (Serquet et al., 2011; Beniston, 2012). At higher elevations, the warming had less of an impact because temperatures remained below the freezing point despite the warming, and thus the changes can be attributed more to modifications in precipitation (Beniston, 2012). However, this interpretation here has to be done with caution as OSHD-CLQM is subject to greater uncertainties and limitations at these elevations (see subsection 2.2.1 and subsection 3.2.2).

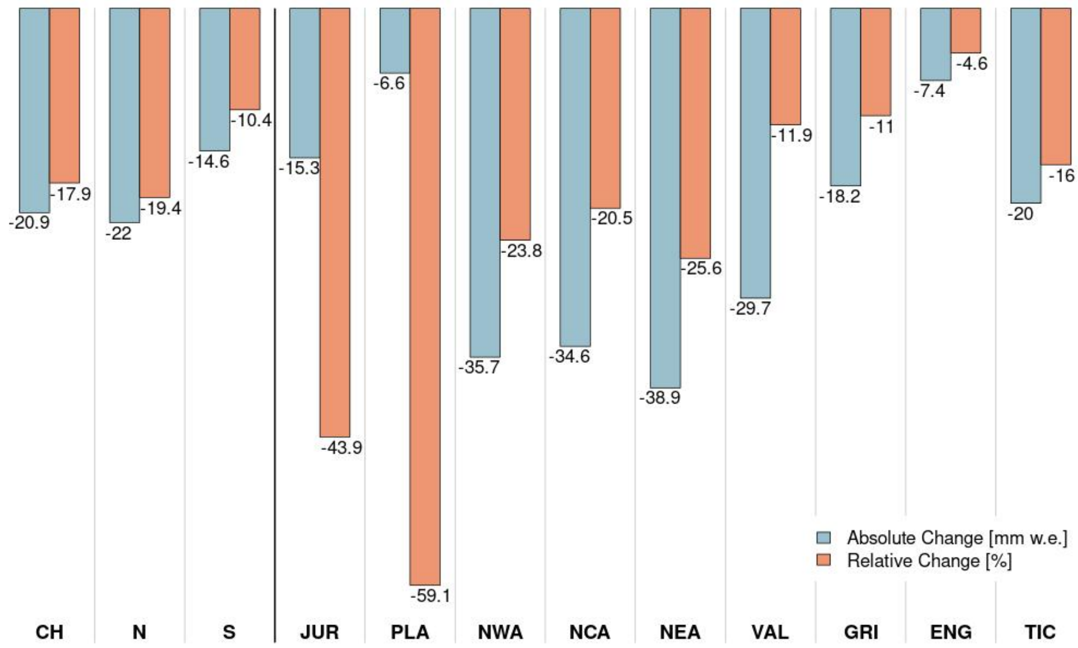

Figure 3.13: Absolute (blue) and relative (orange) change of the mean SWE (Sep - May) from the period 1962 - 1990 to the period 1991 - 2020 in each selected sub-region.

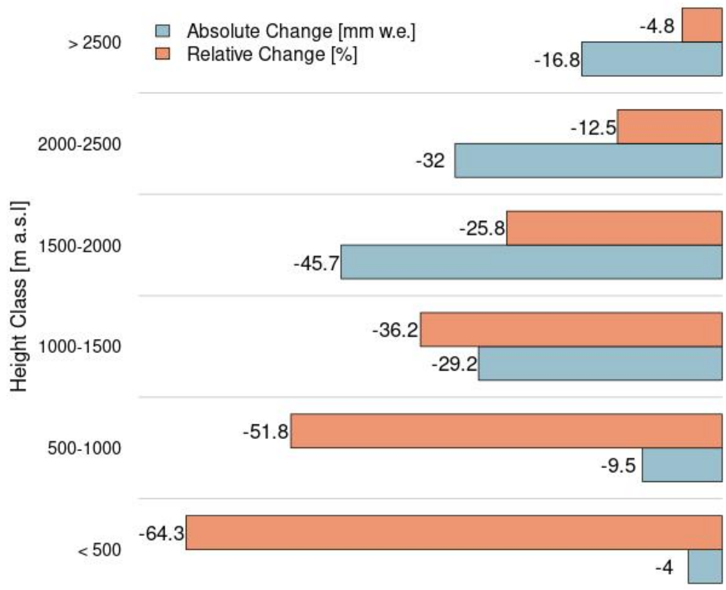

Figure 3.14: Absolute (blue) and relative (orange) change of the mean SWE (Sep - May) from the period 1962 - 1990 to the period 1991 - 2020 for each selected elevation class over entire Switzerland.

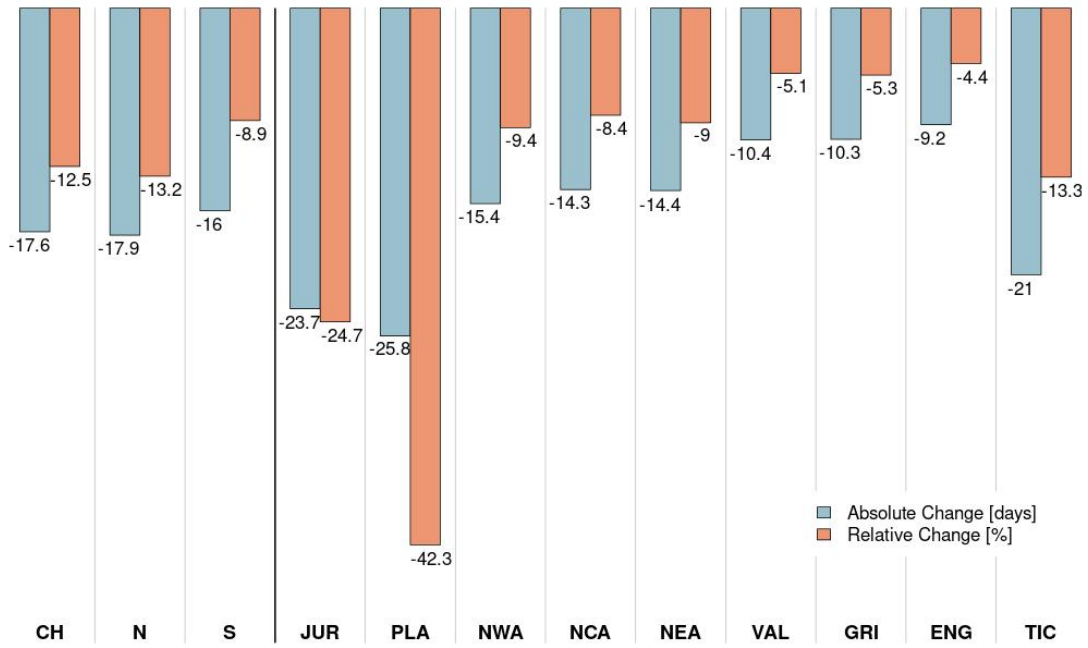

Figure 3.15: Absolute (blue) and relative (orange) change of the mean number of snow days within a snow season from the period 1962 - 1990 to the period 1991 - 2020 in each selected sub-region.

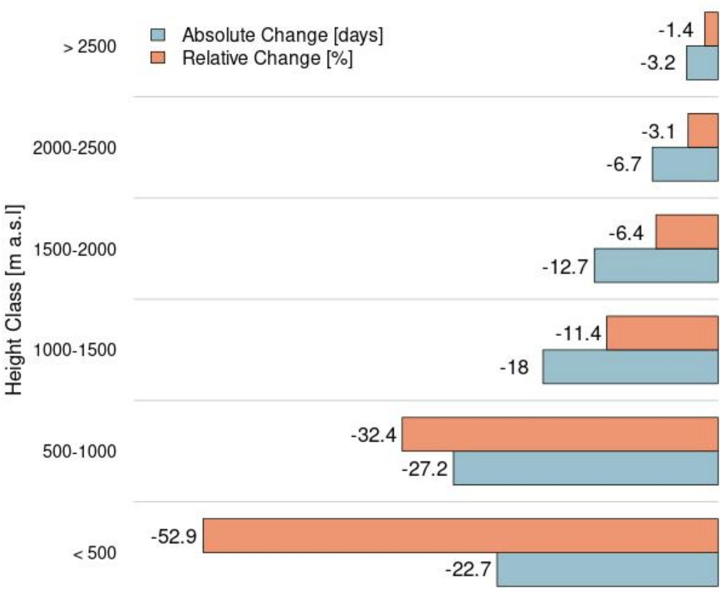

Figure 3.16: Absolute (blue) and relative (orange) change of the mean number of snow days within a snow season from the period 1962 - 1990 to the period 1991 - 2020 for each selected elevation class over entire Switzerland.

3.1.6 Trends

To gain more insights into the evolution of the mean SWE (Sep - May) over time, trends are shown in Figure 3.17. A 10-year (red) and a 30-year (yellow) LOESS smoothing function (De Valk (2020); Scherrer et al. (2023)) according to subsection 2.3.2 were applied to the time series presented in Figure 3.7. More detailed trend analyses including the upper and lower confidence limits are shown in Figure F.1 and F.3 in the Appendix.

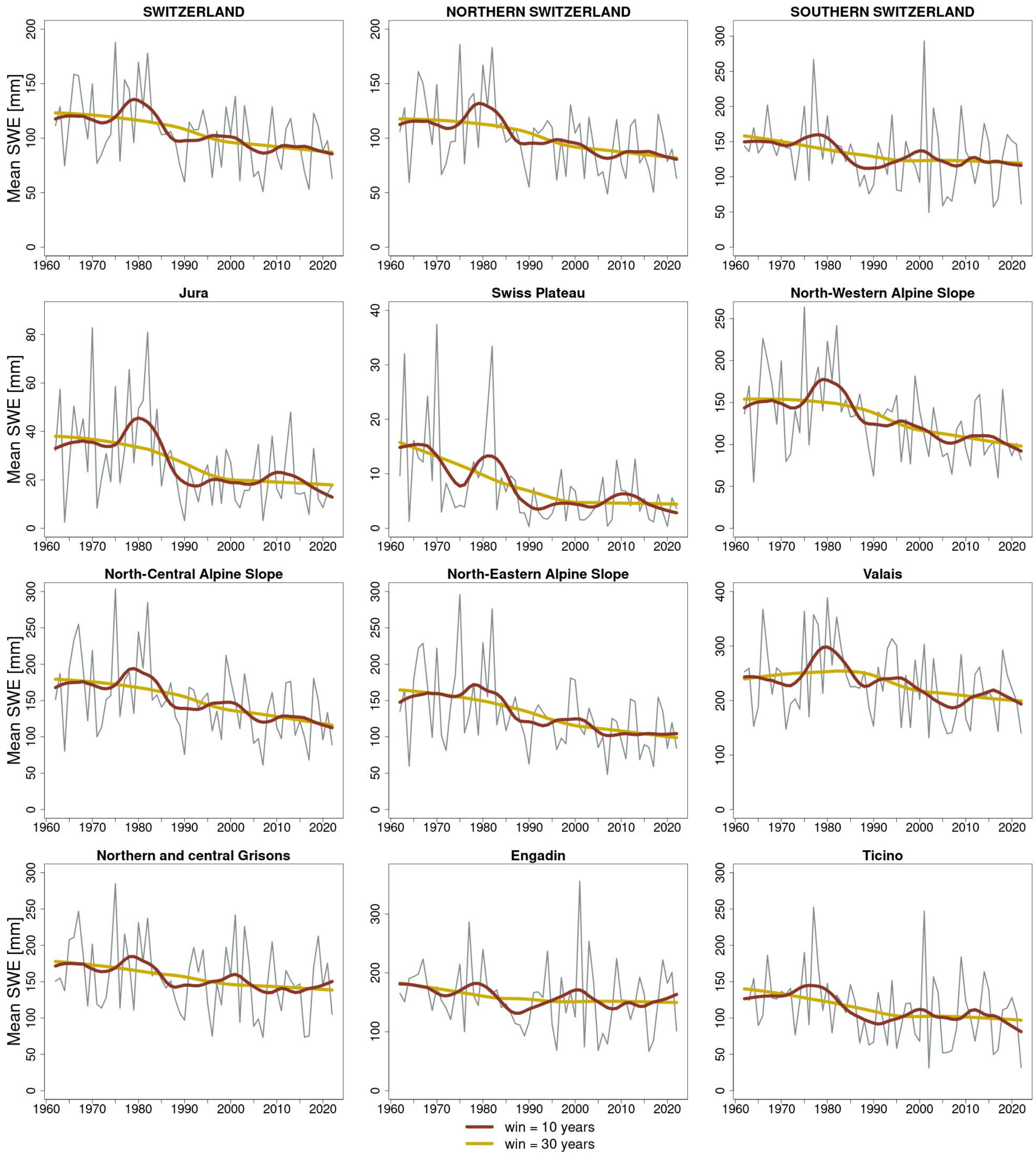

Figure 3.17: LOESS smoothing trend line (De Valk (2020); Scherrer et al. (2023)) applied on the time series of the mean SWE (Sep - May). Red: 10-year smoothing window. Yellow: 30-year smoothing window. Black: time series of the mean SWE between 1962 and 2022.

The 30-year smoothing looks similar to a hypothetical linear trend since it is very smooth, and therefore a lot of short-term variability was smoothed out. In most sub-regions a light, steady decrease is identifiable, which is most pronounced in the first half of the time series up to the 1980s. Towards the end, the strength of the trends is decreasing or even stagnating in some cases. On the other hand, the 10-year smoothing function contains more variability. In all the sub-regions a maximum is visible in the late 1970s / early 1980s. After that, there is a fairly sharp decline in every sub-region followed by a smaller maximum around the turn of the millennium. A last small maximum, with a considerably smaller amplitude than the one from the 1980s, occurs again between 2010 and 2015. The end of the slope of the time series varies depending on the sub-region. While the 10-year smoothed trend in the Engadin and the Northern and central Grisons is slightly increasing, a decrease can be seen in all other sub-regions.

The same analysis for the number of snow days within the snow season is presented in Figure 3.18. The LOESS smoothing function was applied on the snow days time series in Figure 3.8. More detailed trend analysis including the lower and upper confidence limit are depicted in Figure F.2 and F.4 in the Appendix. Compared to the trend analysis of the mean SWE in Figure 3.7, the trend analysis here is very similar. While the 30-year smoothed trend is steadily decreasing over the whole time span in every sub-region, the 10-year smoothing shows more features again. As in the SWE trends the maximum in every sub-region occurs in the late 1970s / early 1980s followed by a sharp decline of the mean number of snow days towards the 1990s. A smaller maximum occurs around 2000 and again between 2010 and 2015. The time series end with an increase in the Engadin and Northern and central Grisons and a further decline in all the other sub-regions.

Not only the annual and inter-annual variability of snow cover over Switzerland is large, but also decadal- and longer-scale variability exists. The most striking result, when looking at the 10-year smoothed trends, is the maximum in the late 1970s / early 1980s and the rather sharp decline thereafter, which is even slightly recognizable in the 30-year smoothed trend. It occurs in both time series, the mean SWE and the mean number of snow days. This prominent feature was already found in other studies by e.g. Laternser et al. (2003); Marty (2008); Scherrer et al. (2013); Matiu et al. (2021). Marty (2008) suggested a regime shift occurring in the late 1980s, which was responsible for a loss of 20 to 60 % of the total snow days found at 34 long-term stations (see Figure 1.1). A trend analysis by Scherrer et al. (2013) also showed an increase in snow between 1960 and 1980 followed by a strong decrease in the late 1980s and 1990s. A more recent Alpine-wide station-based study (Matiu et al., 2021) confirmed those earlier studies.

The cause for this is fairly certain due to the temperature fluctuations and the sensitivity of snow to them (Marty, 2008). Marty (2008) showed that time series of winter temperatures reveal a step-like increase at the end of the 1980s. Most probable reasons include the impact of large-scale flow pattern such as the North Atlantic Oscillation (Scherrer et al., 2006). The occurrence of the contemporaneous solar brightening followed after a period of solar dimming might also have influenced the step-change (Norris et al., 2007). Sippel et al. (2020) suggested random atmospheric circulation variability to be the reason for the abrupt change.

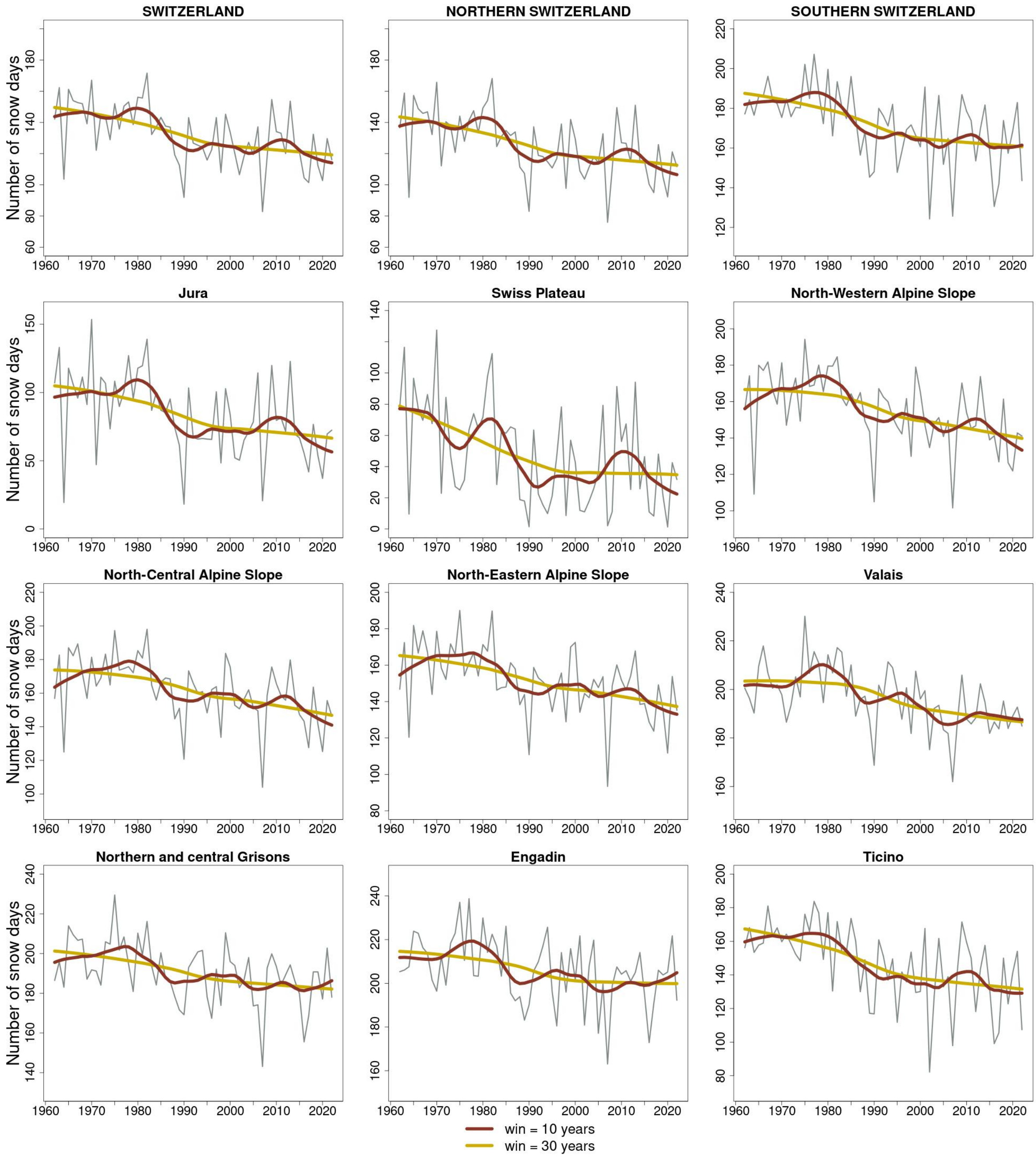

Figure 3.18: LOESS smoothing trend line (De Valk (2020); Scherrer et al. (2023)) applied on the time series of the mean number of snow days within a snow season. Red: 10-year smoothing window. Yellow: 30-year smoothing window. Black: time series of the mean number of snow days within a snow season.

3.2 Uncertainties and limitations

3.2.1 South-western region of Yverdon

The investigation of spatial maps showing absolute and relative SWE anomalies based on OSHD-CLQM revealed a spurious feature in the region south-west to Yverdon, which is strongest during the hydrological year 2002 (see Figure 3.19 and 3.20). More detailed analyses showed that this feature is also visible in the training data set (OSHD-EKF) and the baseline simulation (OSHD-CL) of OSHD-CLQM and thus not an artifact of the quantile mapping in SnowQM. Further investigations led to the forcing data of the OSHD snow model. The main error was found in RhiresD, which is based on daily precipitation totals from high-resolution rain-gauge networks (MeteoSwiss (2021b)). Wrong precipitation values measured between December 25, 2001, and January 22, 2002, at the measurement station in Mathod are responsible for the prominent anomaly (two examples of wrong values in RhiresD are shown in Figure 3.21). The RhiresD product, together with TabsD, is used to force the OSHD snow model, that delivers OSHD-CL (see subsection 2.2.1). Since OSHD-CL is used as the baseline simulation for OSHD-CLQM, the error propagates. In order to minimize this error, the identified region between December 25, 2001, and February 15, 2002 was masked out in all analyses. This period was chosen to consider the temporal memory of snow cover, i.e., the influence of past snowfall events on the present surface snow coverage. The spatial SWE anomaly patterns for OSHD-EKF, OSHD-CL and OSHD-CLQM for the available hydrological years after applying the mask are shown in Appendix E. Even after the mask has been applied, spurious signals are visible in this area, although they are less pronounced. Further errors in RhiresD have to be assumed and this region must be considered with caution.

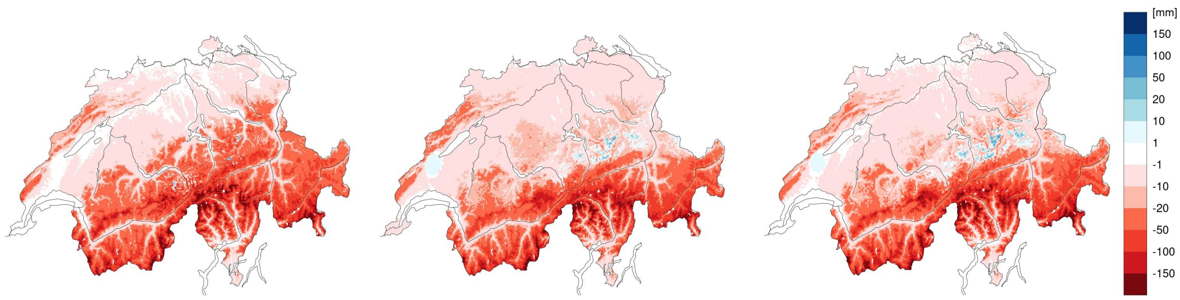

(a) OSHD-EKF (b) OSHD-CL (c) OSHD-CLQM

Figure 3.19: Absolute SWE anomaly of the hydrological year 2002. Reference Period: 1999 - 2020.

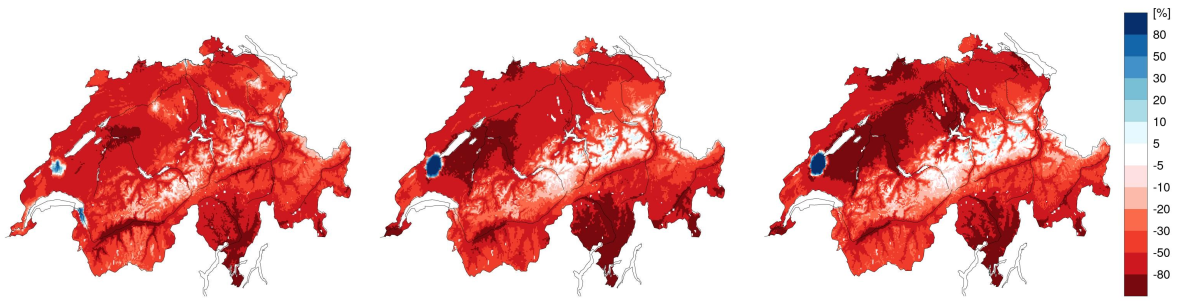

(a) OSHD-EKF (b) OSHD-CL (c) OSHD-CLQM

Figure 3.20: Relative SWE anomaly of the hydrological year 2002. Reference Period: 1999 - 2020.

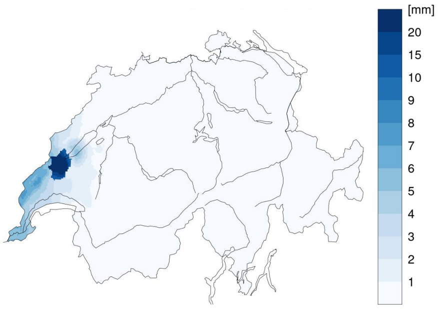

(a) RhiresD on January 15, 2002

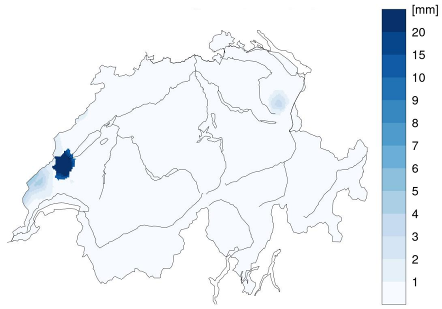

(b) RhiresD on January 22, 2002

Figure 3.21: Two examples of daily precipitation grids (RhiresD) containing wrong values in the region south-west to Yverdon. The plots show daily precipitation (from 06:00 UTC of the day to 06:00 UTC of the day+1) in mm (MeteoSwiss, 2021b).

3.2.2 General Uncertainties

The subsection 3.2.1 has shown a specific example of a limitation in the input data grid RhiresD of the OSHD snow model, which lead to spurious features in in the OSHD-CLQM analysis. Therefore, the question arises whether further artifacts in the input data could influence our results. Consider for example the rather strong positive trends of the mean SWE and especially of the mean winter SWE at high elevations in the Valais and the Bernaise Alps found in Figure 3.1 and 3.3. Even though the positive snow cover trends at high elevations might be explained by the increase of seasonal precipitation with global warming since the temperatures even with warming remain below the freezing point (Beniston, 2012), this may not be the case here. The RhiresD and the TabsD product, which are the input gridded data sets of the OSHD snow model (see subsection 2.2.1), may be affected by spatio-temporal artifacts. These might be caused by temporal inconsistencies of the station network as RhiresD is based on daily precipitation totals measured at high-resolution rain-gauge networks and TabsD on the operational station network SwissMetNet of MeteoSwiss (MeteoSwiss, 2021a; MeteoSwiss, 2021b). In both data sets the number of underlying stations varies over time and thus, RhiresD and TabsD are not necessarily temporally homogeneous and consistent. Possible effects of such inconsistencies can be seen in Figure 3.22 for precipitation and in Figure 3.23 for temperature, in which the RhiresD and TabsD are compared to consistent grids (RnormM and TnormM). The consistent precipitation and temperature grids are corrected for the effects of incomplete temporal coverage as well as for station and instrument changes (MeteoSwiss, 2021c; MeteoSwiss, 2021e). However, since these consistent gridded temperature and precipitation data sets are not available as a daily product, they cannot replace RhiresD and TabsD to force the OSHD snow model. Figure 3.22a shows the ratio of mean precipitation (Sep - May) between the reference periods 1991 - 2020 and 1961 - 1990 for the consistent RnormM product (method based on MeteoSwiss (2021e)), whereas Figure 3.22b shows the same for the RhiresD product. The difference of the two ratios, shown in Figure 3.22c, reveals larger differences in high elevated regions of the south-east Valais, where RhiresD in contrast to RnormM shows an increase in precipitation from the previous to the latter period (blue colors indicate a stronger precipitation increase in TabsD). As this is the area where a mean SWE increase in OSHD-CLQM is visible (subsection 3.1.1), the increase can be attributed to the precipitation increase caused by this inconsistency in RhiresD. For temperature, the effect of inconsistencies in TabsD cannot be localized as precisely. The differences of the mean temperature (Sep - May) between the reference periods 1991 - 2020 and 1961 - 1990 of the consistent TnormM product (Figure 3.23a) respectively the inconsistent TabsD product (Figure 3.23b) are compared in Figure 3.23c (red colors indicate a stronger warming in TabsD). It is shown that the difference is substantial over large parts of the country (around

0.5 °C). It has to be assumed that OSHD-CLQM is also affected by this inconsistency in TabsD. Therefore, especially trend analyses of OSHD-CLQM should be done with caution.

Not only uncertainties resulting from the snow model inputs, but also other aspects have to be considered. Michel et al. (2023) suggested to mask out all pixels above 3000 m a.s.l. in the analysis of OSHD-CLQM, as no monitoring stations for providing data to assimilate into OSHD-EKF are available above 2800 m a.s.l. Additionally, pixels at high elevations, in steep Alpine terrain, might not be represented adequately by the 1 km horizontal resolution. Therefore, these areas contain larger uncertainties from various sources. Moreover, OSHD-CLQM contains further general uncertainties which are not attributable to a specific area or region. As reviewed in section 1.2, snow is highly dynamic and measuring, as well as modeling snow is challenging and subject to important uncertainties. This influences the baseline data set OSHD-CL as well as the training data set OSHD-EKF and thus, OSHD-CLQM. Also, the quantile mapping method used to develop OSHD-CLQM contains uncertainties (Michel et al., 2023). Overall, it is difficult to state which features are the result of uncertainties and artifacts. There are numerous uncertain factors and existing errors have been found. Validation with independent data is therefore urgently required.

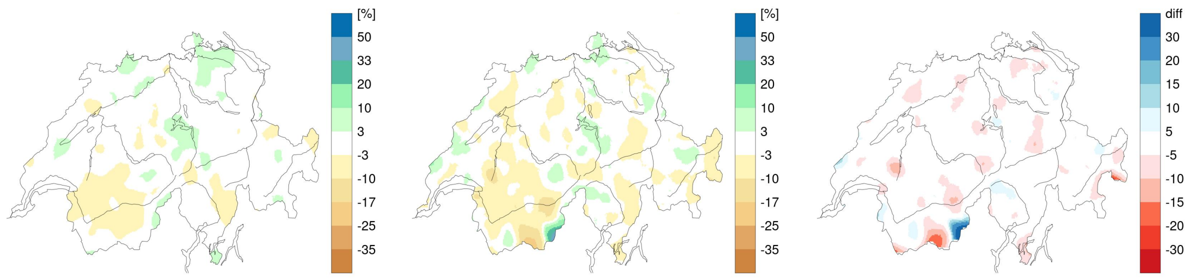

(a) RnormM (MeteoSwiss, 2021e) (b) RhiresD (MeteoSwiss, 2021b) (c) RhiresD minus RnormM

Figure 3.22: Overview of uncertainties originating from RhiresD. (a) Ratio of mean precipitation (Sep - May) between the reference periods 1991 - 2020 and 1961 - 1990 of the consistent RnormM product. (b) Ratio of mean precipitation between the reference periods 1991 - 2020 and 1961 - 1990 of the RhiresD product, which is used to run the baseline snow model OSHD-CL. (c) Difference of the two ratios from (a) and (b). The same analysis on a seasonal base are shown in Figure G.1.

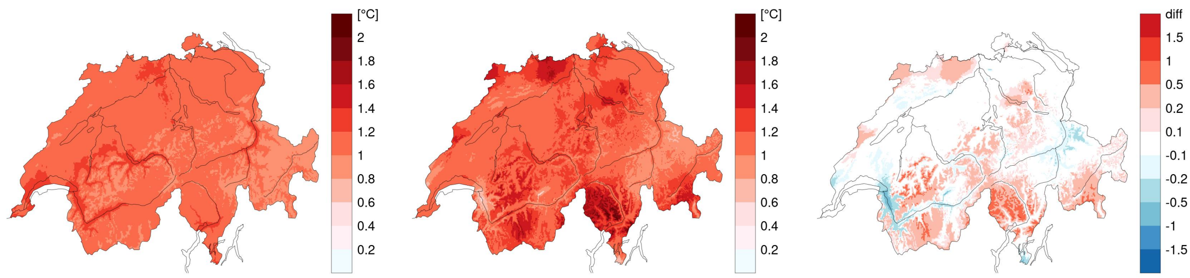

(a) TnormM (MeteoSwiss, 2021c) (b) TabsD (MeteoSwiss, 2021a) (c) TabsD minus TnormM

Figure 3.23: Overview of uncertainties originating from the TabsD. (a) Difference of mean temperature (Sep - May) between the reference periods 1991 - 2020 and 1961 - 1990 of the consistent TnormM product. (b) Difference of mean temperature between the reference periods 1991 - 2020 and 1961 - 1990 of the TabsD product, which is used to run the baseline snow model OSHD-CL. (c) Difference of (a) and (b). The same analysis on a seasonal base are shown in Figure G.2.

3.3 Intercomparison of data sets

In this section, the validation of OSHD-CLQM is shown. First, the validation against in-situ observations is presented and discussed (subsection 3.3.1), followed by the validation against remote sensing data (subsection 3.3.2).

3.3.1 Validation against surface observations

For the validation of OSHD-CLQM against station-based surface observations, maps of Switzerland depicting the absolute and relative difference of (a,b) the mean SWE and (c,d) mean number of snow days over the winter half year (Nov - Apr) from the period 1962 - 1990 to 1991 - 2020 are analyzed first (Figure 3.24). Additionally to the OSHD-CLQM data, the same analyses for stations with a sufficiently long availability were added by dots.

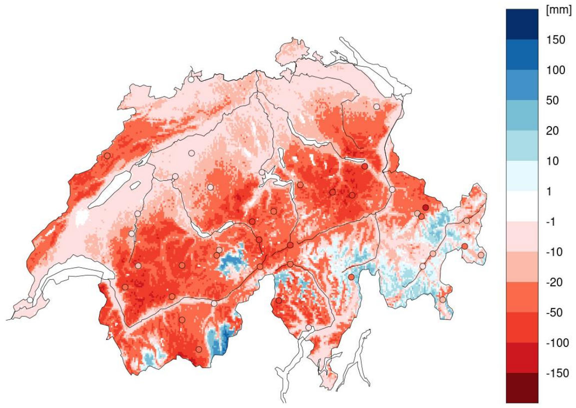

(a) Absolute SWE difference

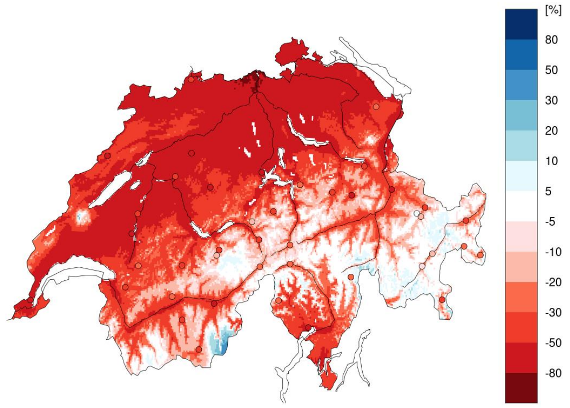

(b) Relative SWE difference

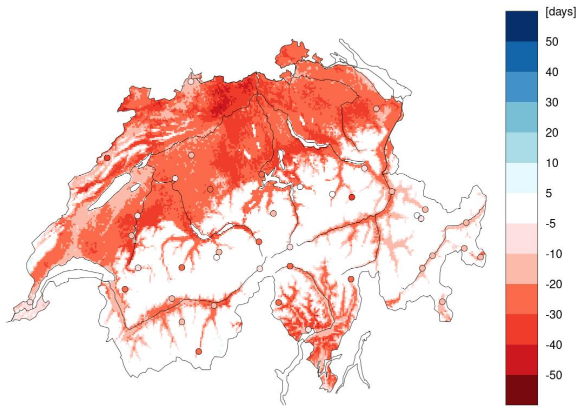

(c) Absolute snow days difference

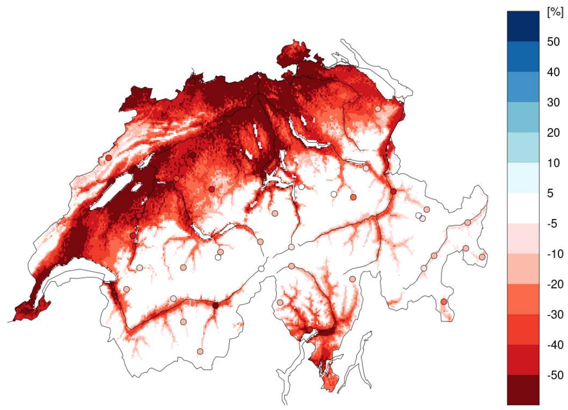

(d) Relative snow days difference

Figure 3.24: Difference of the mean SWE (winter half year) (a,b) and number of snow days within the winter half year (c,d) between the periods 1962 - 1990 and 1991 - 2020. Reference period: 1962 - 1990. Points indicate the same quantities computed from station data.

Overall, the colors of OSHD-CLQM and the station dots match, indicating a comparable evolution of the snow indicators from the previous to the latter period. The station-based changes in terms of magnitude seem to correspond with the OSHD-CLQM development of the indicators. Unfortunately, there are no homogeneous long-term stations available in regions and elevations where the OSHD-CLQM analyses suggests an increase in the mean SWE over the winter half year. Thus, the verification of this pattern is not possible with station-based data. The exact comparison is also difficult because of the resolution of the map. Therefore a local comparison between OSHD-CLQM and the station data, based on an adapted the nearest grid cell approach was made. The procedure as well as the elevation difference for each station was presented in subsection 2.3.3. The relative and absolute differences from the previous to the latter period according to Figure 3.24 at each station and its corresponding nearest grid cell can be found in the Appendix H.

As an example of a local comparison, the time series of the mean SWE over the winter half year and the number of snow days within the winter half year at the station of Andermatt (2AN) and its nearest grid cell are shown in Figure 3.25b. The elevation difference of the station of Andermatt at 1440 m a.s.l. and the corresponding nearest grid cell at 1434 m a.s.l. with just 6 m, is rather small. This may be a reason for the high agreement of, especially, the two mean SWE time series. As mentioned in subsection 2.2.2, possible inhomogeneities as well as other challenges in measuring snow at stations make these analyses of the time series error-prone. Thus, the focus is, besides the root mean squared error (RMSE), more on the correlation of the two corresponding time series. In the case of Andermatt, the correlation between the station and the nearest grid cell equals 0.93 for the mean SWE time series and 0.62 for the snow days time series. The RMSE corresponds to 35.6 mm w.e. for the mean SWE and 14.44 days for the number of snow days. Overall, OSHD-CLQM agrees well at the station of Andermatt, with better performance for SWE than for snow days. A reason for this may be, that the number of snow days is explicitly dependent on a threshold value (SWE $>$ 10 mm, subsection 2.3.1). If the SWE values are close to this value, even a small difference in SWE may lead to differences in the number of snow days. In areas, where the SWE values are above the threshold for an extended period each winter, the sensitivity is largest during snow onset and melt-out periods, which are mostly limited in occurrence and duration to autumn and spring. Therefore the variability is generally lower and so is the correlation.

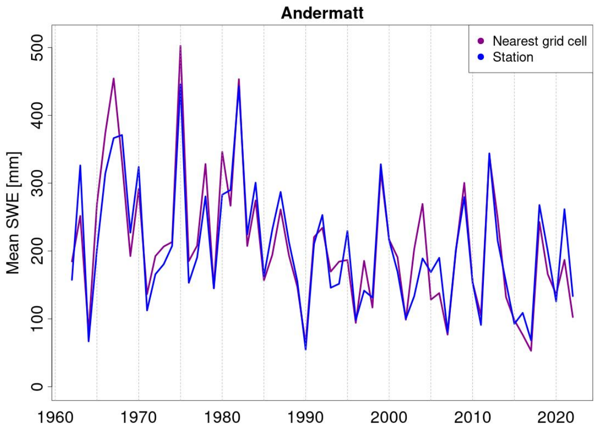

(a) Mean SWE (Nov - Apr)

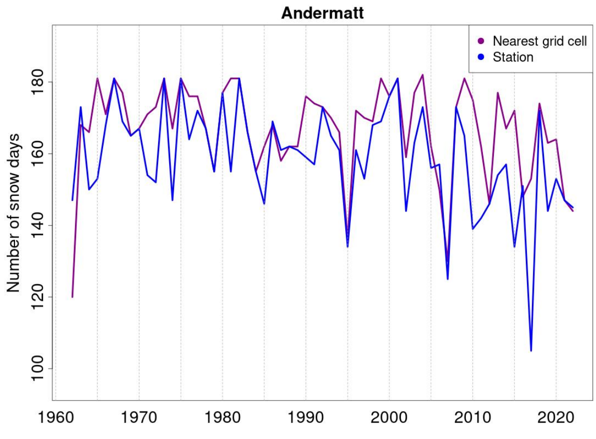

(b) Number of snow days within Nov - Apr

Figure 3.25: Comparison of the time series of (a) the mean SWE (Nov - Apr) and (b) number of snow days within the winter half year between 1962 and 2022. Blue: time series at the station. Purple: time series at the corresponding nearest grid cell.

The performance of all the individual stations and their corresponding nearest grid cells on the basis of the RMSE, and the pearson correlation is presented in Figure 3.26 for the mean SWE over the winter half year and in Figure 3.27 for the number of snow days within the winter half year. The RMSE and

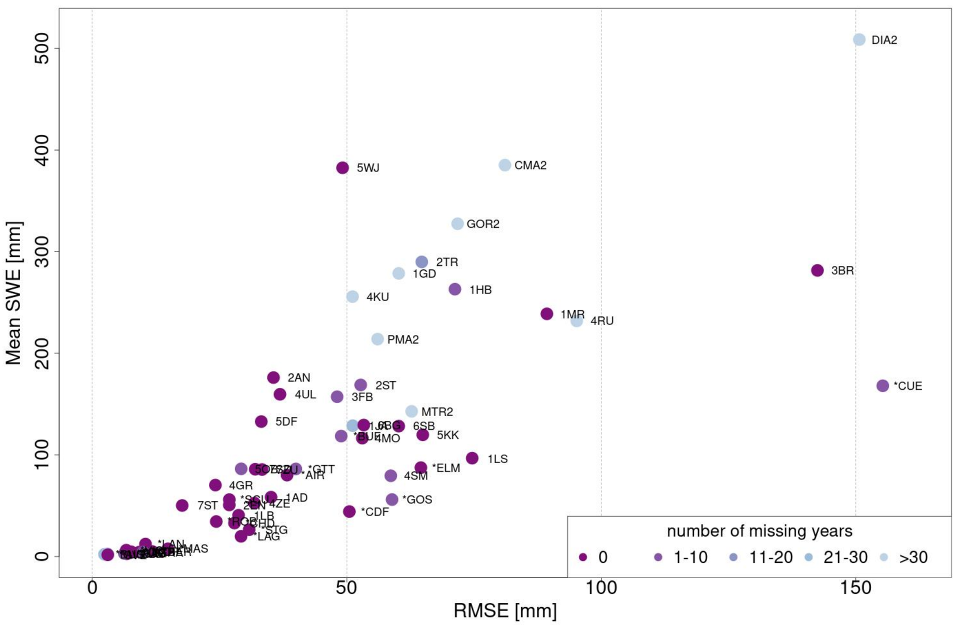

(a) RMSE mean SWE

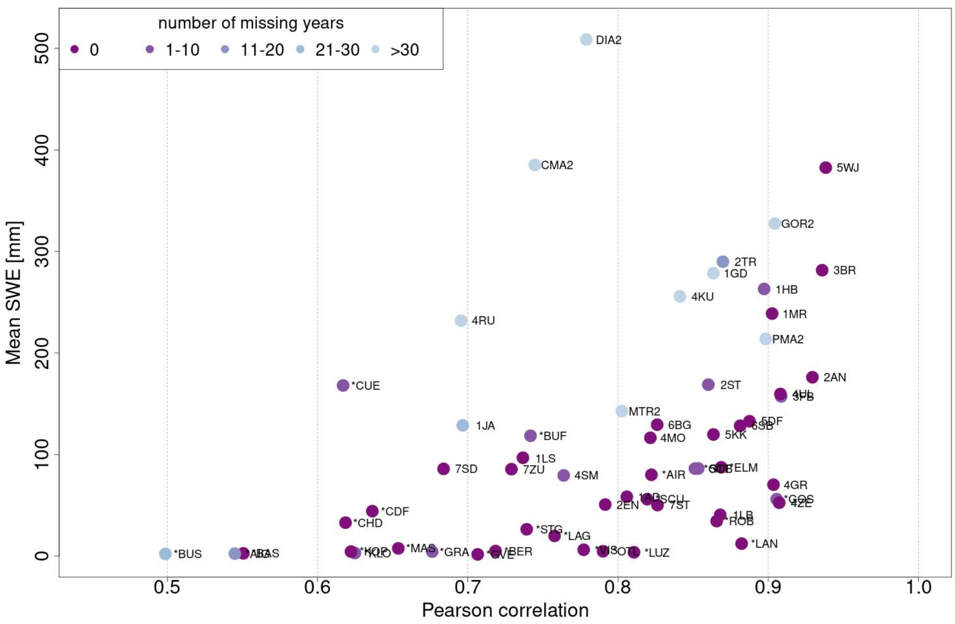

(b) Correlation mean SWE

Figure 3.26: Comparison of the time series of the mean SWE (Nov - Apr) between 1962 and 2022 at the stations and the corresponding nearest grid cells. (a) RMSE. (b) Pearson correlation. Y-axes: average of the mean SWE values over 1991 - 2020 in each corresponding nearest grid cell. The colors indicate the number of missing values in the station time series (lighter colors correspond to more missing years).

correlation are plotted against the average of the mean SWE values and the numbers of snow days over 1991 - 2020 in each nearest grid cell, respectively. As not all stations provide gapless time series, the colors additionally indicate the number of missing half yearly station values. The lighter the color, the more years are missing and the less reliable the validation.

The SWE analysis shows that the RMSE values increase generally with larger mean snow amounts. Thus, the higher the average SWE values in a given area, the higher the absolute error. However, also at two

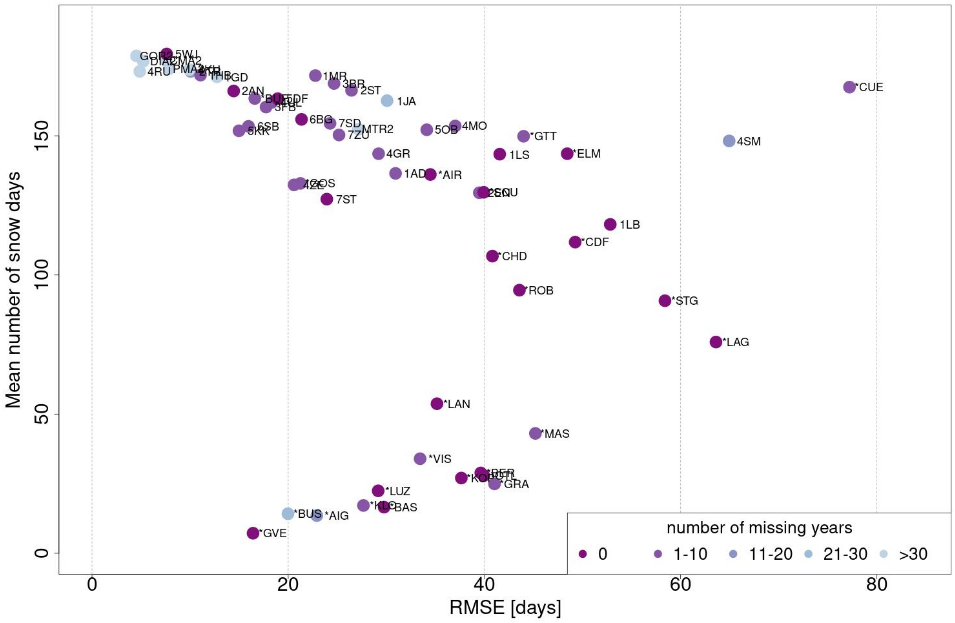

(a) RMSE number of snow days

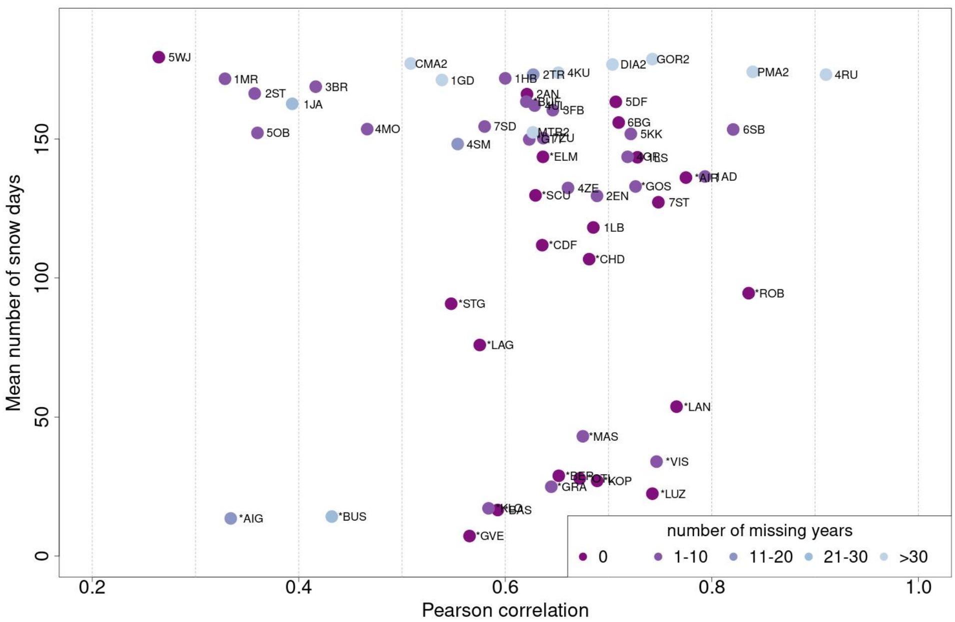

(b) Correlation number of snow days

Figure 3.27: Comparison of the time series of the number of snow days within the winter half year between 1962 and 2022 at the stations and the corresponding nearest grid cells. (a) RMSE. (b) Pearson correlation. Y-axes: average of the numbers of snow days over 1991 - 2020 in each corresponding nearest grid cell. The colors indicate the number of missing values in the station time series (lighter colors correspond to more missing years).

lower stations (Braunwald, 3BR and La Cure, *CUE) with lower mean SWE amounts, the RMSE values between the station and the grid cell are rather large. All the other RMSE values at grid cells with similar mean snow amounts are smaller. The Pearson correlation does not show such a specific result. The median correlation equals 0.82, which indicate a high correlation in general. Overall, it can be stated that stations with larger mean snow amounts generally show a larger correlation. However, also numerous

stations with lower mean snow amounts show large correlations.
The performance of the comparison between the nearest grid cell and the station depends on the elevation as well as on the horizontal distance between each other. Better performances of this validation are expected for stations with a low elevation and horizontal distance to the nearest grid cell. Moreover, also the topographic features to the specific comparison might play a role. Stations in narrow valleys, for example, may correspond less to the nearest grid cells since the representation of such small geographic features is more difficult or not possible at all by the 1 km resolution of OSHD-CLQM.

The same analysis for the number of snow days within a winter half year shows different results (Figure 3.27). The best performance of OSHD-CLQM (i.e. smallest RMSE) occurs at stations with many snow days (at the maximum or close by) with RMSE values of less than 20 days. Also the grid cells at stations with few snow days perform well. In areas with a medium number of snow days, the performance of the data set against the station data is worse. This may be explained by the larger snow variability in these cases. Areas with the largest numbers of snow days often reach the maximum possible number of snow days over the winter half year and areas with very few snow days also do not have a large variability. The result for the correlation between the snow days time series at the station and its corresponding grid cell is more difficult to interpret. Grid cells with many snow days as well as grid cells with few snow days show a large range of the correlation coefficients. It has to be stated that the statistical interpretation of the correlation at the areas reaching the maximal number of snow days in some years, is not fully correct as this specific is bounded by an upper limit. Nevertheless, the comparison of the OSHD-CLQM and the station-based time series allow to extract relevant information about the representation of winters with fewer snow days in OSHD-CLQM.
High performance in the mean SWE time series does not automatically favor high performance in the snow days time series and vice versa. For example, at Ruinettes, the nearest grid cell and the station (4RU) shows the highest Pearson correlation in the snow days time series (> 0.9). On the other hand, the SWE correlation at this station is rather small (< 0.7) compared to other stations with similar mean snow amounts. However, the station of Ruinettes has more than 30 missing years in the period of interest (1962 - 2022), and thus, the correlation has to be considered with caution. The opposite is the case for Weissfluhjoch (shown in Figure 3.28), where the station (5WJ) and the nearest grid cell have the highest correlation of all grid cells for the SWE time series (> 0.9, Figure 3.28a), and the lowest in the snow days time series (< 0.3, Figure 3.28b). As this grid cell is at a rather high elevation and thus has high number of snow days (often nearby or at the maximum), it is a case where the statistical interpretation of the correlation is not fully correct. However, the comparison of the snow days time series at the station with the nearest grid cell allow insights about the representation of winters with fewer snow days. For example, it can be seen that the winter half years 1966 and 1970 are well represented, whereas 1984 or 2011 are worse represented in OSHD-CLQM compared to the station-based data.

To conclude, the validation of OSHD-CLQM against station-based surface observations revealed comparable results between the observations and OSHD-CLQM. Investigations of the evolution of mean SWE and the number of snow days over the winter half year from the period 1962 - 1990 towards 1991 - 2020 showed the same signals at the stations and in OSHD-CLQM (Figure 3.24). The performance, regarding the correlation in the nearest grid cell approach, is better when considering SWE than the number of snow days (Figure 3.26 and 3.27) and there better for sites with higher SWE amounts. As discussed, this may be caused by the dependence of snow days on the threshold of 10 mm. When the SWE values are around that threshold, small differences in SWE may lead to larger differences in the number of snow days. For sites with generally low SWE values (around the threshold) over an extended period each

winter reaching a high performance is more difficult.
Unfortunately, stations are not available all over the country and thus, a complete validation is not possible. Moreover, measuring snow at representative stations itself is challenging and may lead to inhomogeneities (see subsection 2.2.2). There are also some other difficulties which might have affected the validation. Some stations contain measurement errors or gaps. Further, the validation is not fully independent since some station-based data have been assimilated into the training data set (OSHD-EKF) of OSHD-CLQM. The conversion from snow depth to SWE for the station-based data is connected with uncertainties. And, the nearest grid cell approach is not a flawless way to compare the two data sets, as the elevation difference as well as the geographic setting between the station and the nearest grid cell may prevent an accurate comparison.

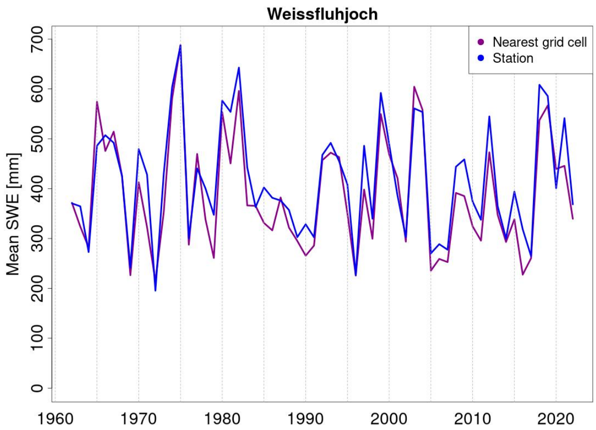

(a) SWE

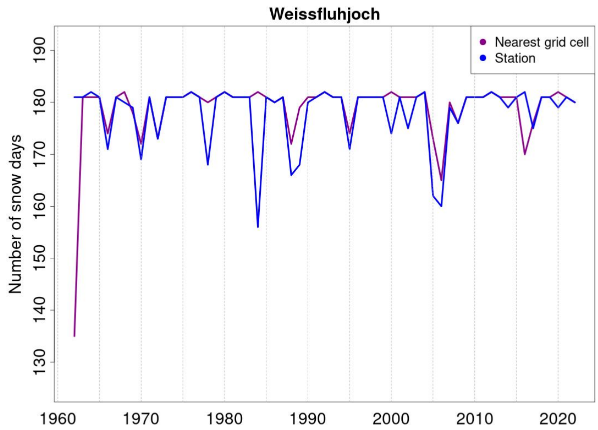

(b) Number of snow days

Figure 3.28: Comparison of the time series of the (a) mean SWE (Nov - Apr) and (b) number of snow days within Nov - Apr between 1962 and 2022. Blue: time series at the station. Purple: time series in the nearest grid cell.

3.3.2 Validation against remote sensing data

The validation of OSHD-CLQM against station-based surface observations indicate an overall high performance of OSHD-CLQM with comparable results between the two data sets. Unfortunately, the validation against station data is not fully independent, not possible during summer and spatially limited. Therefore, a validation against remote sensing data is presented in the following, which should provide further information about the quality of OSHD-CLQM.
A first analysis is shown in Figure 3.29, where the number of snow days calculated from the 10-day fractional snow cover of OSHD-CLQM, the AVHRR and the MODIS data set are compared (according to subsection 2.3.3). The comparison was made over the time horizon 2004 to 2018 since all data sets are available then. The figures present the average number of snow days within the hydrological year over this time span. Since there are numerous missing values in the remote sensing data sets, especially in AVHRR, these grid cells were masked out in all the data sets here. Figure 3.29a presents the overview of OSHD-CLQM, whereas Figure 3.29b shows the AVHRR and Figure 3.29d shows the MODIs data set. The comparison between OSHD-CLQM and the remote sensing data sets was made based on the calculation of the absolute difference within them given in numbers of snow days. Figure 3.29c presents the difference between the OSHD-CLQM and AVHRR and Figure 3.29e shows the difference between OSHD-CLQM and MODIS. Blue colors indicate that OSHD-CLQM suggests longer snow coverage than the remote sensing data sets and red colors indicate larger numbers in the remote sensing data sets.

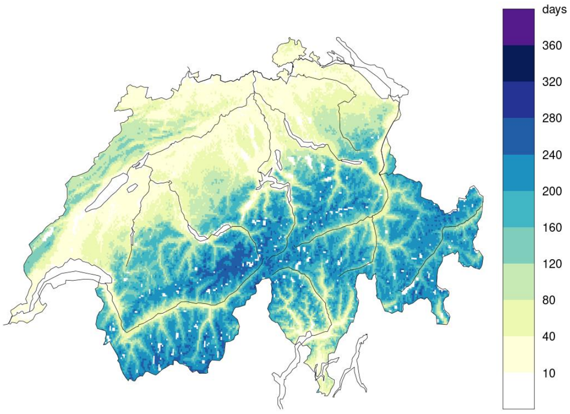

(a) OSHD-CLQM

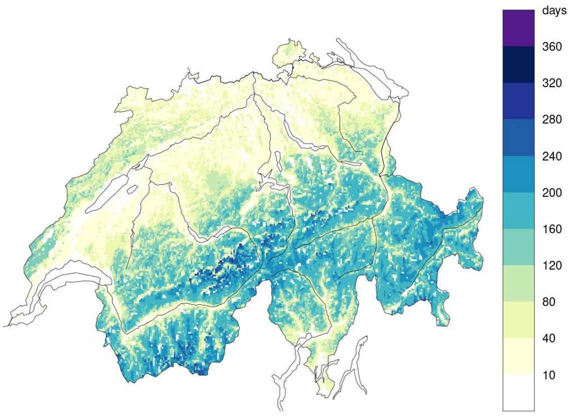

(b) AVHRR

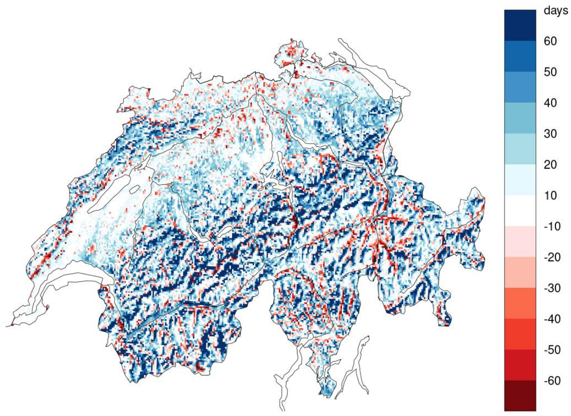

(c) OSHD-CLQM minus AVHRR

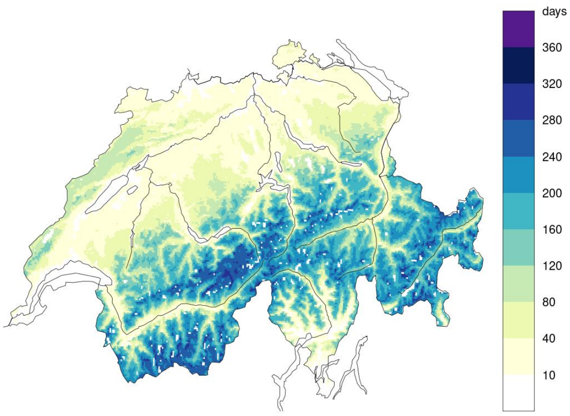

(d) MODIS

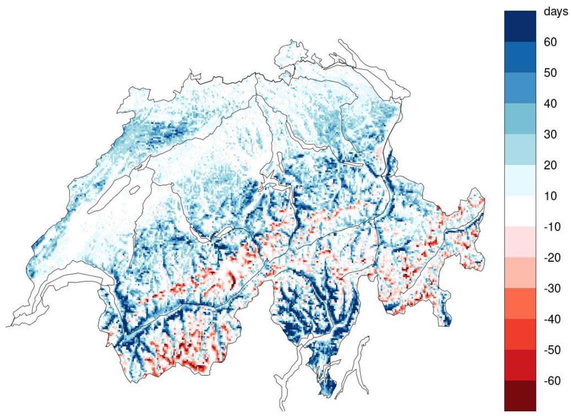

(e) OSHD-CLQM minus MODIS

Figure 3.29: Comparison between OSHD-CLQM and the remote sensing data sets AVHRR and MODIS. Average number of snow days within hydrological years 2004 to 2018. Missing values are masked out in all data sets. The calculation is based on 10-day fractional snow cover composites.

Overall, it can be seen that the range of the number of snow days within the three data sets is relatively wide. It is particularly noticeable that the two remote sensing data sets show rather large discrepancies. AVHRR detects the least snow days, whereas MODIS shows over major parts of the country the largest numbers of snow days. OSHD-CLQM lies in general within the range of the two validation data sets.

Since the remote sensing data sets show large variation, the validation of OSHD-CLQM against them is difficult.
Nevertheless, it is recognizable that the three data sets correspond better in the lowlands where the number of snow days are generally smaller. The comparison of AVHRR with OSHD-CLQM does not show a clear spatial signal over the Alps. On large parts, OSHD-CLQM shows more than 60 snow days more than AVHRR. However, there are also some smaller regions where the opposite is the case. On the other hand, the comparison of OSHD-CLQM and MODIS show clearer spatial signals besides a better agreement in general. Here, the highest elevations show more snow days in MODIS whereas the valleys, especially in the Valais and the Ticino, show larger numbers of snow days in OSHD-CLQM. This might be related to forest coverage. A comparison with Swiss forest coverage (e.g. ESA (2023)) shows that the areas, where AVHRR and OSHD-CLQM matches better than MODIS and OSHD-CLQM, are forested. In contrast to MODIS, AVHRR is corrected for forest canopy layer (Matiu et al., 2019; Weber et al., 2022).

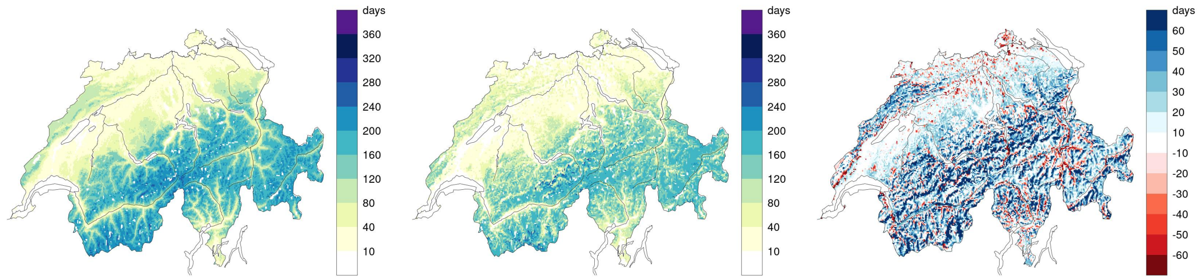

(a) OSHD-CLQM (b) AVHRR (c) OSHD-CLQM minus AVHRR

Figure 3.30: Extended comparison between OSHD-CLQM and AVHRR. Mean number of snow days within hydrological years 1982 to 1985, 1990 to 1995 and 2004 to 2021. A common mask was applied for all three products. The calculation is based on 10-day fractional snow cover composites.

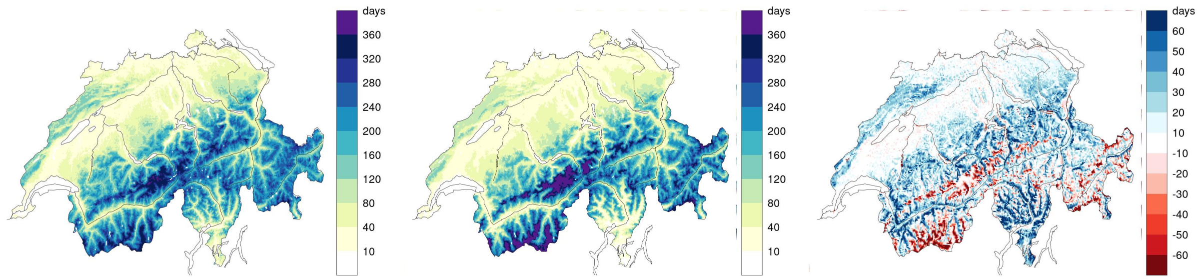

(a) OSHD-CLQM (b) MODIS (c) OSHD-CLQM minus MODIS

Figure 3.31: More complete comparison between OSHD-CLQM and MODIS. Mean number of snow days within hydrological years 2003 to 2018. The calculation is based on daily fractional snow cover data. The same analysis on a monthly base can be found in Appendix I.

An extended investigation of the comparison between OSHD-CLQM and AVHRR is shown in Figure 3.30. The same analysis as in Figure 3.29 was performed, but more years were included since AVHRR reaches back longer. As all available years were included, the plots show an average over the hydrological years 1982 to 1985, 1990 to 1995 and 2004 to 2021. Again, a common mask was applied to exclude the missing values of AVHRR in OSHD-CLQM. In general, the result shows that OSHD-CLQM contains larger numbers of snow days over the major part of the country. In many areas the numbers diverge by more than 60 days. However, there are also some areas where the signal is the opposite and

AVHRR shows higher numbers. Overall, no clear pattern can be detected, since there are always areas in between where the agreement is high.

Figure 3.31 shows a spatially more complete comparison between OSHD-CLQM and MODIS. The same analysis but on a monthly base is presented in Appendix I. In contrast to the previous analyses, the number of snow days here are not calculated on the 10-day fractional snow cover but on daily values. As MODIS contains almost no missing values, no grid cells were masked out. Thus, the average of the full hydrological years between 2003 and 2018 is presented. The comparison shows, as before, that OSHD-CLQM and MODIS show comparable number of snow days over the Swiss Plateau. Larger differences ($>$ 60 days) are found in the Ticino and the Rhone Valley, where OSHD-CLQM has larger snow days values. As mentioned above, this might be related to forest coverage. At the highest elevations the opposite is the case and MODIS shows the larger numbers of snow days. The monthly analysis reveals that this difference is largest in September (Appendix I). It should be noted that the SWE values in OSHD-CLQM are set to zero on September 01 every year. At high elevations, where snow usually remains during summer, the number of snow days in the beginning of the hydrological year are underrepresented in OSHD-CLQM. As this is not the case in the remote sensing based data sets, differences in the beginning of the hydrological year (especially September) can be attributed to that.

To conclude the validation against the remote sensing data sets, it must be stated that a clear statement is very difficult. The large difference in absolute values between the two remote sensing data sets makes the evaluation of OSHD-CLQM challenging. Moreover, the computation of the number of snow days from OSHD-CLQM is based on simple assumptions and thus, affected by numerous uncertainties. As introduced in subsection 2.3.3, we compute snow coverage from OSHD with a simple parameterization, which only depends on SWE. In reality however, the relationship between snow coverage (or fractional snow cover) and SWE is much more complex. Factors like seasonal dependency (accumulation and ablation phase), surface roughness, the complexity of the terrain or the vegetation also determine the sub-grid distribution of snow within a grid cell (Nitta et al., 2014; Jiang et al., 2020; Miao et al., 2022). For simplicity (and in lack of a more complex parameterization suitable and tested for our study region), we decided to apply a simple parameterization. Another source of uncertainty is that in OSHD-CLQM the data are set to zero on September 01. This is a reason for the larger differences between OSHD-CLQM and MODIS in September (as seen in Figure I.1).
In general, however, it seems reassuring that OSHD-CLQM itself does not form an extreme but lies within the range of the validation data sets. Since only a beta version of AVHRR was used here, the analysis should be repeated with the final version as soon as it is released to draw more robust conclusions.

3.4 Case study of the Swiss National Park

In this section, the region of the Swiss National Park (SNP) is investigated in more detail. The SNP, which was established in 1914, is located in the canton of Grisons, more precisely in the region of the Engadin and Val Müstair (see Figure 3.32) (Schweizerischer Nationalpark, 2022). The park has a spatial extent of 170.3 km^2, which corresponds to 172 grid cells in the OSHD grid used. Figure 3.32b shows an overview about the distribution of the elevation classes of the SNP. Most grid cells are located in elevation class 5 (2000 - 2500 m a.s.l.; 87 grid cells) and elevation class 6 (> 2500 m a.s.l., 57 grid cells), whereas 28 grid cells are located in elevation class 4 (1500 - 2000 m a.s.l.).
Flora and fauna are strongly impacted by the snow cover. So far, only little information about snow in the SNP exists. New knowledge about snow distribution and development would therefore allow a better understanding of the natural processes.

(a) The location of the Swiss National Park.

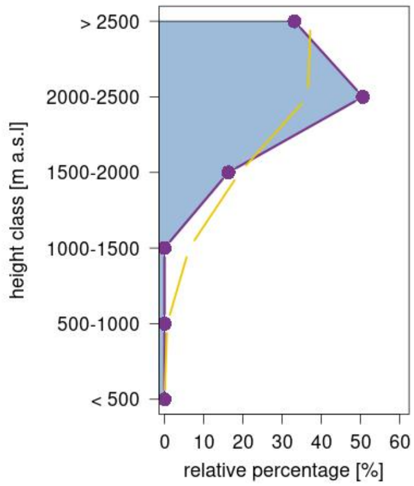

(b) Hypsograph.

Figure 3.32: Overview of the SNP. The hypsograph shows the relative distribution of the number of grid cells among the elevation classes in the SNP in purple. Yellow dashed line indicates the distribution for the Engadine as a whole.

In order to gain a general overview first, the mean SWE (Sep - May) climatologies of the SNP over the periods 1961 - 1990 and 1991 - 2020 are presented in Figure 3.34. In contrast to the same analysis for Switzerland as a whole (Figure 3.1), the individual pixels are clearly recognizable here. Obviously, areas as small as the SNP are not perfectly represented by the 1 km spatial resolution of OSHD-CLQM. Especially the complex mountainous terrain shown in Figure 3.33, which consists of narrow valleys and high mountain peaks makes an accurate representation even more difficult. Nevertheless, the most important topographical and geographical features are identifiable in the results delivered by OSHD-CLQM as the comparison between the topographic map and the climatologies shows. For instance, the valley Val dal Spöl is recognizable in the climatology by lower mean SWE values than the high mountains of the side valleys Il Fuorn, Val Sassa or Val Müschauns.

The absolute and relative change of the mean SWE from 1962 - 1990 to 1991 - 2020 shown in Figure 3.34c respectively 3.34d, reveal a clear reduction in the north-eastern parts of the SNP (in the Val Mingèr, Val Foraz and Val S-charl). Another rather strong reduction is visible in the centre, more precisely in the Val dal Spöl. This corresponds with the results found over Switzerland as a whole, since the reduction

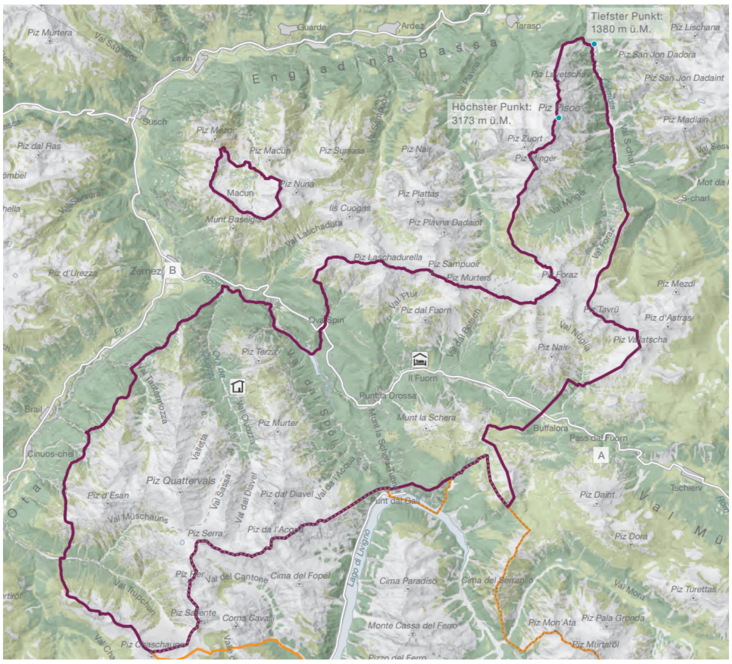

Figure 3.33: Overview of the topography in the SNP. Figure taken from Haller et al. (2014)

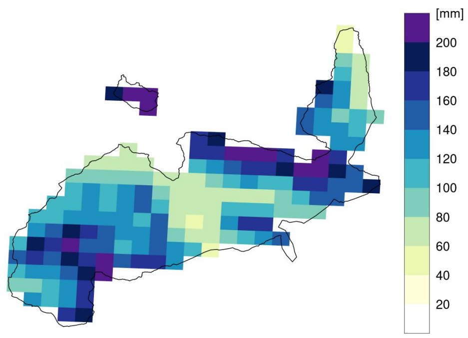

(a) climatology of the period 1962 - 1990

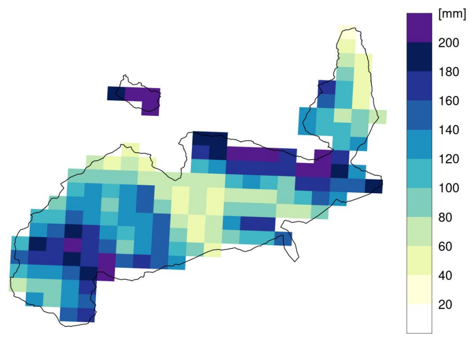

(b) climatology of the period 1991 - 2020

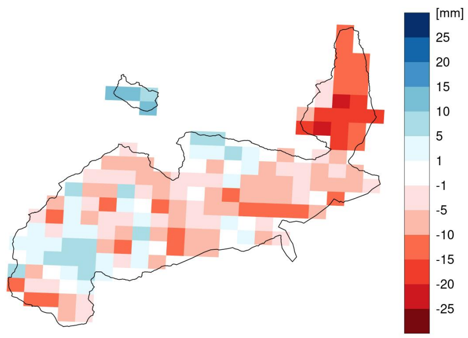

(c) Absolute difference (in mm w.e.)

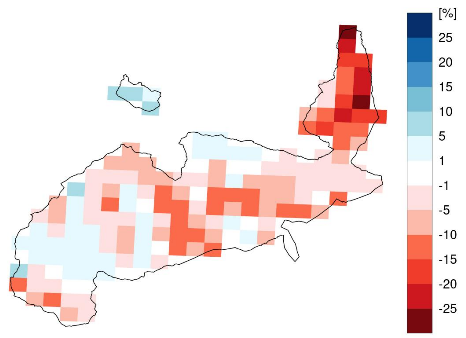

(d) Relative difference (in %)

Figure 3.34: Comparison of the mean SWE between the period 1962 - 1990 and 1991 - 2020. Reference period: 1991 - 2020.

is strongest in the parts with lower mean SWE values. However, a noteworthy part of the SNP shows also a small increase in SWE from 1962 - 1990 to 1991 - 2020. The parts which show an increase lie largely in high areas. It is difficult to say whether this is true or the result of uncertainties or artifacts. The fact is, that uncertainties in OSHD-CLQM exist and are larger over high elevations (see section 3.2).

The validation against stations showed that nearby stations do not show the same signal. Unfortunately, there are no long-term SWE stations at a daily resolution available in the SNP. Therefore, a statement is not possible.

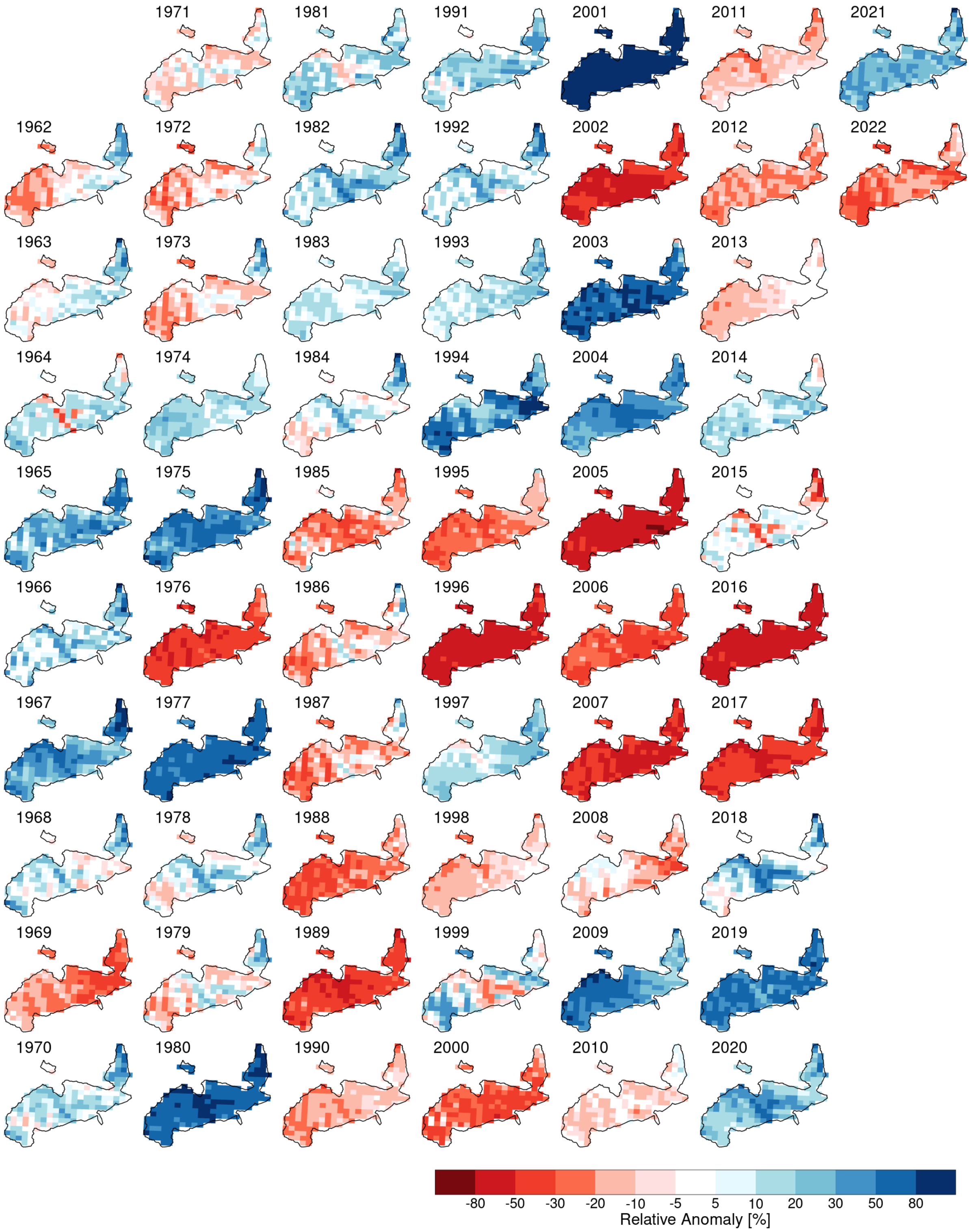

Figure 3.35: Relative SWE anomaly for snow seasons 1962 to 2022 (in %). Reference period: 1991 - 2020.

Figure 3.35 shows the relative anomalies of the mean SWE for the individual snow seasons 1962 to 2022 in comparison to the period 1991 - 2020. In contrast to the same analysis for Switzerland as a whole (Figure 3.5) it is clearly visible that the spatial variability of the anomalies within the SNP is rather small. For most snow seasons, the whole SNP shows either negative or positive anomalies. However, there are also exceptions. For example, the snow seasons 1964, 1981, 1999 and 2015 show larger mean SWE over most parts of the SNP compared to the reference, whereas the Val dal Spöl shows the different signal with less mean SWE. The opposite, in which the Val dal Spöl has larger and the remaining part of the SNP smaller mean SWE values, is the case for the snow seasons 1979 and 1986.

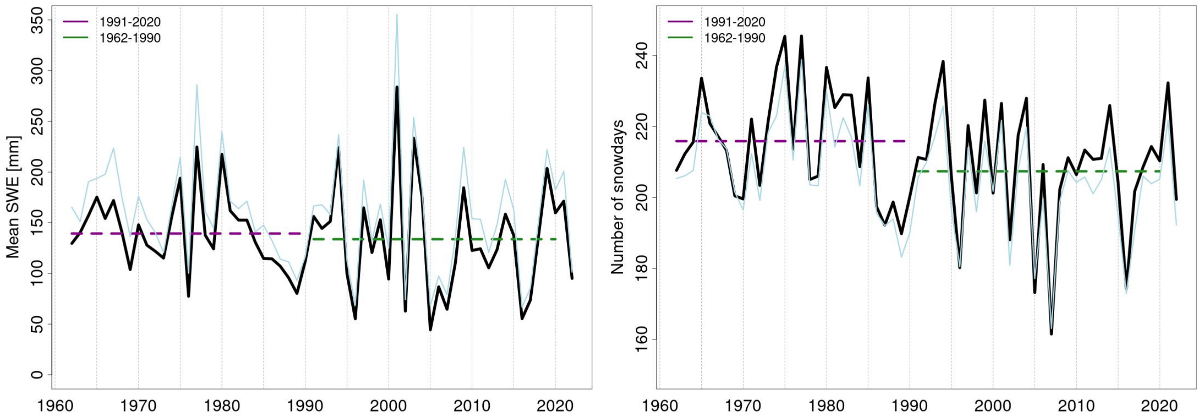

(a) Mean SWE

(b) Number of snow days

Figure 3.36: Comparison of the time series of (a) the mean SWE (Sep - May) and (b) number of snow days within the snow seasons 1962 - 2022 in the SNP (black). Purple: climatological mean over the period 1962 - 1990. Green: climatological mean over the period 1991 - 2020. Light blue: the same time series for the the Engadin as a whole.

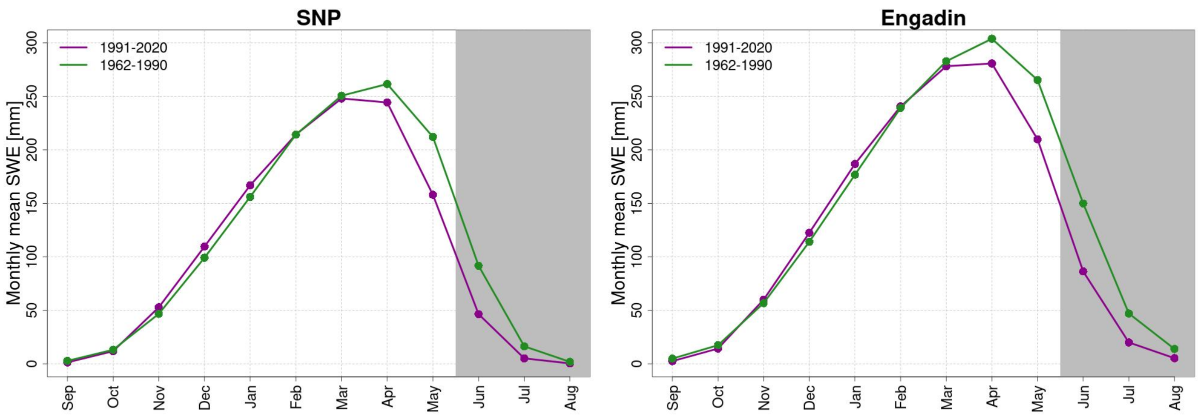

Figure 3.37: Comparison of the mean annual cycle of the period 1962 to 1990 (green) and the period 1991 to 2020 (purple) averaged over (a) the SNP and (b) the Engadin. The gray shading indicates the summer months, which should be considered with caution as they contain larger uncertainties (subsection 3.2.2).

The most extreme relative positive anomaly is present for the snow season 2001, where the whole SNP is dark blue and had over 80 % larger mean SWE values than the climatological reference. The winter 2000/01 is known as a very snow-rich one in southern Switzerland, in which besides the large snow masses, other avalanche-favorable conditions lead to numerous avalanche-related accidents and fatalities (SLF, 2022b). This extreme winter is also visible in the time series of the mean SWE between 1962 and 2022 (Figure 3.36a), in which the snow season 2000/01 has the clear maximum. However, in the time series of the number of snow days within the snow season, this winter does not stand out (Figure 3.36b).

All in all, both the mean SWE as well as the number of snow days time series over the SNP are very comparable to the time series of the Engadin, which is additionally indicated in light blue in Figure 3.36. The same is the case for the annual cycle of the mean monthly SWE (Figure 3.37). The maximal monthly mean SWE in the first period (1962 - 1990) occurs in April. However, it is almost 50 mm smaller in the SNP than in the Engadin as a whole. In contrast to the whole Engadin, the maximum in the SNP does not remain in April, but is shifted to March towards the latter period. The differences between the SNP and the Engadin might arise from the differences in the distribution of the number of grid cells among the elevation classes (shown in Figure 3.32). The SNP has 14 % more grid cells (relative to the total number) in the fifth elevation class (2000 - 2500 m a.s.l.) and 6 % resp. 2 % resp. 4 % less in the elevation classes three (1000 - 1500 m a.s.l.), four (1500 - 2000 m a.s.l.) and six (> 2500 m a.s.l.) respectively, compared to the Engadin as a whole.
The climatological averages of the mean SWE and the number of snow days within the snow season both show a reduction comparable to the Engadin as a whole (Figure 3.36). The climatological mean of the SWE in the SNP declines from 139 mm w.e. to 134 mm w.e. (- 6 mm w.e.), whereas it decreases over the whole Engadin from 162 mm w.e. to 155 mm w.e. (- 7 mm w.e.). For the number of snow days within the snow season, the number declines from 216 days in the previous period to 207 days (- 9 days) in the latter period over the SNP and from 211 days to 201 days (- 10 days) over the Engadin. In both periods, the mean SWE is larger over the Engadin as a whole compared to the SNP. The opposite is the case for the number of snow days within the snow season, where the numbers are higher in both periods over the SNP. Again, this difference may be related to the difference in the distribution of the number of grid cells among the elevation classes. Nevertheless, the reduction is very similar in the SNP and the Engadin for both snow indicators.

Overall, the more detailed analysis of the SNP showed that OSHD-CLQM, with its spatial resolution of 1 km, is able to provide valuable climatological information also over this comparably small region. The results are in good agreement with those expected from the topography and are generally very similar to results from surrounding larger areas such as the Engadin as a whole. However, as the grid cells of the SNP are lying predominantly in the uppermost elevation classes, the uncertainties are larger than in other areas (subsection 3.2.2). In addition, station-based validation was not possible due to the lack of long-term SWE observations. These factors should be considered when looking at the results.

Chapter 4

Synthesis and Conclusion

In the following, the project and its resulted outcomes are synthesized and concluded. Due to the lack of a state-of-the-art spatially highly-resolved and high-quality snow data set at a climatological scale, the SLF and MeteoSwiss developed OSHD-CLQM in a joint research project. OSHD-CLQM provides bias-corrected modeled SWE at a horizontal resolution of 1 km and a daily temporal resolution between September 1961 and today and was used for different in-depth analyses regarding the spatio-temporal variability of Switzerland's snow cover in the last 60 years in the present thesis. Moreover, the data set was validated against station-based surface observations, as well as remote sensing data from AVHRR and MODIS. Uncertainties and limitations of the OSHD-CLQM data set were identified and investigated and a case study of the SNP was conducted.

Overall, it can be stated that OSHD-CLQM allows for new relevant insights about the snow cover of Switzerland and numerous selected sub-regions, as well as elevation classes over the last 60 years. The overall performance of the data set seems to be promising, as OSHD-CLQM is comparable to station-based observations and lies within the range of the remote sensing data sets MODIS and AVHRR. Besides investigating the long-term climatology of the indicators and its evolution, looking at individual snow seasons and looking at comparably small areas like the SNP is possible and enables reasonable findings. The 1 km resolution of OSHD-CLQM is sufficient to capture the main characteristics of Switzerland's complex topography.

Analyses of different snow variables and indicators obtained from OSHD-CLQM, such as the mean SWE or the number of snow days (SWE $>$ 10 mm), show that snow cover has changed strongly over the last decades. The comparison of two long-term climatological periods, 1962 - 1990 and 1991 - 2020, in terms of mean SWE over the snow season (Sep - May) and the number of snow days within the snow season, demonstrate a decrease of both indicators over the majority of the country (subsection 3.1.1 and 3.1.5). These changes correspond to findings from previous studies and display a spatial and elevation-dependent variability. Especially, low elevations ($<$ 1000 m a.s.l.) with generally smaller snow amounts experience a large relative decrease of both snow indicators and a large absolute decrease of the number of snow days. In some areas, the mean SWE shows a relative reduction of more than 50 %, whereas the numbers of snow days within a snow season show reductions around 40 %. At medium elevations between 1500 and 2000 m a.s.l. the largest absolute mean SWE reductions (around - 46 mm w.e.) are found, which correspond to about - 25 % from 1962 - 1990 to 1991 - 2020. Negative signals are less pronounced or absent in some regions at high elevations above 2500 m a.s.l.

Investigations regarding the distribution of mean SWE and the number of snow days within the snow season in the different elevation classes and sub-regions over the periods 1962 - 1990 and 1991 - 2020,

indicate a shift towards more snow seasons with rather low values of mean SWE and number of snow days during the latter period (subsection 3.1.4, Figure 3.11 and 3.12). Again, the signal is strongest at low elevations and less or absent at high elevations.
Also, results of the analysis of the annual cycle (subsection 3.1.3) based on monthly SWE averages suggest a change from the previous to the latter climatological period. The annual cycle shows a shortening and the monthly maximum a decline in all the sub-regions. A shift of the monthly maximum to an earlier month is visible in most sub-regions. According to previous studies (e.g. Klein et al. (2016)), the shortening is largest during the spring months (on average - 45 mm / month over MAM over Switzerland).
Looking at trends on the basis of the LOESS trend smoothing function reveal insights on the evolution of mean SWE and the number of snow days within a snow season since 1962 (subsection 3.1.6). The 30-year window, which is very smooth and therefore comparable to a hypothetical linear trend, shows a steady, light decrease of these indicators in every sub-region. On the other hand, the 10-year smoothing window reveals decadal variability. Most pronounced in every sub-region is the period of high snow amounts during the end of the 1970s / the beginning of the 1980s followed by a rather sharp decline in both variables, which is already known from other studies by Marty (2008); Laternser et al. (2003); Matiu et al. (2021).

In addition to the analyses of OSHD-CLQM revealing comparable results to previous studies, there are also limitations in OSHD-CLQM (section 3.2). For instance, an artifact south-west to Yverdon was found, for which a measurement error at a station was the cause (subsection 3.2.1). This error lead to wrong values in the RhiresD grid, which is one of the inputs of the OSHD snow model, which in turn is the baseline of OSHD-CLQM. After masking out this region, the results improve. However, some artefacts remain despite applying this correction and more errors have to be expected.
Signals revealing an increase of mean SWE are found, in particularly at high elevations. Discussions have shown that the input data grids RhiresD and TabsD of the OSHD snow model have problems due to temporal inconsistencies (subsection 3.2.2). Other uncertainties may originate from the absence of stations at elevations above 3000 m a.s.l. and thus, from the lack of assimilation data into the training data set of OSHD-CLQM. In conclusion these factors suggest that results, especially trend analyses, at high elevations and regions impacted by the inconsistencies of the model input grids, have to be interpreted with caution.

A full independent validation over the whole time horizon of OSHD-CLQM was not possible. The validation made against station-based and remote sensing observations reveal results which speak for an overall accurate performance of OSHD-CLQM. The validation against 59 snow measurement stations shows generally high correlations of the time series of the snow indicators, especially for the mean SWE (Nov - Apr), at most stations and their corresponding nearest OSHD-CLQM grid cells (the median correlation equals 0.82 for the mean SWE including all stations) (subsection 3.3.1) .
The assessment of the validation against the remote sensing data sets AVHRR (beta-version) and MODIS is more difficult as the range among the two validation data sets is large (subsection 3.3.2). Nevertheless, it is reassuring that OSHD-CLQM seems to be within this range.

To conclude, OSHD-CLQM is a good base for further analyses in the future. Once the errors in the input data grid RhiresD due to measurement errors will be corrected, the analyses should be repeated. In addition, the handling of grid cells lying at high elevations and areas impacted by inconsistencies in the input grids of the OSHD snow model should be well regarded in the future. Masking out regions impacted by larger uncertainties could be considered. In addition, further validation with the final version of AVHRR and other independent data may be envisaged.

Acknowledgments

I would like to thank my supervisors Dr. Sven Kotlarski, Dr. Regula Mülchi, Dr. Stefanie Gubler, Dr. Christian Steger and Dr. Christoph Marty for the invaluable support I have received during all steps of my Master's Thesis. I am especially grateful for the on-going day-to-day support provided by Dr. Sven Kotlarski and Dr. Regula Mülchi, in the handling, analysis and interpretation of the data, as well as during the writing process. I also highly appreciated the support of Dr. Stefanie Gubler in the case study of the SNP and of Dr. Christian Steger and Dr. Christoph Marty with the pre-processing and handling of the remote sensing data and the in-situ observations, respectively. Further, I would like to thank Prof. Dr. Christoph Schär for his inputs on the project. Dr. Michel Adrien I would like to thank for providing advice on OSHD-CLQM. Last but not least, I would like to thank Dr. Simon Scherrer for his help with the trend analysis, Dr. Christoph Frei and Dr. Francesco Isotta for their inputs regarding the identification of uncertainties in OSHD-CLQM and Dr. Helga Weber for providing the AVHRR data.

References

AMS, American Meteorological Society (2021). *Glossary of Meteorology.* URL: https://glossary.ametsoc.org/wiki/Climatology (visited on 05/01/2022).

Anghileri, D., M. Botter, A. Castelletti, H. Weigt, and P. Burlando (2018). "A Comparative Assessment of the Impact of Climate Change and Energy Policies on Alpine Hydropower". In: *Water Resources Research* 54(11), pp. 9144–9161. ISSN: 0043-1397. DOI: 10.1029/2017WR022289.

Armstrong, R.L. and E. Brun (2008). *Snow and climate: physical processes, surface energy exchange and modeling.* Cambridge University Press: Cambridge. ISBN: 9780521854542.

Beniston, M. (2012). "Is snow in the Alps receding or disappearing?" In: *Wiley Interdisciplinary Reviews: Climate Change* 3(4), pp. 349–358. ISSN: 17577780. DOI: 10.1002/wcc.179.

Beniston, M. et al. (2018). *The European mountain cryosphere: A review of its current state, trends, and future challenges.* ISSN: 19940424 Issue: 2 Publication Title: Cryosphere Volume: 12. DOI: 10.5194/tc-12-759-2018.

Brown, R.D. and D.A. Robinson (2005). "Snow and Snow Cover". In: *Encyclopedia of World Climatology.* Springer Netherlands, pp. 658–663. DOI: 10.1007/1-4020-3266-8_187.

Buchmann, M., M. Begert, S. Brönnimann, and C. Marty (2021). "Evaluating the robustness of snow climate indicators using a unique set of parallel snow measurement series". en. In: *International Journal of Climatology* 41(S1). ISSN: 0899-8418, 1097-0088. DOI: 10.1002/joc.6863.

Buchmann, M., J. Coll, J. Aschauer, M. Begert, S. Brönnimann, B. Chimani, G. Resch, W. Schöner, and C. Marty (2022). "Homogeneity assessment of Swiss snow depth series: Comparison of break detection capabilities of (semi-) automatic homogenisation methods". In: *The Cryosphere.* DOI: 10.5194/tc-16-2147-2022.

Da Ronco, P., C. De Michele, M. Montesarchio, and P. Mercogliano (2016). "Comparing COSMO-CLM simulations and MODIS data of snow cover extent and distribution over Italian Alps". en. In: *Climate Dynamics* 47(12), pp. 3955–3977. ISSN: 0930-7575, 1432-0894. DOI: 10.1007/s00382-016-3054-2.

De Valk, C.F. (2020). *Technical report; TR-389. Standard method for determining a climatological trend.* Tech. rep. Royal Netherlands Meteorological Institute, Ministry of Infrastructure and Water Management. URL: https://cdn.knmi.nl/system/ckeditor_assets/attachments/161/TR389.pdf (visited on 04/04/2023).

DeWalle, D.R. and A. Rango (2008). *Principles of snow hydrology.* Publication Title: Principles of Snow Hydrology. Cambridge University Pres. ISBN: 978-0-521-82362-3. DOI: 10.1017/CBO9780511535673.

Doesken, N.J. and D.A. Robinson (2009). "The Challenge of Snow Measurements". In: *Historical Climate Variability and Impacts in North America.* Springer Netherlands: Dordrecht, pp. 251–273. DOI: 10.1007/978-90-481-2828-0_15.

EDA, Eidgenössisches Departement für auswärtige Angelegenheiten (2021). *Geography.* URL: https://www.eda.admin.ch/aboutswitzerland/en/home/umwelt/geografie/geografie---fakten-und-zahlen.html (visited on 04/03/2023).

Egli, L. (2008). "Spatial variability of new snow amounts derived from a dense network of Alpine automatic stations". en. In: *Annals of Glaciology* 49, pp. 51–55. ISSN: 0260-3055, 1727-5644. DOI: 10.3189/172756408787814843.

Elsasser, H. and R. Bürki (2002). "Climate change as a threat to tourism in the Alps". In: *Climate Research* 20(3). ISSN: 0936577X. DOI: 10.3354/cr020253.

ESA, The European Space Agency (2023). *Land use map for Switzerland.* URL: https://www.esa.int/ESA_Multimedia/Images/2005/11/Land_use_map_for_Switzerland (visited on 02/23/2023).

Göldi, M. (2021). "Spatial snow climatologies for Switzerland: Intercomparison and validation". Place: Zürich Publisher: ETH Zürich. MA thesis.

Groisman, P.Y. and T.D. Davies (2001). "Snow Cover and the Climate System". In: *Snow ecology: An Interdisciplinary Examination of Snow-Covered Ecosystems.*

Grünewald, T., Y. Bühler, and M. Lehning (2014). "Elevation dependency of mountain snow depth". In: *Cryosphere* 8(6). ISSN: 19940424. DOI: 10.5194/tc-8-2381-2014.

Gutzler, D. S. and R.D. Rosen (1992). "Interannual Variability of Wintertime Snow Cover across the Northern Hemisphere". In: *Journal of Climate* 5(12). ISSN: 0894-8755. DOI: 10.1175/1520-0442(1992)005<1441:ivowsc>2.0.co;2.

Haberkorn, A. (2019). *European Snow Booklet (ESB) – an Inventory of Snow Measurements in Europe.* EnviDat. URL: https://www.envidat.ch/dataset/european-snow-booklet (visited on 04/04/2023).

Hall, A. (2004). "The role of surface albedo feedback in climate". In: *Journal of Climate* 17(7). ISSN: 08948755. DOI: 10.1175/1520-0442(2004)017<1550:TROSAF>2.0.CO;2.

Haller, H., A. Eisenhut, and R. Haller (2014). *Atlas des Schweizerischen Nationalparks. Die ersten 100 Jahre.* Haupt Verlag: Bern.

Hüsler, F., T. Jonas, M. Riffler, J. P. Musial, and S. Wunderle (2014). "A satellite-based snow cover climatology (1985-2011) for the European Alps derived from AVHRR data". In: *Cryosphere* 8(1). ISSN: 19940416. DOI: 10.5194/tc-8-73-2014.

IPCC (2021). *IPCC Climate Change 2021: The Physical Science Basis*. Tech. rep. ISBN: 978-92-9169-158-6. Working Group I Contribution to the Sixth Assessment Report of the Intergovernmental Panel on Climate Change Summary for Policymakers. URL: www.ipcc.ch.

Jiang, Y., F. Chen, Y. Gao, C. He, M. Barlage, and W. Huang (2020). "Assessment of Uncertainty Sources in Snow Cover Simulation in the Tibetan Plateau". en. In: *Journal of Geophysical Research: Atmospheres* 125(18). ISSN: 2169-897X, 2169-8996. DOI: 10.1029/2020JD032674.

Jonas, T., C. Marty, and J. Magnusson (2009). "Estimating the snow water equivalent from snow depth measurements in the Swiss Alps". In: *Journal of Hydrology* 378(1-2). ISSN: 00221694. DOI: 10.1016/j.jhydrol.2009.09.021.

Klein, G., Y. Vitasse, C. Rixen, C. Marty, and M. Rebetez (2016). "Shorter snow cover duration since 1970 in the Swiss Alps due to earlier snowmelt more than to later snow onset". In: *Climatic Change* 139(3-4), pp. 637–649. ISSN: 0165-0009. DOI: 10.1007/s10584-016-1806-y.

Kotlarski, S., A. Gobiet, S. Morin, M. Olefs, J. Rajczak, and R. Samacoïts (2022). "21st Century alpine climate change". In: *Climate Dynamics 2022* 1. ISBN: 0123456789 Publisher: Springer, pp. 1–22. ISSN: 1432-0894. DOI: 10.1007/S00382-022-06303-3.

Laternser, M. and M. Schneebeli (2003). "Long-term snow climate trends of the Swiss Alps (1931-99)". en. In: *International Journal of Climatology* 23(7), pp. 733–750. ISSN: 0899-8418, 1097-0088. DOI: 10.1002/joc.912.

Lehning, M., H. Löwe, M. Ryser, and N. Raderschall (2008). "Inhomogeneous precipitation distribution and snow transport in steep terrain: Snow drift and inhomogeneous precipitation". en. In: *Water Resources Research* 44(7). ISSN: 00431397. DOI: 10.1029/2007WR006545.

Luetschg, M., M. Lehning, and W. Haeberli (2008). "A sensitivity study of factors influencing warm/thin permafrost in the Swiss Alps". In: *Journal of Glaciology* 54(187). ISSN: 00221430. DOI: 10.3189/002214308786570881.

Magnusson, J., D. Gustafsson, F. Hüsler, and T. Jonas (2014). "Assimilation of point SWE data into a distributed snow cover model comparing two contrasting methods". In: *Water Resources Research* 50(10). ISSN: 19447973. DOI: 10.1002/2014WR015302.

Marty, C. (2008). "Regime shift of snow days in Switzerland". In: *Geophysical Research Letters* 35(12). ISSN: 00948276. DOI: 10.1029/2008GL033998.

Marty, C., S. Schlögl, M. Bavay, and M. Lehning (2017a). "How much can we save? Impact of different emission scenarios on future snow cover in the Alps". In: *Cryosphere* 11(1). ISSN: 19940424. DOI: 10.5194/tc-11-517-2017.

Marty, C., A.M. Tilg, and T. Jonas (2017b). "Recent evidence of large-scale receding snow water equivalents in the European alps". In: *Journal of Hydrometeorology* 18(4). ISSN: 15257541. DOI: 10.1175/JHM-D-16-0188.1.

Matiu, M. and F. Hanzer (2022). “Bias adjustment and downscaling of snow cover fraction projections from regional climate models using remote sensing for the European Alps”. en. In: *Hydrology and Earth System Sciences* 26(12), pp. 3037–3054. ISSN: 1607-7938. DOI: 10.5194/hess-26-3037-2022.

Matiu, M., A. Jacob, and C. Notarnicola (2019). “Daily MODIS Snow Cover Maps for the European Alps from 2002 onwards at 250 m Horizontal Resolution Along with a Nearly Cloud-Free Version”. en. In: *Data* 5(1), p. 1. ISSN: 2306-5729. DOI: 10.3390/data5010001. URL: https://zenodo.org/record/3601891 (visited on 04/04/2023).

Matiu, M. et al. (2021). “Observed snow depth trends in the European Alps: 1971 to 2019”. In: *Cryosphere* 15(3). ISSN: 19940424. DOI: 10.5194/tc-15-1343-2021.

MeteoSwiss, Federal Office of Meteorology and Climatology (2018). *National Climate Observing System (GCOS Switzerland)*. Tech. rep. URL: https://www.meteoswiss.admin.ch/services-and-publications/publications/scientific-publications/2018/national-climate-observing-system.html.

MeteoSwiss, Federal Office of Meteorology and Climatology (2021a). *Daily Mean, Minimum and Maximum Temperature: TabsD, TminD, TmaxD*. Publication Title: Documentation of MeteoSwiss Grid-Data Products. URL: https://www.meteoswiss.admin.ch/dam/jcr:818a4d17-cb0c-4e8b-92c6-1a1bdf5348b7/ProdDoc_TabsD.pdf (visited on 02/22/2023).

MeteoSwiss, Federal Office of Meteorology and Climatology (2021b). *Daily Precipitation (final analysis): RhiresD*. Publication Title: Documentation of MeteoSwiss Grid-Data Products. URL: https://www.meteoswiss.admin.ch/dam/jcr:4f51f0f1-0fe3-48b5-9de0-15666327e63c/ProdDoc_RhiresD.pdf (visited on 02/22/2023).

MeteoSwiss, Federal Office of Meteorology and Climatology (2021c). *Daily, Monthly and Yearly Norm Temperature (1991-2020): TnormD9120, TnormM9120 and TnormY9120*. Publication Title: Documentation of MeteoSwiss Grid-Data Products. URL: https://www.meteoschweiz.admin.ch/dam/jcr:c6e697aa-194b-41d6-bb8b-d85085a01b4e/ProdDoc_TnormM9120.pdf (visited on 02/28/2023).

MeteoSwiss, Federal Office of Meteorology and Climatology (2021d). *Klimabulletin Januar 2021*. URL: https://www.meteoschweiz.admin.ch/service-und-publikationen/publikationen/berichte-und-bulletins/2021/klimabulletin-januar-2021.html (visited on 02/09/2023).

MeteoSwiss, Federal Office of Meteorology and Climatology (2021e). *Monthly and Yearly Precipitation: RhiresM and RhiresY*. Publication Title: Documentation of MeteoSwiss Grid-Data Products. URL: https://www.meteoschweiz.admin.ch/dam/jcr:d4f53a4a-d7f4-4e1e-a594-8ff4bfd1aca5/ProdDoc_RhiresM.pdf (visited on 02/28/2023).

MeteoSwiss, Federal Office of Meteorology and Climatology (2021f). *Projektinitialisierungsauftrag - SPASS – A Spatial Snow Climatology for Switzerland.*

MeteoSwiss, Federal Office of Meteorology and Climatology (2022a). *Climate normals*. URL: https://www.meteoswiss.admin.ch/weather/weather-and-climate-from-a-to-z/climate-normals.html (visited on 01/02/2023).

MeteoSwiss, Federal Office of Meteorology and Climatology (2022b). *GCOS Switzerland projects.* URL: https://www.meteoschweiz.admin.ch/ueber-uns/forschung-und-zusammenarbeit/internationale-zusammenarbeit/gcos/gcos-switzerland-projects.html (visited on 01/03/2023).

Miao, X., W. Guo, B. Qiu, S. Lu, Y. Zhang, Y. Xue, and S. Sun (2022). "Accounting for Topographic Effects on Snow Cover Fraction and Surface Albedo Simulations Over the Tibetan Plateau in Winter". en. In: *Journal of Advances in Modeling Earth Systems* 14(8). ISSN: 1942-2466, 1942-2466. DOI: 10.1029/2022MS003035.

Michel, A., J. Aschauer, T. Jonas, S. Gubler, S. Kotlarski, and C. Marty (2023). "SnowQM 1.0: A fast R Package for bias-correcting spatial fields of snow water equivalent using quantile mapping". In: *Geoscientific Model Development (GMD), in review.*

Morán-Tejeda, E., J.I. López-Moreno, and M. Beniston (2013). "The changing roles of temperature and precipitation on snowpack variability in Switzerland as a function of altitude". en. In: *Geophysical Research Letters* 40(10), pp. 2131–2136. ISSN: 00948276. DOI: 10.1002/grl.50463.

Neukom, R. (2006). "Flächige Visualisierung der Schneedecke im Vergleich zum langjährigen Mittel". Diplomarbeit. ETH Zürich.

Nitta, T., K. Yoshimura, K. Takata, R. O'ishi, T. Sueyoshi, S. Kanae, T. Oki, A. Abe-Ouchi, and G. E. Liston (2014). "Representing Variability in Subgrid Snow Cover and Snow Depth in a Global Land Model: Offline Validation". en. In: *Journal of Climate* 27(9), pp. 3318–3330. ISSN: 0894-8755, 1520-0442. DOI: 10.1175/JCLI-D-13-00310.1.

Norris, J.R. and M. Wild (2007). "Trends in aerosol radiative effects over Europe inferred from observed cloud cover, solar "dimming," and solar "brightening"". en. In: *Journal of Geophysical Research* 112(D8), p. D08214. ISSN: 0148-0227. DOI: 10.1029/2006JD007794.

OSHD, operational snow-hydrological service (2023). *The SLF's operational snow-hydrological models.* URL: https://www.slf.ch/en/snow/snow-as-a-water-resource/snow-hydrological-forecasting/oshd-models.html (visited on 03/27/2023).

Philipona, R., C. Marty, B. Duerr, and A. Ohmura (Jan. 2023). "Rising solar and thermal greenhouse radiation drive rapid warming over the continents". en. In: *Meteorologische Zeitschrift.* ISSN: , DOI: 10.1127/metz/2022/1148.

Rabiei, E. and U. Haberlandt (2015). "Applying bias correction for merging rain gauge and radar data". In: *Journal of Hydrology* 522, pp. 544–557. ISSN: 00221694. DOI: 10.1016/j.jhydrol.2015.01.020.

Rebetez, M. and M. Reinhard (2008). "Monthly air temperature trends in Switzerland 1901–2000 and 1975–2004". en. In: *Theoretical and Applied Climatology* 91(1-4), pp. 27–34. ISSN: 0177-798X, 1434-4483. DOI: 10.1007/s00704-007-0296-2.

Robeson, S.M. (2005). "Statistical climatology". In: *Encyclopedia of Earth Sciences Series.* ISSN: 1871756X. DOI: 10.1007/1-4020-3266-8_198.

Sanchez-Lorenzo, A. and M. Wild (2012). "Decadal variations in estimated surface solar radiation over Switzerland since the late 19th century". en. In: *Atmospheric Chemistry and Physics* 12(18), pp. 8635–8644. ISSN: 1680-7324. DOI: 10.5194/acp-12-8635-2012.

Scherrer, S.C. and C. Appenzeller (2006). "Swiss alpine snow pack variability: Major patterns and links to local climate and large-scale flow". In: *Climate Research* 32(3). ISSN: 0936577X. DOI: 10.3354/cr032187.

Scherrer, S.C., M. Begert, and M. Croci-Maspoli (2023). *Eine neue Beschreibung des Klimaverlaufs und Bestimmung des aktuellen Klimazustands.* Fachbericht MeteoSchweiz 285. MeteoSchweiz, p. 24. URL: https://doi.org/10.18751/PMCH/TR/285.KlimaVerlauf/1.0.

Scherrer, S.C., P. Ceppi, M. Croci-Maspoli, and C. Appenzeller (2012). "Snow-albedo feedback and Swiss spring temperature trends". In: *Theoretical and Applied Climatology* 110(4). ISSN: 14344483. DOI: 10.1007/s00704-012-0712-0.

Scherrer, S.C., C. Wüthrich, M. Croci-Maspoli, R. Weingartner, and C. Appenzeller (2013). "Snow variability in the Swiss Alps 1864-2009". In: *International Journal of Climatology* 33(15). ISSN: 10970088. DOI: 10.1002/joc.3653.

Schweizerischer Nationalpark (2022). *Zahlen und Fakten.* URL: https://www.nationalpark.ch/de/about/ueber-uns/naturoase/zahlen-und-fakten/ (visited on 12/20/2022).

Serquet, G., C. Marty, J.P. Dulex, and M. Rebetez (2011). "Seasonal trends and temperature dependence of the snowfall/precipitation-day ratio in Switzerland: snowfall/precipitation-day ratio in Switzerland". en. In: *Geophysical Research Letters* 38(7), n/a–n/a. ISSN: 00948276. DOI: 10.1029/2011GL046976. (Visited on 02/10/2023).

Sippel, S., E.M. Fischer, S.C. Scherrer, N. Meinshausen, and R. Knutti (Aug. 2020). "Late 1980s abrupt cold season temperature change in Europe consistent with circulation variability and long-term warming". en. In: *Environmental Research Letters* 15(9), p. 094056. ISSN: 1748-9326. DOI: 10.1088/1748-9326/ab86f2.

SLF, WSL-Institut für Schnee-und Lawinenforschung SLF (2022a). *Division into regions.* URL: https://www.slf.ch/en/avalanche-bulletin-and-snow-situation/about-the-avalanche-bulletin/division-into-regions.html (visited on 04/21/2022).

SLF, WSL-Institut für Schnee-und Lawinenforschung SLF (2023a). *Information about snow measurement.* URL: https://www.slf.ch/en/avalanche-bulletin-and-snow-situation/measured-values/information-about-snow-measurement.html (visited on 01/02/2023).

SLF, WSL-Institut für Schnee-und Lawinenforschung SLF (2022b). *Schnee und Lawinen in den Schweizer Alpen 2000/01.* URL: https://www.slf.ch/de/lawinenbulletin-und-schneesituation/wochen-und-winterberichte/200001/winterbericht.html (visited on 12/25/2022).

SLF, WSL-Institut für Schnee-und Lawinenforschung SLF (2023b). *Snow and climate change.* URL: https://www.slf.ch/en/snow/snow-and-climate-change.html (visited on 03/12/2023).

Stähli, M. and D. Gustafsson (2006). "Long-term investigations of the snow cover in a subalpine semi-forested catchment". In: *Hydrological Processes* 20(2), pp. 411–428. ISSN: 0885-6087. DOI: 10.1002/hyp.6058.

Steger, C., S. Kotlarski, T. Jonas, and C. Schär (2013). "Alpine snow cover in a changing climate: A regional climate model perspective". In: *Climate Dynamics* 41(3-4). ISSN: 09307575. DOI: 10.1007/s00382-012-1545-3.

Weber, H. and S. Wunderle (2022). *GCOS Switzerland Project: Fractional snow cover time series (1981 – 2021) – a novel dataset from space to support climate studies in Switzerland - Final Report*. Tech. rep. Bern. URL: https://www.meteoswiss.admin.ch/dam/jcr:391750ca-cf20-4a0b-8000-68be092b4f3c/Fractional_snow_cover_time_series-_final_project_report_2022.pdf (visited on 02/22/2023).

Winkler, M., H. Schellander, and S. Gruber (2021). "Snow water equivalents exclusively from snow depths and their temporal changes: the snow model". In: *Hydrology and Earth System Sciences* 25(3), pp. 1165–1187. ISSN: 1607-7938. DOI: 10.5194/hess-25-1165-2021.

Wirz, V., M. Schirmer, S. Gruber, and M. Lehning (2011). "Spatio-temporal measurements and analysis of snow depth in a rock face". In: *The Cryosphere* 5(4), pp. 893–905. ISSN: 1994-0424. DOI: 10.5194/tc-5-893-2011.

WMO, World Meteorological Organization (2007). *The role of climatological normals in a changing climate*. WMO/TD. WMO: Geneva. URL: https://library.wmo.int/doc_num.php?explnum_id=4546 (visited on 04/04/2023).

WMO, World Meteorological Organization (2017). *WMO Guidelines on the Calculation of Climate Normals — World Meteorological Organization*. ISBN: 978-92-63-11203-3. URL: https://public.wmo.int/en/resources/library/wmo-guidelines-calculation-of-climate-normals (visited on 04/03/2022).

WSL (2012). *Alpine Schnee- und Wasserressourcen gestern, heute, morgen*. Tech. rep. Eidgenössische Forschungsanstalt für Wald, Schnee und Landschaft WSL. URL: https://www.wsl.ch/de/publikationen/alpine-schnee-und-wasserressourcen-gestern-heute-morgen.html.

Appendices

Appendix A

Grid cell distribution

Table A.1: Number of grid cells for every height class [m a.s.l.] in every sub-region.

# number of grid cells (Sub-) Region — Height class	<500	500-1000	1000-1500	1500-2000	2000-2500	>2500	Total
Switzerland	6975	12549	6635	5638	5425	4325	41547
Northern Switzerland	6532	11989	5780	4396	3912	3277	35886
Southern Switzerland	443	560	855	1242	1513	1048	5661
Jura	828	2093	1301	17	0	0	4239
Swiss Plateau	4717	6116	96	0	0	0	10929
North-Western Alpine Slope	188	1565	1631	1309	593	440	5726
North-Central Alpine Slope	288	858	850	595	424	207	3222
North-Eastern Alpine Slope	427	669	680	546	300	74	2696
Valais	82	334	541	826	1171	1865	4819
Northern and central Grisons	2	354	681	1103	1424	691	4255
Engadin	0	17	151	459	875	892	2394
Ticino	443	543	704	783	638	156	3267

Appendix B

Station names

Table B.1: Overview of the stations used for the validation (station abbreviation and station name).

Abbr.	Name	Abbr.	Name	Abbr.	Name
***BAS**	Basel-Binningen	**3FB**	Flumserberg	**1GD**	Grindel
***OTL**	Locarno-Monti	**1AD**	Adelboden	***BUF**	Buffalora
***AIG**	Aigle	**4UL**	Ulrichen	**4RU**	Ruinettes
***BUS**	Buchs-Suhr	**7ST**	Sta.Maria	**4KU**	Kühboden
***GVE**	Geneve-Cointrin	**5OB**	Obersaxen	**CMA2**	La Fuorcla
***KLO**	Zürich-Kloten	**2AN**	Andermatt	**PMA2**	Colms da Parsonz
***LUZ**	Luzern	**4SM**	Simplon Dorf	**5WJ**	Weissfluhjoch
***KOP**	Öschberg-Koppigen	**1JA**	Jaunpass	**DIA2**	Tsanfleuron
***LAN**	Landquart	**6BG**	Bosco Gurin	**GOR2**	Gornergratsee
***BER**	Bern-Zollikofen	**4GR**	Grimentz		
***GRA**	Fribourg-Posieux	**5DF**	Davos Flüelastr.		
***VIS**	Visp	**4MO**	Montana		
***MAS**	Marsens	**4ZE**	Zermatt		
***LAG**	Langnau i.E.	**6SB**	San Bernardino		
***STG**	St. Gallen	**1MR**	Mürren		
1LB	Lauterbrunnen	**7ZU**	Zuoz		
***ELM**	Elm	**7SD**	Samedan		
***CHD**	Chateau d'Oex	**2TR**	Trübsee		
***CDF**	La Chaux-de-Fonds	**1HB**	Hasliberg		
2EN	Engelberg	**MTR2**	MTR2		
***GTT**	Guttannen	**5KK**	Klosters KW		
***ROB**	Robbia	**2ST**	Stoos		
***GOS**	Göschenen	***SCU**	Scuol		
***AIR**	Airolo	**1LS**	Leysin		
***CUE**	La Cure	**3BR**	Braunwald		

Appendix C

Monthly overview

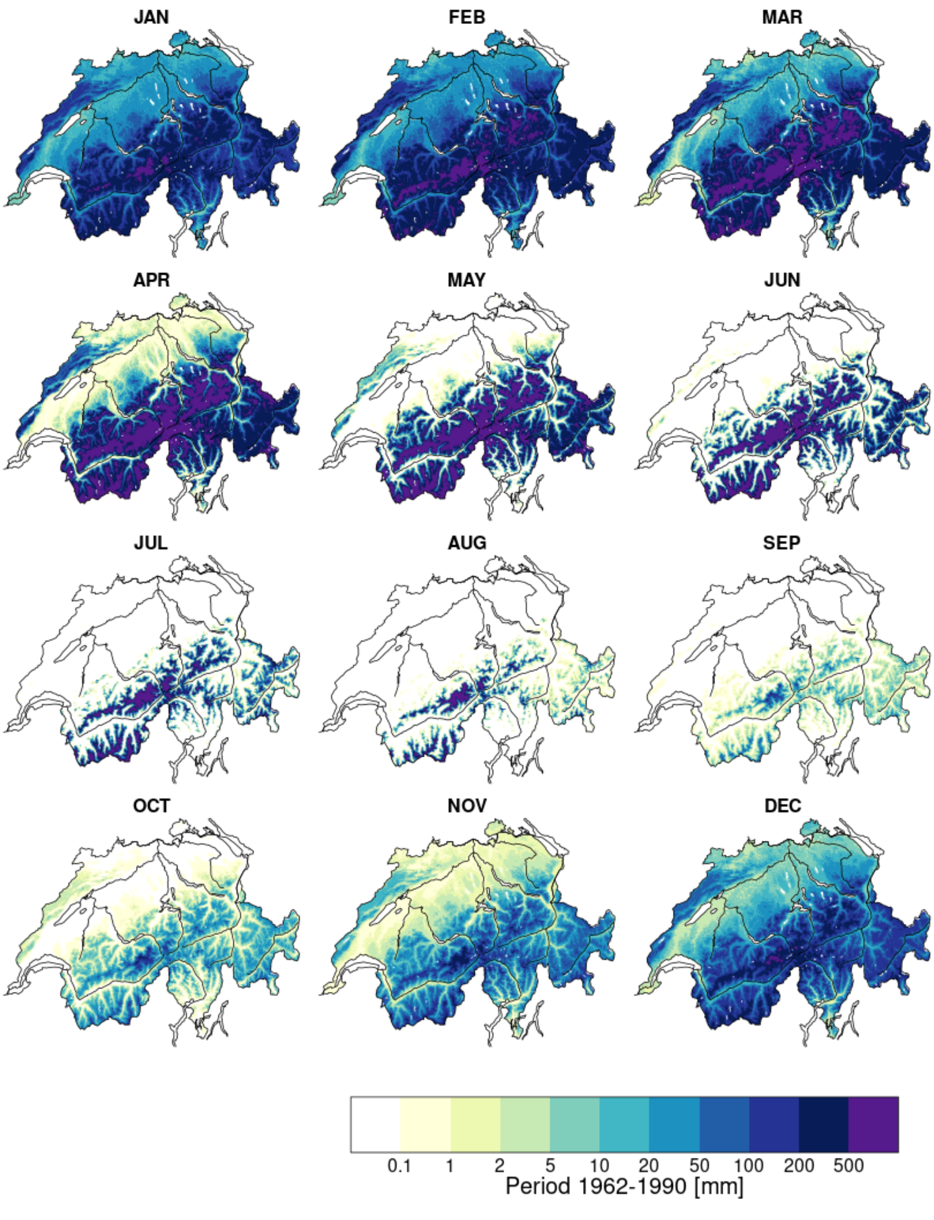

Figure C.1: Monthly SWE climatology between 1962 and 1990.

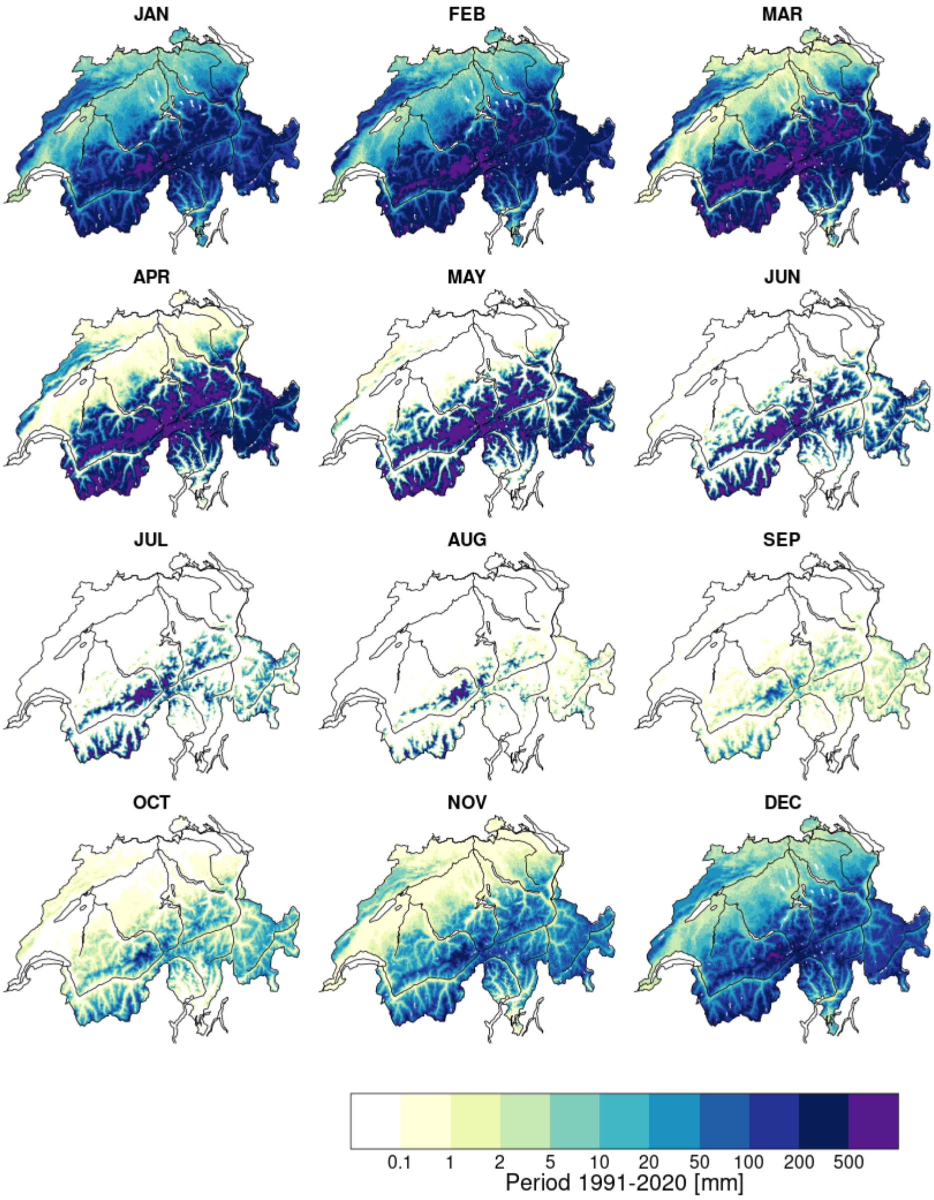

Figure C.2: Monthly SWE climatology between 1991 and 2020.

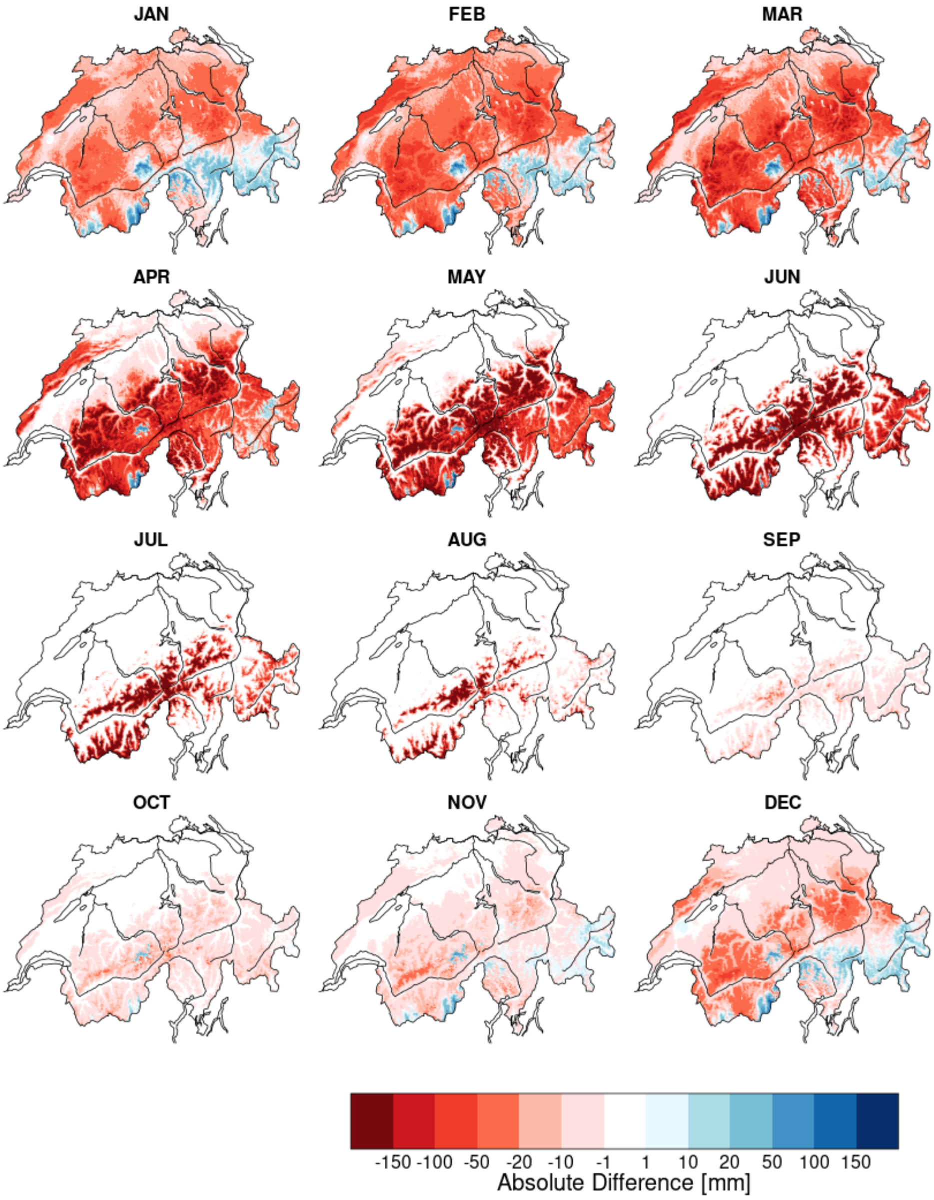

Figure C.3: Absolute monthly SWE difference between the period 1962 - 1990 and 1991 - 2020 (in mm w.e.). Reference period: 1962 - 1990.

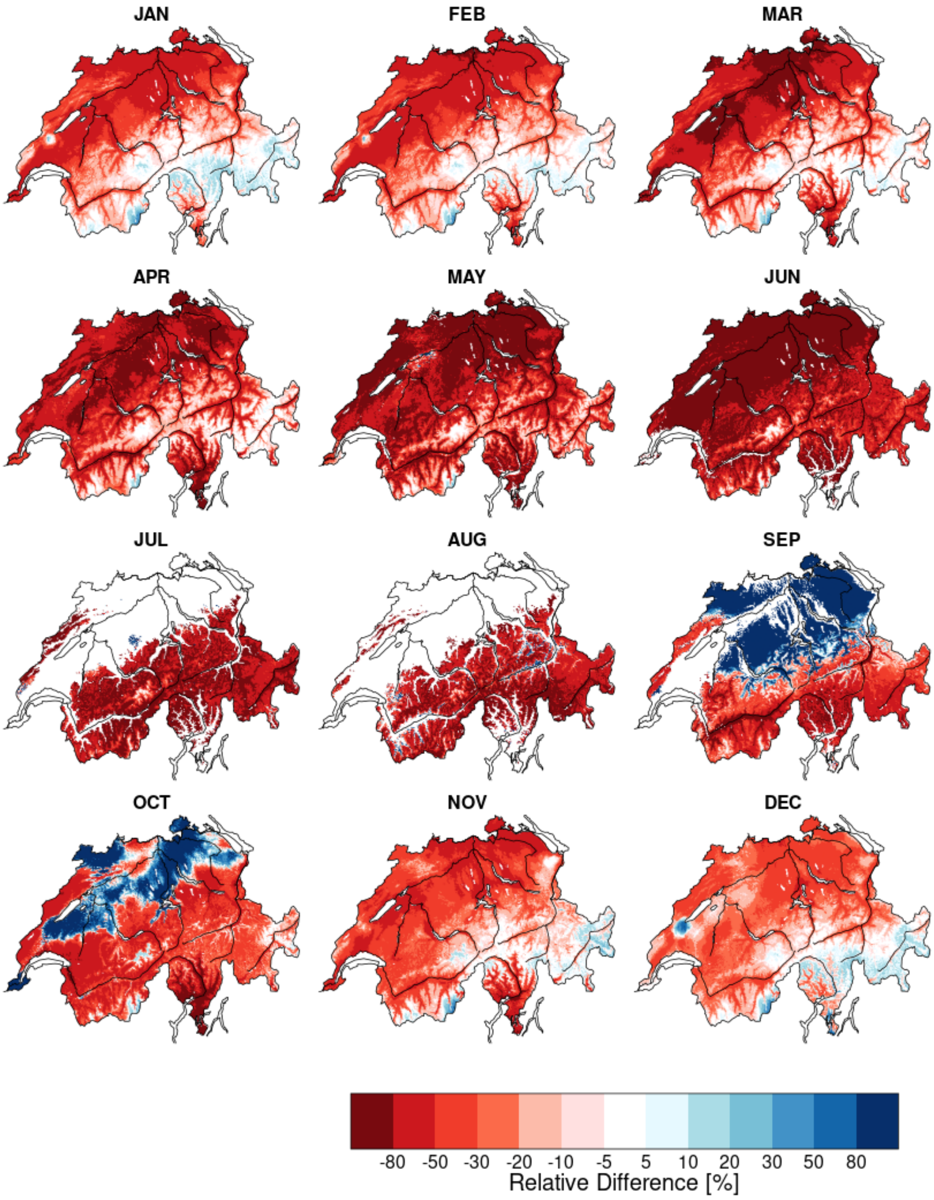

Figure C.4: Relative monthly SWE difference between the period 1962 - 1990 and 1991 - 2020 (in %). Reference period: 1962 - 1990.

Appendix D

Mean SWE over snow seasons

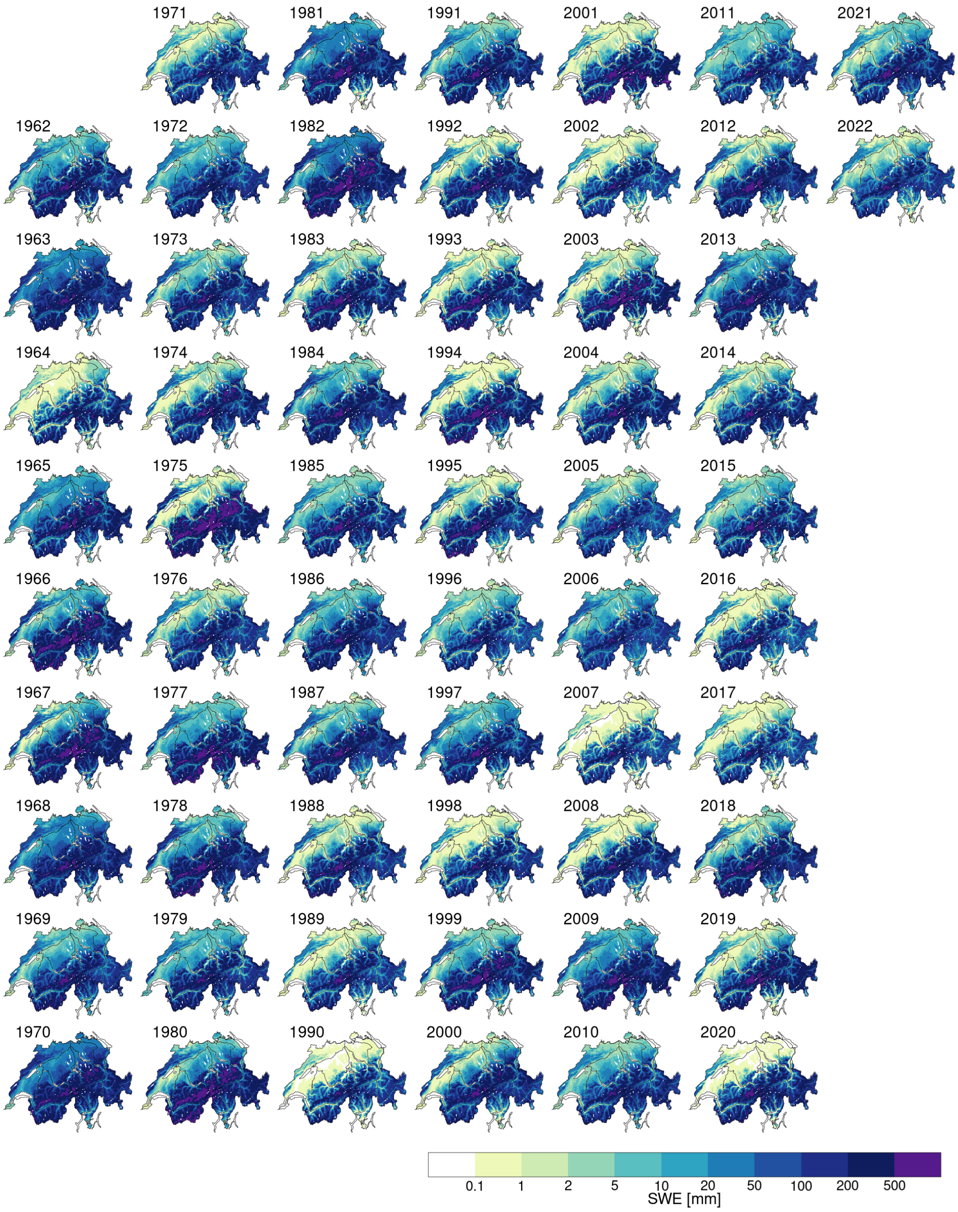

Figure D.1: Mean SWE in mm w.e. over Switzerland for the snow seasons 1962 - 2022.

Appendix E

Annual anomaly patterns

E.1 OSHD-EKF

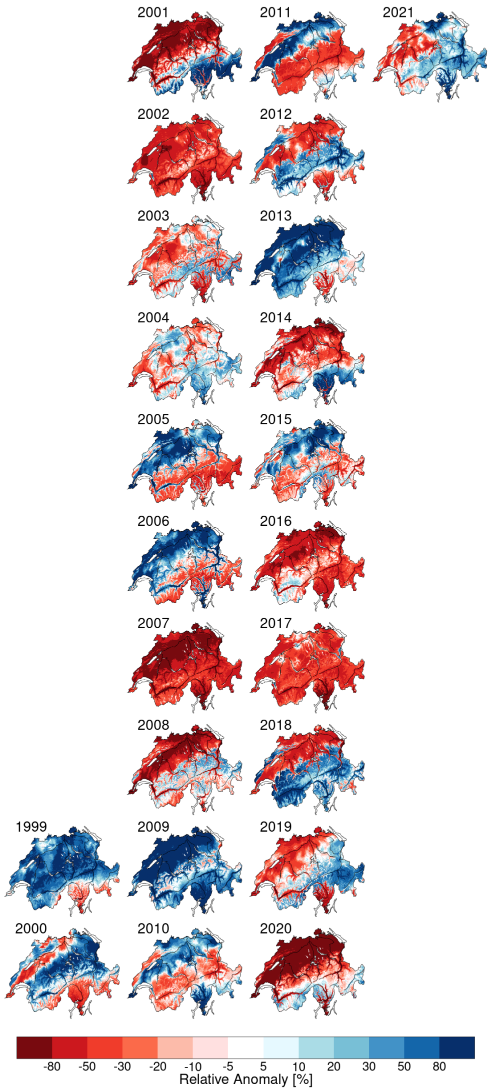

Figure E.1: OSHD-EKF data set. Relative SWE anomaly for the snow seasons 1999 to 2021 (in %). Reference period: 1999 - 2020.

E.2 OSHD-CL

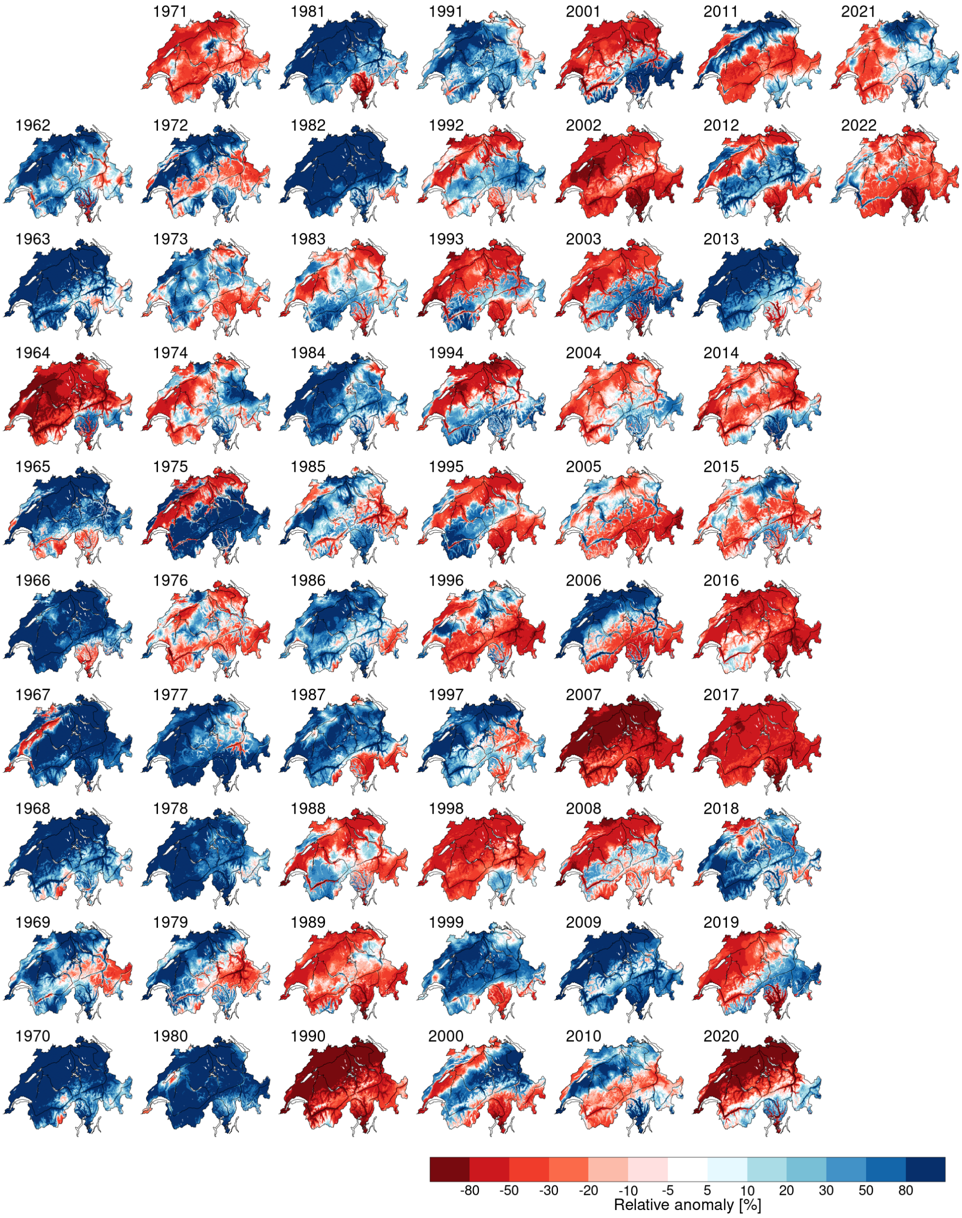

Figure E.2: OSHD-CL data set. Relative anomaly for hydrological years 1962 to 2022 (in %). Reference period: 1999-2020.

E.3 OSHD-CLQM

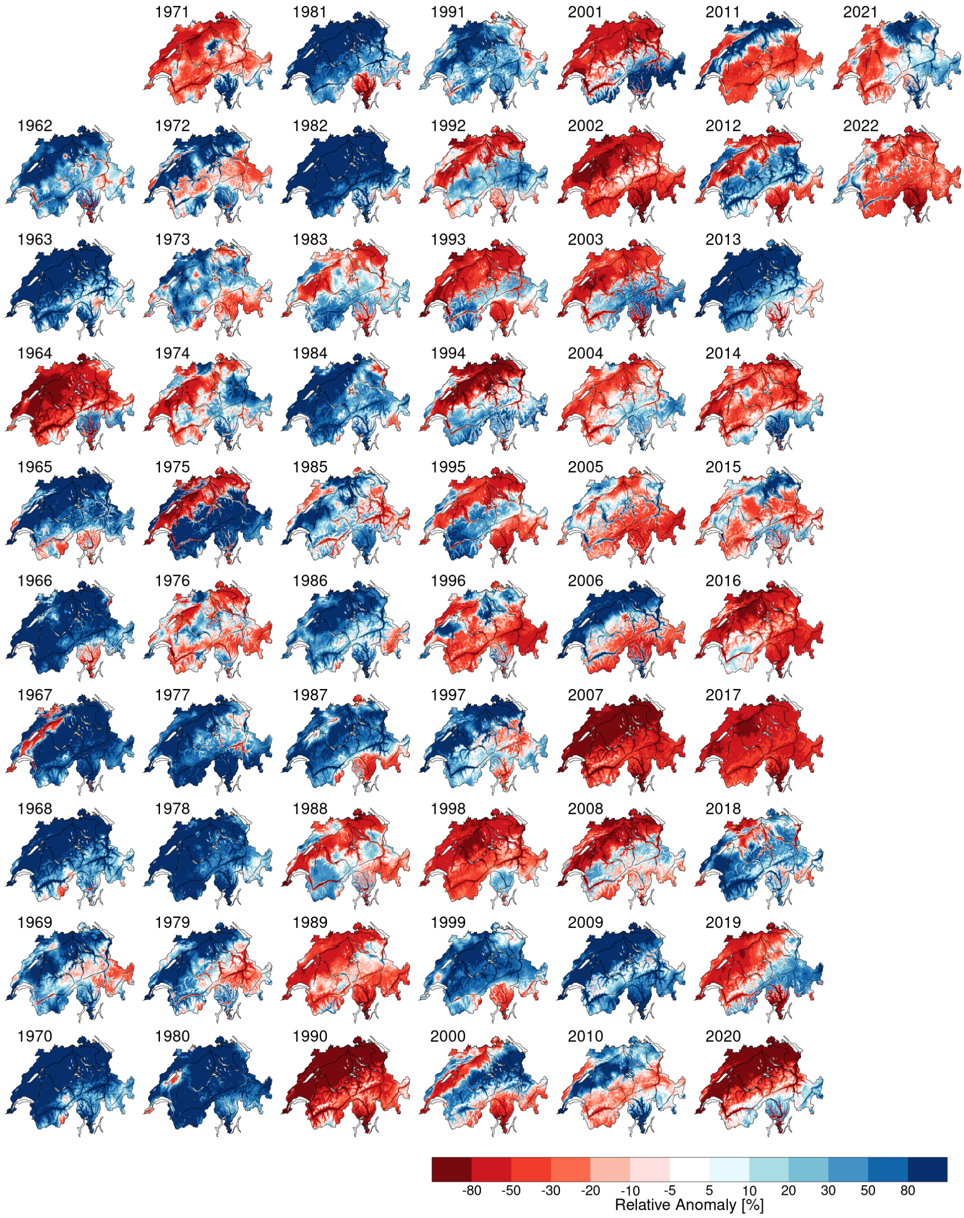

Figure E.3: OSHD-CLQM data set. Relative anomaly for hydrological years 1962 to 2022 (in %). Reference period: 1999-2020.

Appendix F

Trends

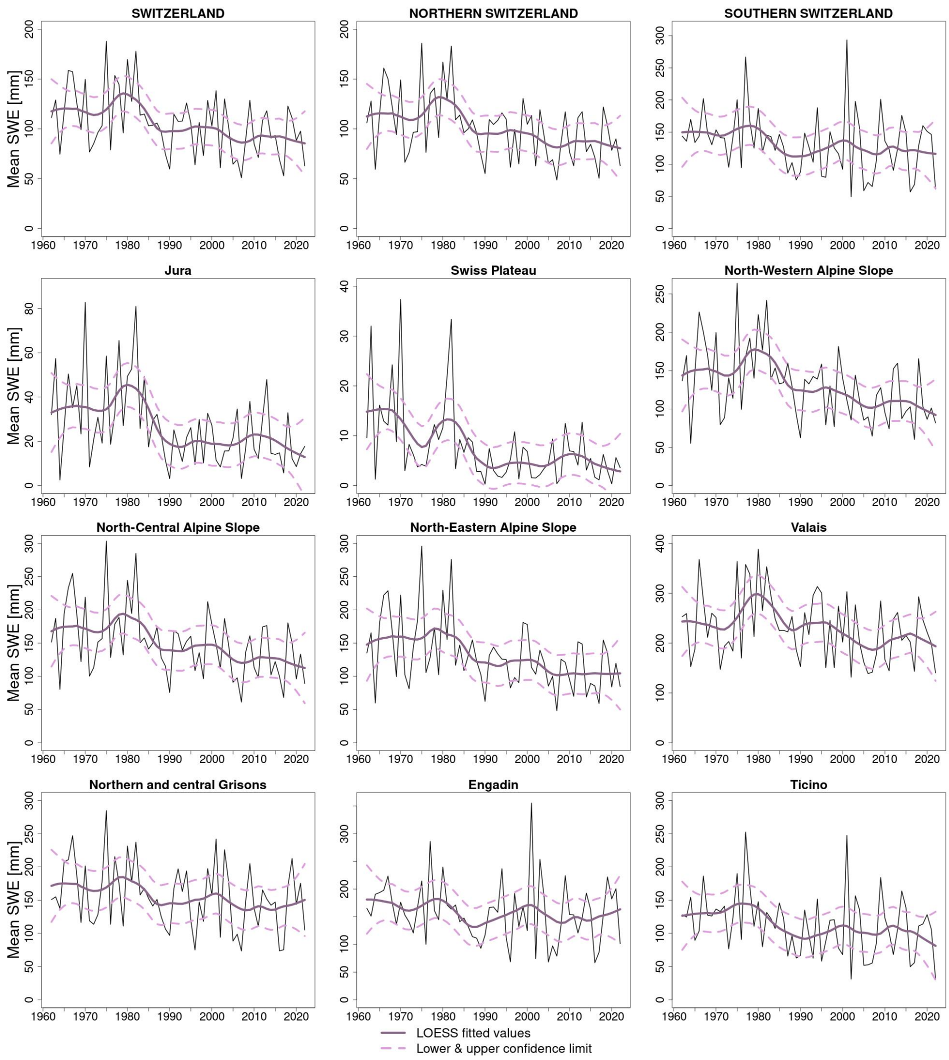

Figure F.1: LOESS smoothing trend line (De Valk (2020); Scherrer et al. (2023)) applied on the time series of the mean SWE (Sep-May). Black: time series of the mean SWE. Solid purple line: applied 10-year LOESS smoothing function. Dashed purple lines: lower and upper confidence limit of the LOESS smoothing function.

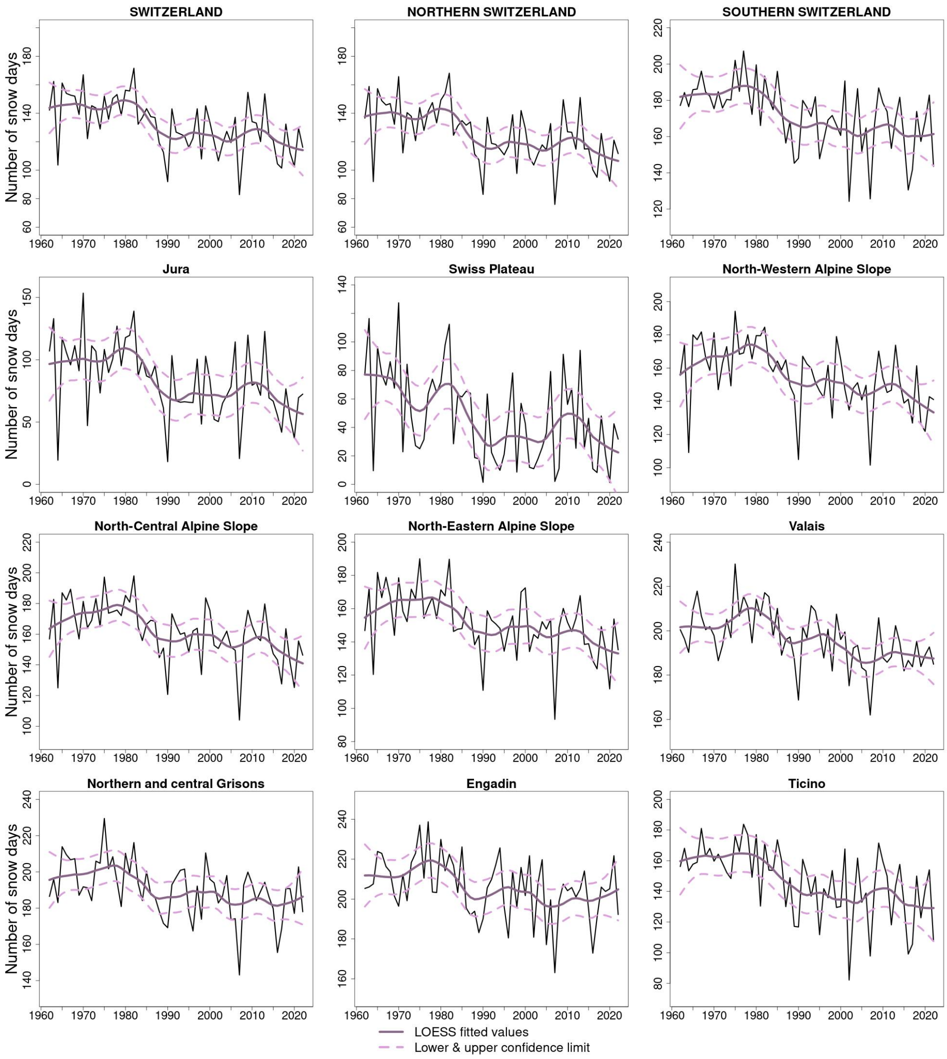

Figure F.2: LOESS smoothing trend line (De Valk (2020); Scherrer et al. (2023)) applied on the time series of the mean number of snow days within a snow season. Black: time series of the mean number of snow days within a snow season. Solid purple line: applied 10-year LOESS smoothing function. Dashed purple lines: lower and upper confidence limit of the LOESS smoothing function.

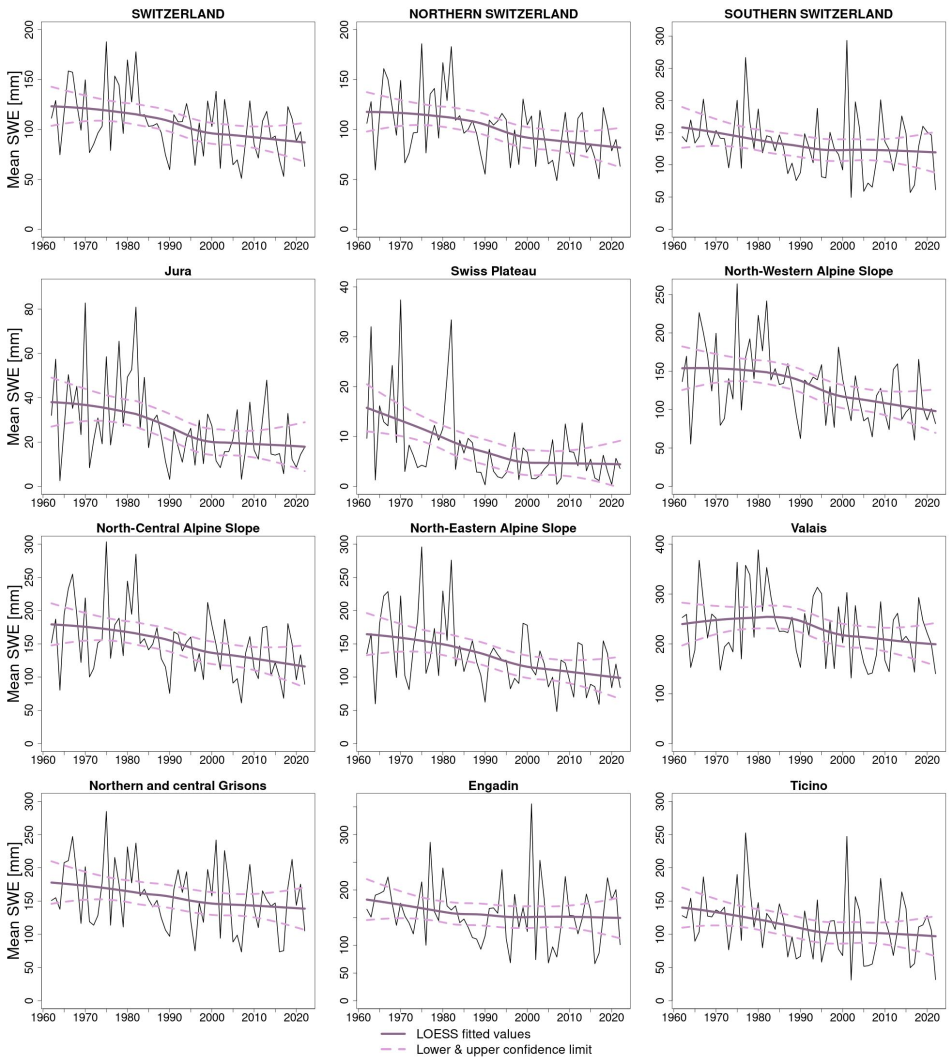

Figure F.3: LOESS smoothing trend line applied (De Valk (2020); Scherrer et al. (2023)) on the time series of the mean SWE (Sep-May). Black: time series of the mean SWE. Solid purple line: applied 30-year LOESS smoothing function. Dashed purple lines: lower and upper confidence limit of the LOESS smoothing function.

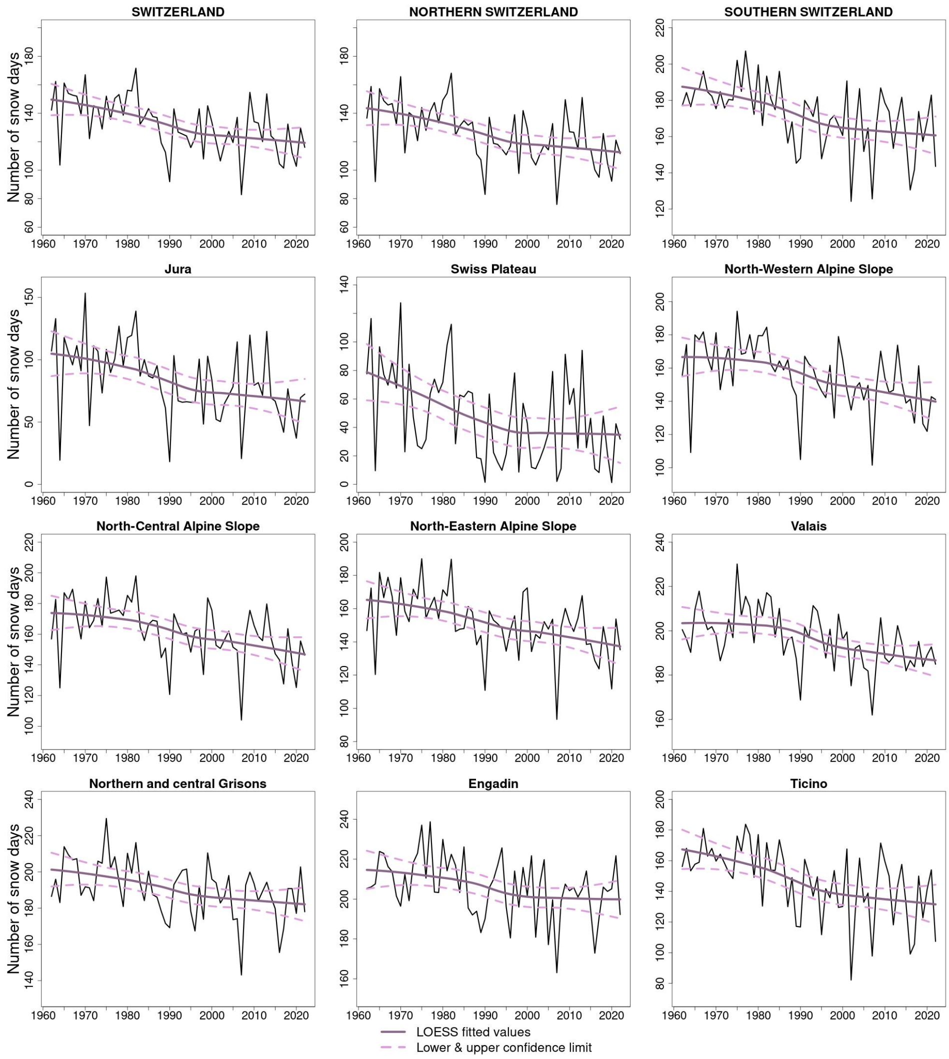

Figure F.4: LOESS smoothing trend line (De Valk (2020); Scherrer et al. (2023)) applied on the time series of the mean number of snow days within a snow season. Black: time series of the mean number of snow days within a snow season. Solid purple line: applied 30-year LOESS smoothing function. Dashed purple lines: lower and upper confidence limit of the LOESS smoothing function.

Appendix G

Seasonal uncertainties from input grids

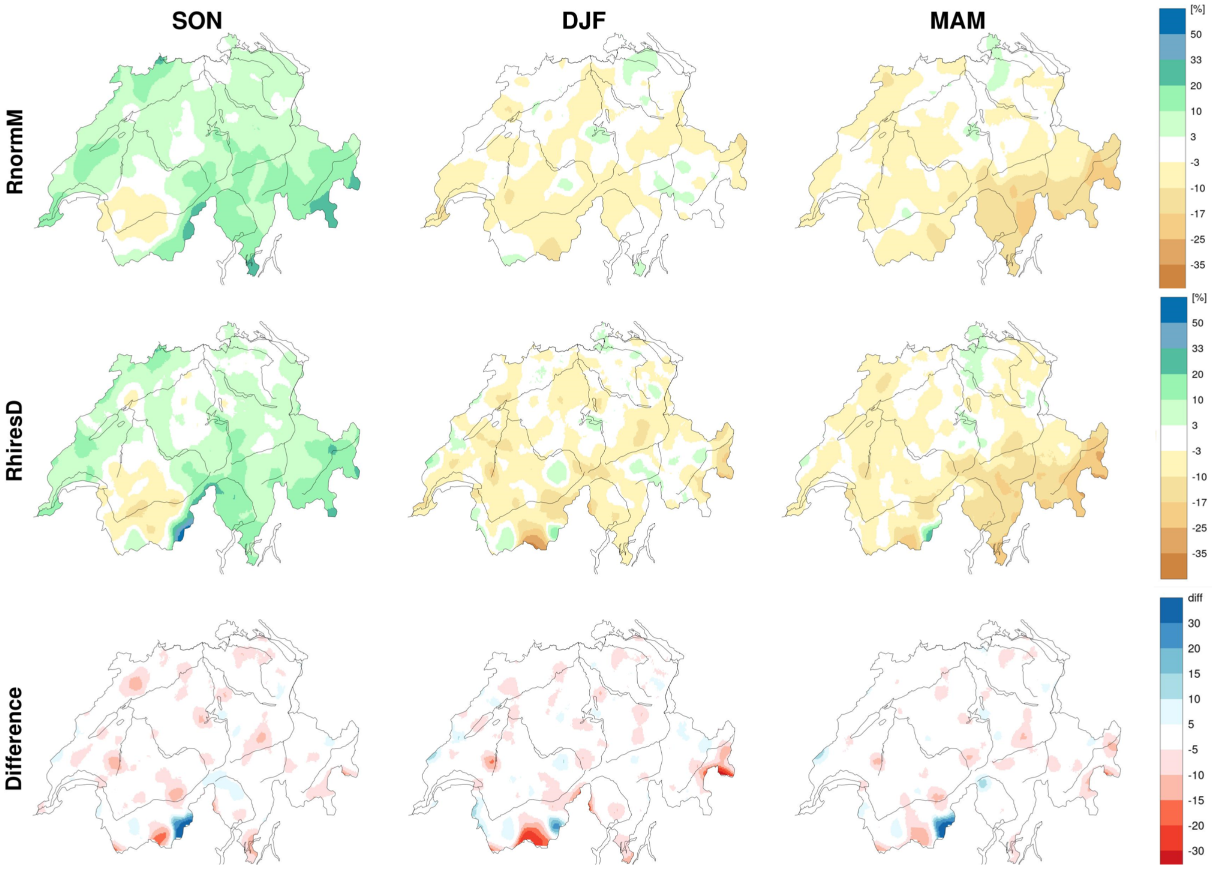

Figure G.1: Seasonal analysis of the uncertainties from the precipitation input grid. Top row: Ratio of mean seasonal precipitation between the reference periods 1991 - 2020 and 1961 - 1990 of the consistent RnormM product. Middle row: Ratio of mean seasonal precipitation between the reference periods 1991 - 2020 and 1961 - 1990 of the RhiresD product, which is used to run the baseline snow model OSHD-CL. Bottom row: Difference of the two upper ratios from (blue color indicate larger precipitation increase between the two periods in RhiresD compared to RnormM).

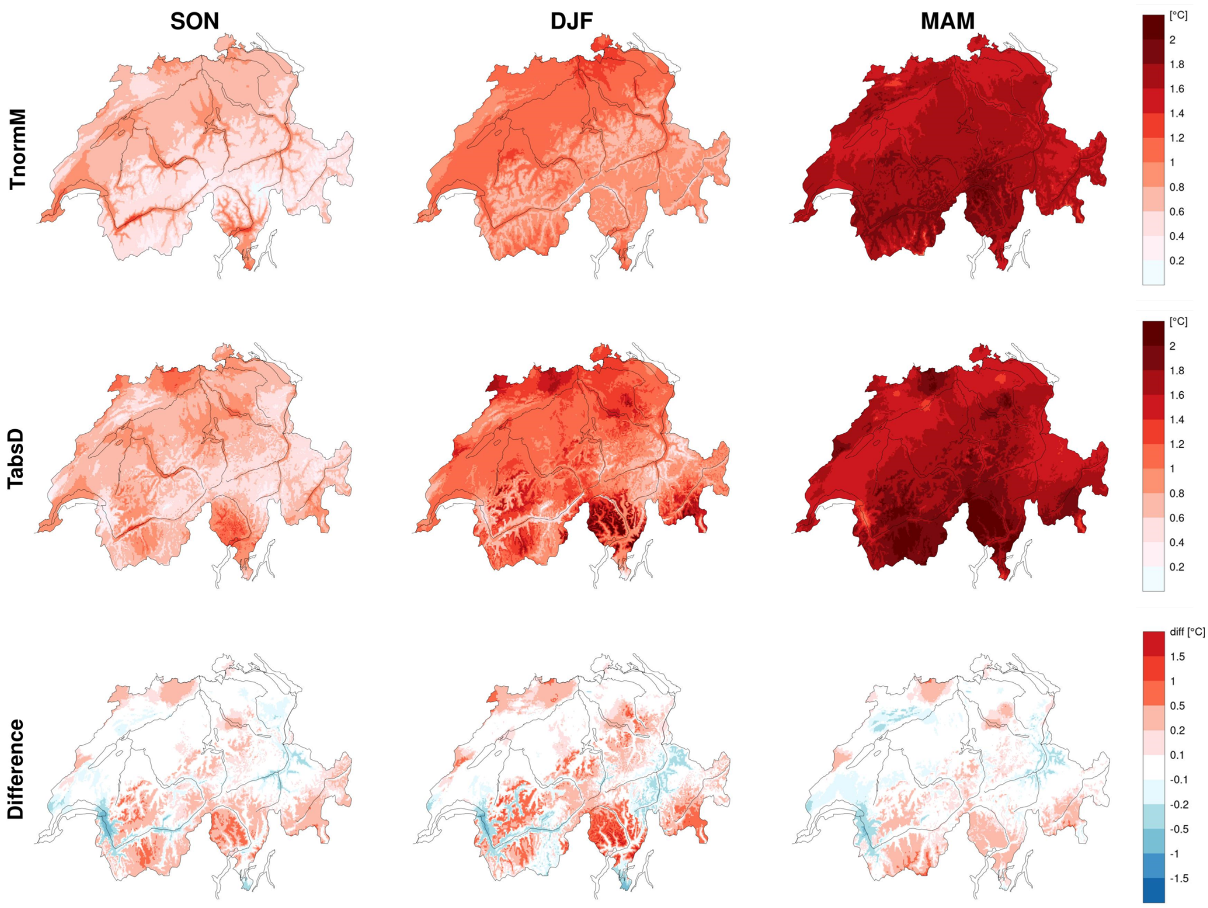

Figure G.2: Seasonal analysis of the uncertainties from the temperature input grid. Top row: Difference of mean seasonal temperature between the reference periods 1991 - 2020 and 1961 - 1990 of the consistent TnormM product. Middle row: Difference of mean seasonal temperature between the reference periods 1991 - 2020 and 1961 - 1990 of the TabsD product, which is used to run the baseline snow model OSHD-CL. Bottom row: Difference of the upper two rows (red colors indicate a stronger warming between the two periods in TabsD compared to TnormM.

Appendix H

Station-based trend validation

Table H.1: Comparison of the difference from period 1962 - 1990 mean to 1990 - 2020 mean winter SWE at the nearest grid cell (GC) and at the corresponding station (STAT). Red: relative difference (in %). Blue: absolute difference (in mm).

STAT	GC [%]	STAT [%]	GC [mm]	STAT [mm]
*BAS	-60.78	-48.94	-4.11	-0.83
*OTL	-53.91	-75.13	-5.49	-2.95
*GVE	-56.27	-57.91	-2.14	-0.79
*LUZ	-67.33	-73.36	-7.60	-4.05
*KOP	-59.25	-55.68	-6.41	-2.17
*LAN	-45.01	-54.62	-10.03	-7.55
*BER	-65.78	-45.26	-9.51	-1.67
*GRA	-67.93	-45.22	-9.26	-1.09
*VIS	-50.37	-68.19	-6.32	-6.65
*MAS	-62.61	-53.84	-12.70	-3.24
*LAG	-52.68	-54.34	-22.11	-6.65
*STG	-39.91	-24.60	-17.51	-3.56
1LB	-28.82	-39.13	-16.44	-11.77
*ELM	-43.90	-60.05	-68.43	-59.11
*CHD	-47.00	-29.95	-29.16	-11.76
*CDF	-53.01	-62.46	-49.90	-35.01
2EN	-32.02	-38.77	-23.90	-23.35
*GTT	-32.03	-46.90	-40.61	-52.22
*ROB	-25.17	-47.38	-11.57	-12.80
*GOS	-34.90	-38.88	-30.04	-54.16
*AIR	-36.01	-25.61	-45.06	-25.32
5KK	-22.78	-44.70	-35.32	-101.21
2ST	-24.41	-21.32	-54.53	-41.90
*SCU	-26.18	-31.25	-19.86	-17.57
1LS	-40.24	-30.60	-65.17	-26.89
3BR	-28.29	-34.87	-111.05	-86.79
3FB	-31.91	-40.95	-73.69	-99.71
1AD	-45.27	-43.26	-48.30	-33.67
4UL	-22.65	-21.10	-46.74	-43.42
7ST	-20.73	-25.51	-13.12	-16.21
5OB	-26.66	-17.58	-31.36	-17.75
2AN	-28.22	-26.42	-69.23	-62.69

Table H.2: Continuation of table Table H.1.

STAT	GC [%]	STAT [%]	GC [mm]	STAT [mm]
6BG	-39.67	-25.70	-85.07	-52.74
4GR	-39.81	-35.86	-46.48	-37.79
5DF	-17.76	-18.81	-28.66	-27.31
4MO	-34.78	-23.33	-62.11	-36.72
4ZE	-46.08	-32.73	-44.90	-37.98
6SB	-9.10	-22.65	-12.84	-44.79
1MR	-10.64	-11.11	-28.42	-20.03
7ZU	-18.38	-14.50	-19.28	-12.53
7SD	-15.67	-5.34	-15.95	-4.73
1HB	-21.73	-19.73	-73.01	-72.35
***BUF**	-9.28	-20.91	-12.12	-35.25
5WJ	-2.41	-2.58	-9.43	-10.87

Table H.3: Comparison of the difference from period 1962 - 1990 mean to 1990 - 2020 mean number of snow days over the winter months at the nearest grid cell (GC) and at the corresponding station (STAT). Red: relative difference (in %). Blue: absolute difference (in days).

STAT	GC [%]	STAT [%]	GC [days]	STAT [days]
*BAS	-50.06	-50.37	-16.61	-5.82
*OTL	-44.54	-48.60	-22.41	-6.87
*GVE	-56.23	-63.90	-9.25	-5.49
*LUZ	-55.50	-67.74	-27.98	-20.30
*KOP	-47.28	-56.10	-24.24	-12.65
*LAN	-28.16	-42.17	-21.06	-19.91
*BER	-47.08	-32.00	-25.69	-6.40
*GRA	-55.34	-44.04	-30.89	-7.17
*VIS	-42.83	-52.12	-25.45	-18.54
*MAS	-40.56	-46.23	-29.38	-16.10
*LAG	-28.84	-42.21	-30.76	-20.38
*STG	-23.11	-19.27	-27.27	-11.89
1LB	-12.06	-16.19	-16.21	-13.89
*ELM	-7.00	-25.38	-10.81	-30.97
*CHD	-16.20	-8.47	-20.65	-7.59
*CDF	-14.61	-33.52	-19.13	-33.02
2EN	-9.70	-12.01	-13.91	-12.95
*GTT	-1.31	-17.29	-1.99	-21.55
*ROB	-10.70	-23.06	-11.33	-16.17
*GOS	-9.17	-9.94	-13.41	-13.64
*AIR	-11.21	-17.22	-17.18	-22.03
5KK	-4.28	-11.18	-6.79	-17.69
2ST	0.68	0.59	1.13	0.87
*SCU	-9.58	-16.19	-13.75	-18.30
1LS	-3.24	-16.94	-4.81	-20.50
3BR	0.33	-3.03	0.56	-4.63
3FB	-1.09	-5.11	-1.77	-7.90
1AD	-7.16	-16.08	-10.53	-20.38
4UL	-1.43	-3.78	-2.34	-5.84
7ST	-13.35	-13.25	-19.59	-17.32
5OB	-6.57	-7.48	-10.70	-10.28
2AN	-1.52	-5.11	-2.56	-8.35
6BG	-6.14	-13.28	-10.20	-21.49
4GR	-8.25	-12.07	-12.92	-16.24
5DF	-1.34	-5.65	-2.22	-8.77
4MO	-3.14	-8.94	-4.98	-11.92
4ZE	-14.07	-13.61	-21.67	-20.00
6SB	-6.17	-12.66	-10.08	-20.44
1MR	0.78	2.34	1.32	3.55
7ZU	-8.22	-10.82	-13.46	-15.98
7SD	-7.35	-9.47	-12.26	-14.42
1HB	1.00	-0.83	1.70	-1.39
*BUF	-2.40	-10.24	-4.01	-17.32
5WJ	0.69	0.48	1.23	0.85

Appendix I

Monthly comparison with MODIS

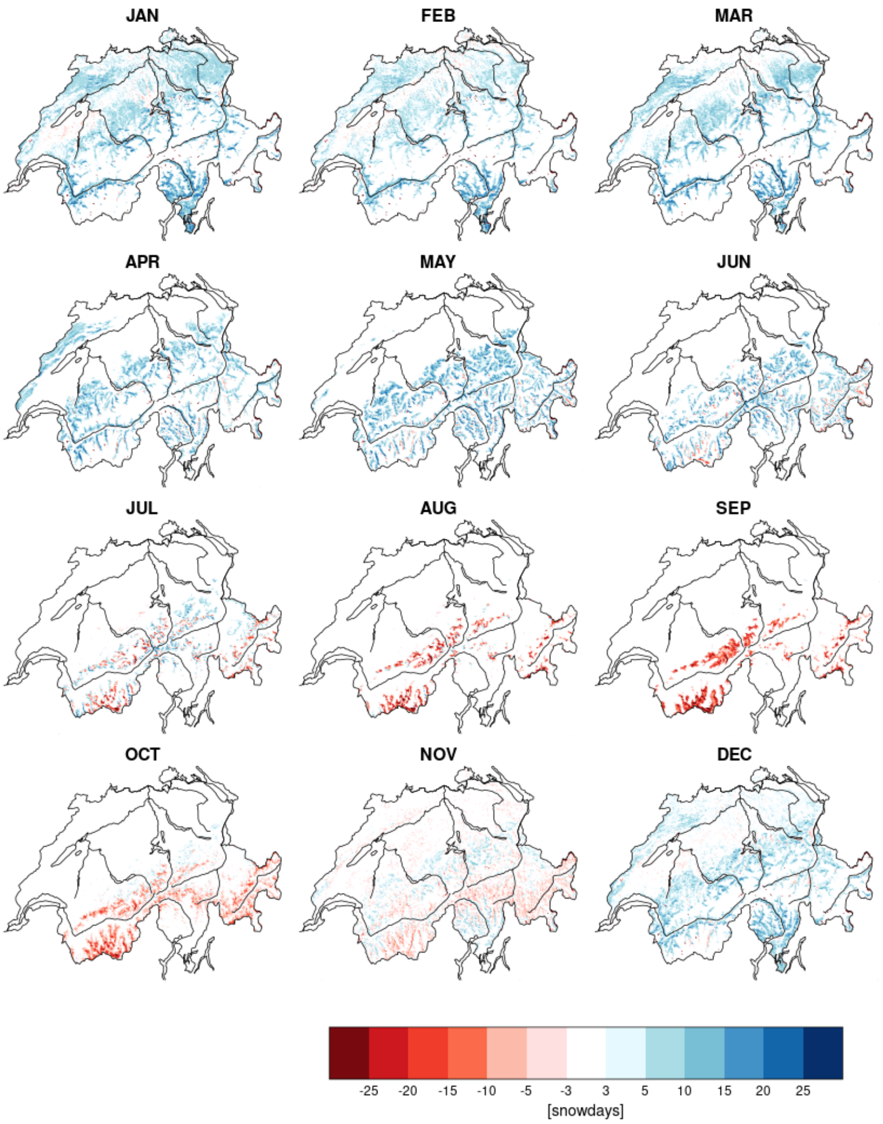

Figure I.1: Monthly comparison between OSHD-CLQM and MODIS. The plot shows the absolute difference between the mean number of snow days within the hydrological years 2003 - 2018 (OSHD-CLQM minus MODIS).

ETH

Eidgenössische Technische Hochschule Zürich
Swiss Federal Institute of Technology Zurich

Declaration of originality

The signed declaration of originality is a component of every semester paper, Bachelor's thesis, Master's thesis and any other degree paper undertaken during the course of studies, including the respective electronic versions.

Lecturers may also require a declaration of originality for other written papers compiled for their courses.

I hereby confirm that I am the sole author of the written work here enclosed and that I have compiled it in my own words. Parts excepted are corrections of form and content by the supervisor.

Title of work (in block letters):

Swiss snow cover in a changing climate: Evaluation of a long-term high-resolution SWE analysis

Authored by (in block letters):
For papers written by groups the names of all authors are required.

Name(s):	**First name(s):**
Danioth	Sarina

With my signature I confirm that
- I have committed none of the forms of plagiarism described in the 'Citation etiquette' information sheet.
- I have documented all methods, data and processes truthfully.
- I have not manipulated any data.
- I have mentioned all persons who were significant facilitators of the work.

I am aware that the work may be screened electronically for plagiarism.

Place, date	**Signature(s)**
Andermatt, April 6th 2023	Danioth

For papers written by groups the names of all authors are required. Their signatures collectively guarantee the entire content of the written paper.